NTNU – Trondheim
Norwegian University of
Science and Technology

Ice Abrasion and Bond Testing of Repair Mortars and High Performance Concrete

Joakim Rydningen Kirkhaug

Civil and Environmental Engineering
Submission date: June 2013
Supervisor: Stefan Jacobsen, KT
Co-supervisor: Kjell Tore Fosså, Kværner

Norwegian University of Science and Technology
Department of Structural Engineering

Department of Structural Engineering
Faculty of Engineering Science and Technology
NTNU- Norwegian University of Science and Technology

ACCESSIBILITY

MASTER THESIS 2013

SUBJECT AREA: Concrete Technology	DATE: 10/06/2013	NO. OF PAGES:122

TITLE:
Ice Abrasion and Bond Testing of Repair Mortars and High Performance Concrete

Isabrasjons- og heftprøving av reparasjonsmørtler og høyfast betong

BY:

Joakim Rydningen Kirkhaug

SUMMARY:
The purpose of this thesis has been to investigate ice abrasion properties for three different repair mortars, and evaluate their behavior and properties in relation to a typical B60 offshore concrete and a B70 concrete. Bond strength to a B60 concrete has been tested for all mortars. To increase understanding and knowledge in the field of research, a literature study was made. Roughness parameters, bond strength properties and parameters affecting ice abrasion resistance were reviewed. Testing equipment and procedures are described for ice abrasion and bond strength tests. Test conditions were chosen to evaluate the influence of sliding distance, contact pressure, sliding velocity and initial surface roughness on the abrasion rate. Seven different products; Densit, Reforcetech, Rockbond, B60 concrete, B70 concrete, MapeCoat (elastic epoxy) and Polyurethane (rigid epoxy) are ice abrasion tested. MapeCoat and Polyurethane showed no visible signs of abrasion, while all repair mortars were found to have higher abrasion resistance than the standard B60 reference concrete. Observed abrasion rate [mm/km]were 0,011-0,026 for Densit, 0,014-0,033 for Reforcetech, 0,024-0,041 for Rockbond, 0,024-0,052 for B70 and 0,025-0,090 for B60. Bond tests are performed according to NS-EN 1542. Average measured bond strength was 2,27 MPa for Densit, 1,82 MPa for Reforcetech and 2,93 MPa for Rockbond. All tested repair mortars are found to have good abrasion resistance and bond strength and should therefore be suitable as offshore repair products on ice abrasion exposed structures. High compressive strength, density and the use of steel reinforcement fibers are parameters found to reduce abrasion

RESPONSIBLE TEACHER: Stefan Jacobsen
SUPERVISOR(S): Prof. Stefan Jacobsen (NTNU), Kjell Tore Fosså (Kværner ASA)

CARRIED OUT AT: Institute of Structural Engineering, NTNU, Trondheim

Preface

This master thesis is the final work of my master degree at Norwegian University of Science and Technology (NTNU). The thesis is a continuation of my 9^{th} semester project thesis and has been carried out in the winter and spring of 2013, at department of structural engineering at NTNU.

This thesis is a product of a close collaboration with Kværner Engineering, who initiated the study.

The purpose has been to investigate ice abrasion properties for repair mortar and concretes considered to be used as repair products on ice abrasion exposed offshore structures.

It has been an interesting and educational work where most of the time has been spent in the laboratory performing tests or making repairs on testing equipment. Average testing time in the ice abrasion rig is supposed to be ≈ 14 hours, including surface measurements. Due to a series of unforeseen events and problems with test equipment, the laboratory work demanded even more time than originally planned.

Acknowledgements

For all the help, guidance and constructive feedback I have received I would like show my appreciation to my supervisor prof. Stefan Jacobsen at NTNU. I would also like to thank Kjell Tore Fosså at Kværner for his close follow-up, inputs, and help in all phases of the project and for making it possible to write my thesis on such an interesting subject.

Gratitude is also extended to the technical staff at the NTNU concrete laboratory.
Especially I want to thank Steinar Seehuus, Ove Loraas and Gøran Loraas for always being there to help me in the laboratory and the ice abrasion rig. Without them it would never been possible to perform all the laboratory tests.

In the end I would like to extend my appreciation to my uncle, Ulf Rydningen for feedback and help with the structure and layout of the report. Also thanks to my father Stein Rydningen and my brother Jonas Rydningen Kirkhaug, for feedback and help with the proofreading of the report.

Joakim Rydningen Kirkhaug
Trondheim 10.06.2013

Abstract

This report is about ice abrasion testing of concrete, consisting of a literature review and a part with description of laboratory experiments, results and discussion of the results.
The purpose has been to investigate ice abrasion properties for three different repair mortars, and evaluate their behavior and properties in relation to a typical B60 offshore repair concrete and a B70 concrete which according to ISO 19906 has acceptable properties. To properly assess the suitability as repair mortar, bond strength was tested.

To increase understanding and knowledge in the field of research, a literature study was made. Roughness parameters, bond strength properties and parameters affecting ice abrasion resistance were reviewed. The literature review indicated that the sliding contact test machine at NTNU should give good and reliable results. In general there seemed to be agreed upon that sliding velocity, temperature, ice contact pressure and compressive strength are parameters influencing ice abrasion of concrete. Literature also indicated that good bond strength is achieved by addition of silica fume, good preparation of the surface and that repair product should have better compressive strength than substrate concrete.

In «Experiments and Research plan» testing equipment and procedures are described for ice abrasion and bond strength tests. Test conditions were chosen to evaluate the influence of sliding distance, contact pressure, sliding velocity and initial surface roughness on the abrasion rate.

Seven different products; Densit, Reforcetech, Rockbond, B60 reference concrete, B70 concrete, MapeCoat (elastic epoxy) and Polyurethane (rigid epoxy) has been ice abrasion tested. Specimens were plane cut to get a representative fraction between aggregates and paste on the surface.

MapeCoat and Polyurethane showed no visible signs of abrasion, while all repair mortars were found to have higher abrasion resistance than the standard B60 reference concrete. Observed abrasion rates were 0,011-0,026 for Densit, 0,014-0,033 for Reforcetech, 0,024-0,041 for Rockbond, 0,024-0,052 for B70 and 0,025-0,090 for B60.
Results indicate that increased sliding velocity and compressive strength together with decreased contact pressure reduces the abrasion. Abrasion rates of sandblasted surfaces are found to be some lower than those who were plane cut.

Bond tests were performed according to NS-EN 1542. Average measured bond strength was 2,27 MPa for Densit, 1,82 MPa for Reforcetech and 2,93MPa for Rockbond.

All tested repair mortars were found to have good abrasion resistance and bond strength and should therefore be suitable as offshore repair products on ice abrasion exposed structures.

Possible sources of error and reliability of performed experiments are also discussed.

Sammendrag

Rapporten omhandler isabrasjonstesting av betong og er todelt med en litterturstudiedel og en del som inneholder beskrivelse av forsøk, resultater og diskusjon.
Formålet med oppgaven har vært å gjennomføre isabrasjonsforsøk for å bestemme abrasjonsmotstanden på reparasjonsmørtler sammenlignet med en standard B60 offshore betong og en B70 betong, som i henhold til ISO 19906 skal ha akseptable abrasjonsegenskaper. To epoxyer, MapeCoat og Polyuretan, er også testet. For å bestemme egnethet som reparsjonsmørtel er heftstyrken for reparasjonsmørtlene testet.

For å øke forståelsen for det omhandlede temaet er det i den første delen av oppgaven ble det gjort et lilitteraturstudie på ruhetsparametere, heftstyrke, testmetoder for isabrasjon og parametere som påvirker abrasjonsraten for betong. Gjennomgangen viser at testriggen på NTNU som er av «glidekontaktstypen» skal gi representative isabrasjonsresultater. Generelt synes det å være enighet om at isens hastighet, kontaktrykk, temperatur og betongens fasthet er de parameterne som kan antas å påvirke isabrasjon av betong. Silikastøv, riktig overflatebehandling av underlaggsbetong og en reparasjonsmørtel med høyere fasthet enn underlagsbetongen synes å være viktig for å oppnå god heft.

I «Experiments and Research plan» er prøvestutstyr og testprosedyrer beskrevet. Prøvebetingelser ble valgt for blant annet å kunne vurdere effekten av glidehastighet, istrykk og overflateruhet. Prøvestykkene ble planslpit for å få en represntativ fordeling mellom tilslag og pasta på overflaten.

Abrasjonsmotstand er testet i laboratoriet for tre aktuelle reparasjonsmørtler, to referansebetonger og to epoxyer; Densit, Reforcetech, Rockbond, B60 referansebetong, B70 betong, MapeCoat og Polyuretan. MapeCoat og Polyuretan viste ingen tegn til abrasjon. Reparasjonsmørtlene er funnet å ha betydelig bedre abrasjonsmotstand enn B60 betongen. Målte abrasjonsrater [mm/km] er; 0,011-0,026 for Densit, 0,014-0,033 for Reforcetech, 0,024-0,041 for Rockbond, 0,024-0,052 for B70 og 0,025-0,090 for B60. Resultatene indikerer at økt glidehastighet, økt trykkfasthet og redusert istrykk gir redusert abrasjon. Sandblåste overflater har noe lavere abrasjonsrater enn planslipte overflater.

Hefttesten er gjennomført i henhold til NS-EN 1542. Gjennomsnittlig målt heftstyrke er 2,27 MPa for Densit, 1,82 MPa for Reforcetech and 2,93 MPa for Rockbond.

Alle reparasjonsmørtlene er funnet å ha god abrasjonsmotstand og heftstyrke, og de vil være å foretrekke fremfor en standard B60 reparasjonsbetong. Feilkilder og pålitelighet av resultatene er vurdert. Usikerheten rundt prøvebetingelser som glidehastighet ser ut til å være betydelig. Målt abrasjon er ikke nok pålitelig til å foreta konkrete konklusjoner om hvordan produktene oppfører seg i virkeligheten. Resultatene bør imidletid gi et bra bilde av forholdet mellom produktene, da feilkildene syntes å være like for tilsvarende prøvebetingelser.

Contents

1 Introduction

1.1 Introduction

High demand of natural recourses makes it profitable to extract natural resources in harsh environments like the arctic regions. Concrete installations are built further and further north, and new challenges have to be considered in the design process. In the North Sea, where many concrete oil platforms have been built, there is no problem with drifting sea ice. However, in areas near Sakhalin, Russia, drifting sea ice has an abrasive effect on concrete structures. Ice abrasion of concrete is therefore a subject to be considered. Better understanding on how ice and concrete interacts makes it possible to take the necessary precautions to prevent damages and can improve the knowledge on how structures can be repaired.

Kværner is a contractor building this type of concrete structures. A structure at Sakhalin was equipped with protective steel shields in the ice abrasion zone. In Sakhalin, the sea ice can drift with velocities up to 2 m/s (Jacobsen, et al., 2012) creating large mechanical forces and local stress concentrations when interacting with a structure. Steel shields are an expensive investment (Fosså, 2007) and from Figure 1 it can be seen how the ice can tear them up, exposing the concrete underneath for the forces of the ice.

Figure 1 Steel shield at Sakhalin. (Kim, et al., 2012)

By performing tests and experiments on ice abrasion of concrete, it is possible to learn more about the process and which parameters to include. Improved knowledge would make it possible to develop better estimation models and increase the chance of choosing a concrete with sufficient abrasion resistance, and thus avoiding difficult and costly repairs on new structures. For already existing structures it is necessary to find a product bonding properly to the existing concrete at the same time as abrasion resistance is acceptable.

The last decades some research on ice abrasion has been performed, both at NTNU in Norway, and other countries like Canada, Russia, Finland and Japan, to mention some. A challenge is that there seem to be somewhat different opinion on which parameters to include. Since there is no international standardized test method for ice abrasion it can also be difficult to properly compare research from different studies and it is still necessary to get more and improved knowledge on the subject.

1.2 Purpose

Kværner delivers concrete oil rig sub-structures operating in arctic environments, exposed to drifting sea ice. The company has therefore initiated this study to improve knowledge on ice abrasion. The purpose has been to study ice abrasion on different repair mortars and concretes considered to be used on ice abrasion exposed structures. It is intended to evaluate how repair mortars behave compared to standard concretes. B60 is normally used as a standard concrete on offshore structures, while B70 is supposed to have acceptable abrasion properties, according to ISO 19906. Results from bond and ice abrasion tests shall be used to evaluate which of the products that is suitable as repair products, and if they are improving the abrasion resistance of an existing structure. Results should also be used to find parameters that can improve abrasion resistance of concrete in general and extend the extend service time of concrete structures exposed to ice abrasion.

1.3 Research topics

In this research, the objective has been to find how repair mortars behave compared to standard offshore concretes like B60/ B70. It is also of interest to evaluate how different parameters like sliding velocity, contact pressure and surface roughness are influencing the abrasion properties in the concrete. As the ice abrasion test rig is self-built at NTNU and no international standard for ice abrasion tests exists, it has also been of interest to evaluate how the equipment is working and the reliability of the results. With help of pull-out strength tests it can be decided if the repair products have sufficient bond strength for offshore repairs.

1.4 Limitations

In this study abrasion rate has been evaluated for all tested products, for a given set of test conditions. There is little research on how results from the NTNU test rig can be compared to actual ice abrasion on a real structure in the field. Test conditions, methods and equipment which are used in this study do not necessarily represent real life field abrasion values. Possible comparison of obtained results to real field abrasion is therefore limited.

The main objective has been to investigate and evaluate the mechanical properties of the tested products. Therefore parameters like price and workability of fresh concrete and so on is not taken into consideration.

Large amounts of data have been analyzed, many calculations are performed and unintentional mistakes can have been done. All data have been checked at least twice, but there is still a chance that such mistakes have not been found.

1.5 Methodology

The methods used in this work are literature review and laboratory testing. To increase understanding and knowledge in the field of research, a literature study was made. This literature study included gathering information from the internet, previous dissertations, textbooks and journal articles. First a comprehensive literature search based on topics relating to my thesis subjects was made, by search on keywords like "ice abrasion concrete testing", "ice abrasion", and "concrete abrasion" using the databases available by the NTNU University library. All papers that were not relevant to my research were discarded, and the resulting literature, gathered from the literature review, was used for summing up state of the art. The literature review is presented in Chapter 2 "Background".
After the literature review, the second step was testing in the laboratory to find which and how different parameters influence the abrasion resistance of concrete products. The experiments are also used to see which products are best suited to protect against ice abrasion. All experiments in the laboratory were made in ice abrasion laboratory test rig at department of structural engineering at NTNU. The laboratory test results are presented in chapter 3.

2 Background

2.1 Ice

2.1.1 Introduction

When studying ice abrasion, mechanical properties of ice are important. For offshore concrete structures there are two main challenges in regard to ice and cold temperatures; freeze-thaw processes and ice collision. In this chapter a brief description of ice and ice properties are given in order to create a background for understanding the ice abrasion mechanism and evaluate the properties of the ice used in the ice abrasion laboratory tests of this study.

2.1.2 Ice properties

Ice is the solid state of water and can be anything from snow, glaciers, hail and so on. It can have up to 12 different crystal structures, with hexagonal and cubic ice as the two most closely related and ordinary versions (Schulson, 1999). Hexagonal ice, typically termed ordinary ice (Schulson, 1999), is created by freezing water at temperatures lower than 0^{0}C (at 100 kPa). Cubic ice can be obtained by condensation of water vapor at low temperatures, typically less than < -80^{0}C (Chaplin, 2012) , and has a diamond-cubic crystal structure. Microstructure of hexagonal ice is subject to large variations depending on the thermal history and conditions of formation (Schulson, 1999). On a molecule level, water molecules are held together by hydrogen bound to four other molecules. Liquid water molecules are usually bound to 3-4 other molecules. Figure 2 shows molecule structure of water and hexagonal ice.

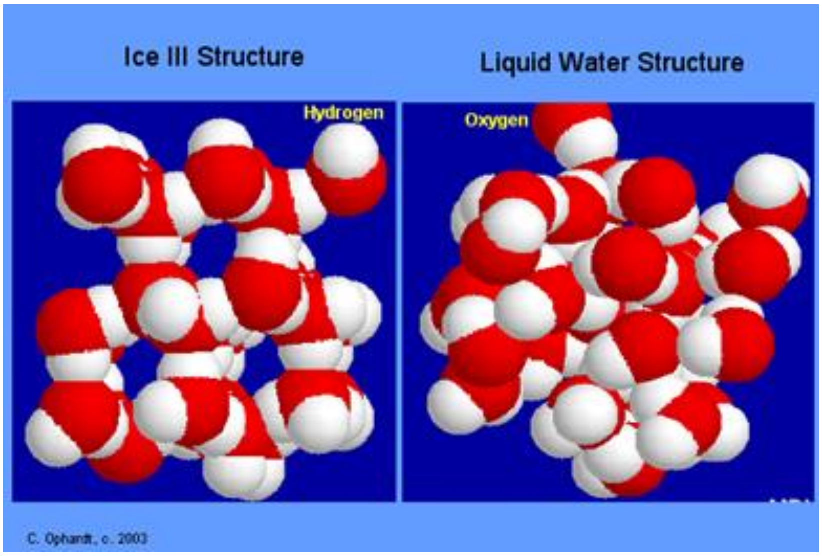

Figure 2 Molecule structure of ice and water (Ophardt, 2003)

This makes theoretical density of ice 0.917 kg/m^3 which is less dense than liquid water (0,998 kg/m^3)(2013a). Reduced density means that volume of frozen water increases about 9 % compared to its liquid state. This volume expansion creates huge forces. Figure 3 is a picture of a plastic container which has cracked due to volume expansion of freezing water.

Figure 3 Cracked ice container

Actual density differs from the theoretical one and depends on parameters like air content and the thermal history. For sea ice the density are varying for ice above and under the waterline, salinity levels and age. Multi-year ice has slightly lower density over the waterline compared to first year ice. Reported measurements (Timco and Weeks, 2009) is 0.84-0.91kg/m^3 for ice above the waterline and 0.9-0.94 kg/m^3 under the waterline. It is also stated that unless a precise value is available, a density of 0.92 kg/m^3 can, and should be assumed. Figure 4 shows density of sea ice plotted against temperature for four different salinities (Timco, et al., 2009). Density is increasing with increased salinity and reduced temperatures. In sea ice, salinity varies with the depth in the ice sheet as well as seasonal changes. This is because salt migrates through the ice. Typical salinity reported in (Timco, et al., 2009) is 1.5-5 ‰.

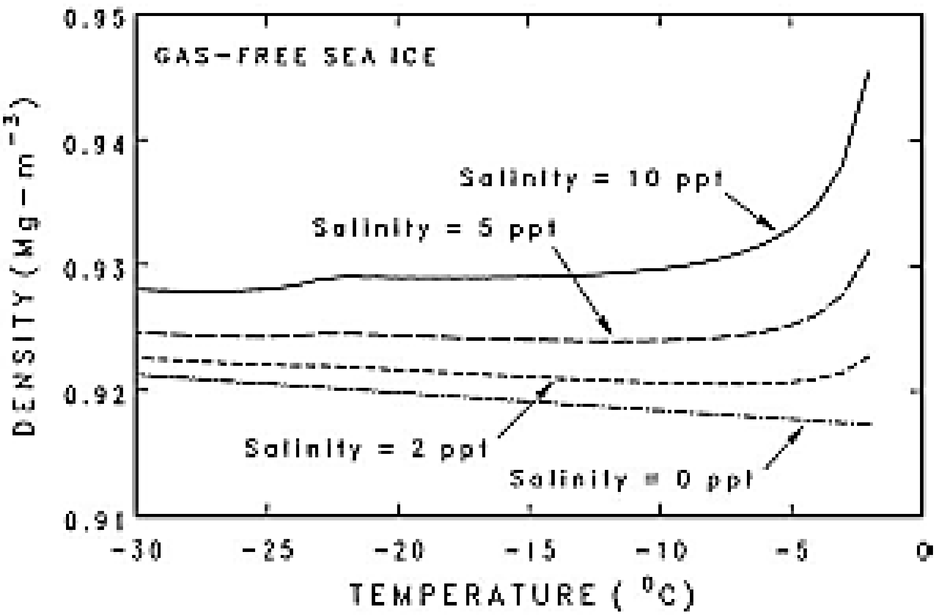

Figure 4 Density of sea ice for different salinity levels and temperatures (Timco, et al., 2009)

Sea ice growth-history can result in different structures depending on the orientation of the molecules. The two most common are columnar and granular ice. Granular ice can be made if water is frozen from different sides at the same time, and the middle is freezing last, resulting in a chaotic structure. This type of ice is in most cases isotropic, also in sea ice with salt incisions. This is because salt particles occur between and not within the ice crystals. Columnar ice can form at sea surface under calm conditions or underneath the surface on an initial granular layer when the vertical movement have subsided. Columnar crystals will be orientated so that they extend through the thickness of the ice sheet and orientated parallel to the heat flow, in most cases vertically.

When studying ice abrasion mechanical ice properties are of interest. Relevant parameters are compressive- and tensile strength, fracture toughness, shear strength, hardness, age and density.

Strength of ice depends on variables such as temperature, strain rate, volume, salinity, density, ice type, loading direction and grain size (Timco and Weeks, 2009, Petrovic, 2003). For sea ice, a multi-year ice is considerably stronger than first year ice. This is mainly because of lower salinity and lower porosity due to melting processes during the summer (Timco, et al., 2009).

Shear strength: Ice interacting with structures is often subject to conditions involving both tensile and compressive forces. Shear strength could therefore be a useful parameter. For granular sea ice the average shear strength is reported to be in the range of 550±120 kPa and high temperatures is found to reduce the strength (Timco, et al., 2009). Since ice problems occur at high loading rates and as compressive strength are much higher than the tensile strength, ice will in most cases fail in tensile rather than shear.

Compressive strength: Compressive strength is an important property of ice. In the temperature range of -10^{0}C to -20^{0}C the compressive strength has been reported between 5-25 MPa for fresh water ice (Petrovic, 2003). For multi-year sea ice it has been reported to be 7-15 MPa (Timco and Weeks, 2009). According to (Petrovic, 2003) decreasing temperature gives an increase in compressive strength. Compressive strength is actually increased by a factor of 4 when temperature is decreased from 0^{0}C to - 40 ^{0}C. Compressive strength is also strain rate sensitive. Ductile behavior can be experienced at low and intermediate strain rates while a high strain rates causes brittle behavior (Timco and Weeks, 2009).

Tensile strength: Tensile strength is another of fundamental property of ice and represents a key failure mode when ice interacts with structures (Timco and Weeks, 2009). Average tensile strength of published investigations evaluated in (Petrovic, 2003) are 1.43 MPa, varying from 0.7 to 3.1 MPa. Reduced temperature is found to increase tensile strength. However, the temperature effect is much smaller than for compressive strength. Tensile strength increases only by a factor of 1.3 (0°C to-40°C). Tensile strength also decreases when the diameter of the ice grain size is increasing. Higher salinity is reducing tensile strength.

Fracture toughness describes the stress required to make a crack propagate. The fracture toughness of ice is generally in the range of 50-150 kPa (Timco, et al., 2009). In comparison glass is typically in the range of 700-1000 kPa. This parameter seems to have a weak relation to temperature, but ice exhibits a decrease of toughness with increased grain size.

For the interaction between ice and materials such as concrete the coefficient of friction will also be a factor to take into account. Various tests and experiments on the subject on friction of ice against various materials have been performed. It has been found that friction tends to increase for lower contact velocities and rough materials. Average friction coefficient of sea ice against smooth metals was 0,05 and 0,1 for velocities over 50 mm/sec. Slightly larger values were observed at -20°C than for -10°C (Timco, et al., 2009).

2.2 Ice Abrasion

2.2.1 Introduction

Ice abrasion is a possible, and likely, wear mechanism to occur on concrete structures built to operate in areas with drifting ice. Since concrete is harder than ice it is easy to imagine that the ice will be crushed, leaving the concrete undamaged. In arctic and sub-arctic areas, friction induced forces between concrete and ice can, over time, become so large that the concrete starts to experience wear in the form of ice abrasion. This may cause reduced capacity and reduction of the reinforcement cover depth. Reduced cover depth means that protection against for instance reinforcement corrosion is reduced. If this is not taken into account in the design process this could impact the serviceability time, and/or demand costly and challenging repair of the structure.

2.2.2 Mechanism

Ice abrasion is the result of drifting ice colliding with a structure. The friction created between moving ice and concrete will generate contact forces. These forces start to wear down the concrete surface by the mechanism of abrasion. One way to measure this abrasion is as an abrasion rate, the wear in millimeter per kilometer of ice sliding [mm/km]. Size of abrasion forces depends on the properties of both ice and concrete, sliding (collision) velocity, contact pressure and temperature. Sea and fresh water ice have different impact on abrasion for different temperatures. Ice containing sand or other particles may also contribute to increased abrasion. According to (Huovinen, 1990) wear due to abrasion can be divided three main stages, illustrated in Figure 5.

a) Abrasion of cement paste
b) Abrasion of cement paste + loosening of aggregate: The wear of cement paste is so large that the aggregate starts to become ”peaks”.
c) Removal of the loosened aggregate and continued cement paste abrasion.

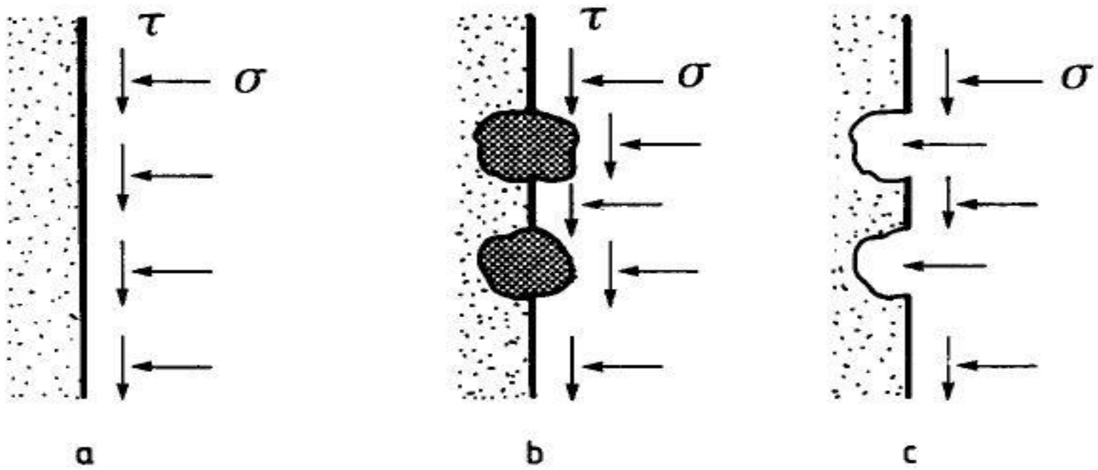

Figure 5 Stages of concrete abrasion (Huovinen, 1990)

Predicting the abrasion rate [mm/km] is a complicated matter. Knowing the connection between different parameters like concrete strength, contact pressure and ice temperature and how they influence on each other and the concrete abrasion rate is therefore of great interest.

The surface condition of concrete is important in regard to how large friction forces are being created. Previous research has also indicated that geographical properties like weather and climate influence how large the abrasion effect is going to be. Repeating freeze/taw cycles reduces the matrix strength and therefore also the bond between aggregate and paste, leaving the concrete more exposed to abrasion (Janson, 1988a).

2.2.3 Forces

The size of stress and forces that is occurring on the concrete surface depends on the strength and fracture toughness of the ice. Fracture toughness can due to redistribution of forces be increased with a factor 3 compared to the un-axial compressive strength of ice (Janson, 1988). As described in chapter 2.1, ice properties depend on parameters like salinity, temperature and strain rate. In (Janson, 1988) a model of how stress induced by contact force leads to abrasion is presented. Figure 6 shows a model of how the distribution of contact forces can give locally large stress concentrations.

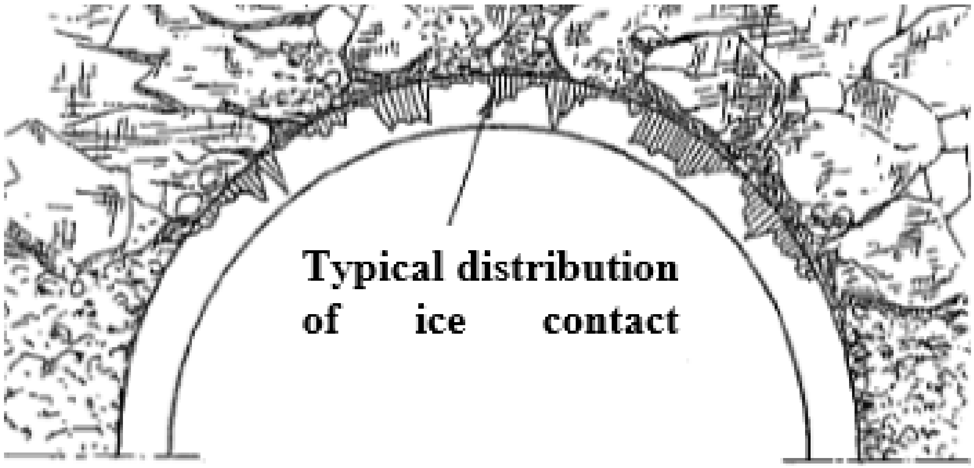

Figure 6 Typical distribution of ice contact pressure on the concrete surface. (Janson, 1988)

Uneven distribution of contact forces results in high local stress concentrations. The location of these stress concentrations are changing in time and space, creating a fatigue effect on the concrete surface. When the concrete is being exposed to stress and fatigue for longer time periods, it starts to experience wear, and abrasion is initiated. Loading direction is also an important parameter in regards to ice abrasion. When the ice is moving parallel to a structure the abrasion is larger compared to when it collides in a perpendicular direction (Janson, 1988a). Variations in sliding direction are assumed to create a rocking effect on the aggregate, with increased abrasion as the result. Figure 7 shows sliding direction variations.

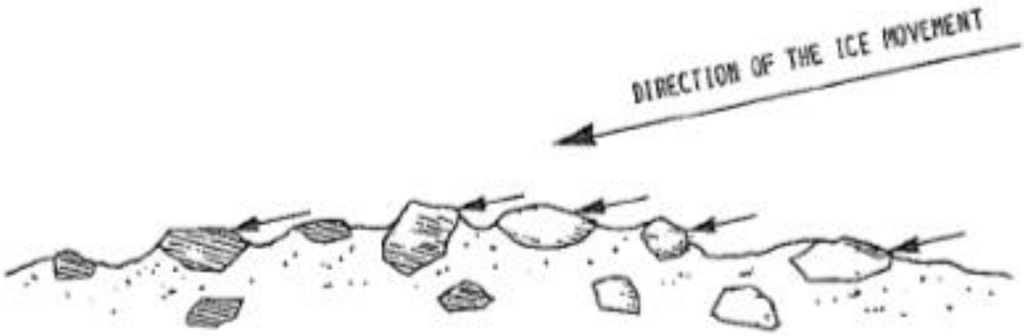

Figure 7 The direction of the Ice movement affects the abrasion of concrete. Ice sliding parallel to the surface will generate larger wear than ice colliding with an angle of 90 °. (Janson, 1988)

2.3 Surface Roughness

The topology and roughness of a surface may help predict how materials are interacting with each other. In most cases, increased roughness are increasing the contact/ interaction between two materials, thus also the friction. In order to evaluate a surface in particular, it is necessary to quantify the surface roughness in a suitable way. A range of methods and equipment for measuring surfaces exists. Based on factors like size, material, time and accuracy an acceptable method/ equipment should be chosen. There is of course also the question regarding how to characterize roughness. Numerous different parameters can be used, all with their own strength and weaknesses.

In the following chapter a selection of different methods on how to measure and characterize surface roughness, and how these characterizations methods differ from each other are described. Then there is a short literature review on how surface roughness and surface condition affects abrasion of materials. Even though concrete has not been the material in focus in all the reviewed literature, it could be interesting to see how roughness are influencing the behavior of other materials and compare this to the behavior of concrete.

2.3.1 Surface Measurement techniques

Numerous instruments for measuring surface roughness/ texture have been developed over the years, including everything from more or less simple stylus instruments (digital indicators) to more advanced optical 3D-scanning devices and 3D- microscopes. Measurement instruments can be divided into two main categories: contact and non-contact methods. Examples of non-contact methods are laser profiling, and other photo- and light structuring techniques, while a typical contact method is a standard digital indicator.

In the following sections the basic principles of methods used for characterizing the surface of concrete specimens in the experiments of this study is presented; linear profiling and optical 3D photogrammetry. A 3D microscope was also considered but left out because concrete specimens were too large for the microscope available at NTNU. The same equipment used for roughness measurements can, and have, been used for measurements of abrasion.

Linear profiling/ Stylus Techniques

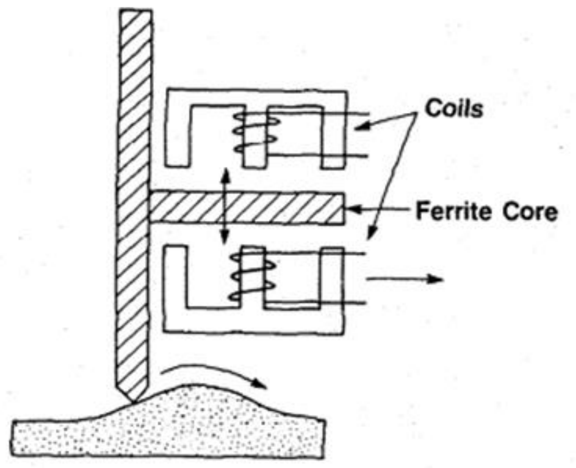

Figure 8 Schematic diagram of LVDT stylus (Kobrick, et al., 2011)

Linear profiling using a profilometer is one of the most commonly used measuring techniques (Tatone, 2009), and is classified as a contact measuring method. A schematic principal sketch can be seen on Figure 8. The principle is that the indicator is moved in a grid over the surface. The stylus is moving vertically as the indicator changes it position on the surface, allowing deviations to be measured. Deviations can be recorded manually by writing down deviations for selected intervals on the surface, or the measuring device can be connected to a computer which is recording the deviations automatically. A disadvantage with this method is that it requires a load to create contact between surface and stylus. This creates a contact pressure on the surface, which may leave a permanent deformation (Kobrick et al., 2011). The shape and size of the tip /stylus interacting with the surface specimen is also a possible source of error. If too large the, tip could be resting on an edge and therefore give inaccurate measurements. Lateral resolution depends on the width of the stylus tip, and can be as small as 0,1 µm, this is illustrated in Figure 9. If too small there is an increased risk for the tip to break.

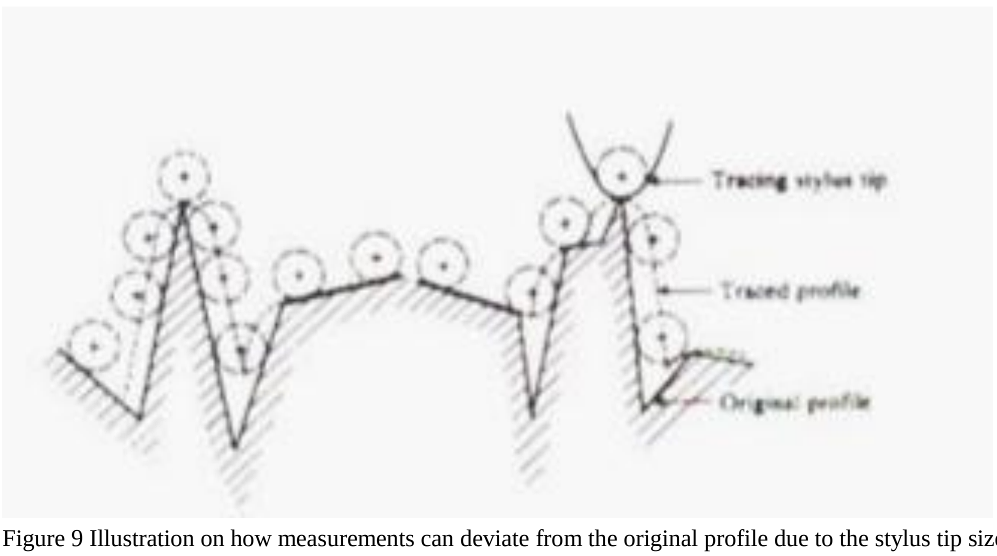

Figure 9 Illustration on how measurements can deviate from the original profile due to the stylus tip size (Kobrick, et al., 2011).

This type of device is limited to linear 2D profile measurements. In order to do areal measurements, parallel recordings of the surface close to each other have to be performed. Good accuracy and calibration are important and requires a highly linear transducer. Meaning that measurements of the same surface height should not change over the range of the transducer (Vorburger, 2010). A transducer is the part converting deviations to an electrical signal (Amaral, et al., 2002).

Optical instruments /Photogrammetry

Another option is to use optical instruments. A huge advantage with this type of measurements is that the risk of damaging the surface is reduced, as it is a non-contact method. Common techniques are based on the ability to detect a light beam on the surface. Interferometry uses superposition to combine light waves. When two waves with equal frequency are combined, the phase difference can be used to interpret the surface.

Photogrammetry is a method meaning that minimum two 2D images taken from different angels are used to create a digital 3D profile of the surface. Different type of equipment and products are available, using different types of technology. One method is to project structured light with a known pattern on the surface. Disorientations of these lines are captured by CCD (Charged-coupled device) cameras and used to create the digitalized version of the surface. Figure 10 shows the principle of the technique. Light is projected, reflected before it is captured by the cameras.

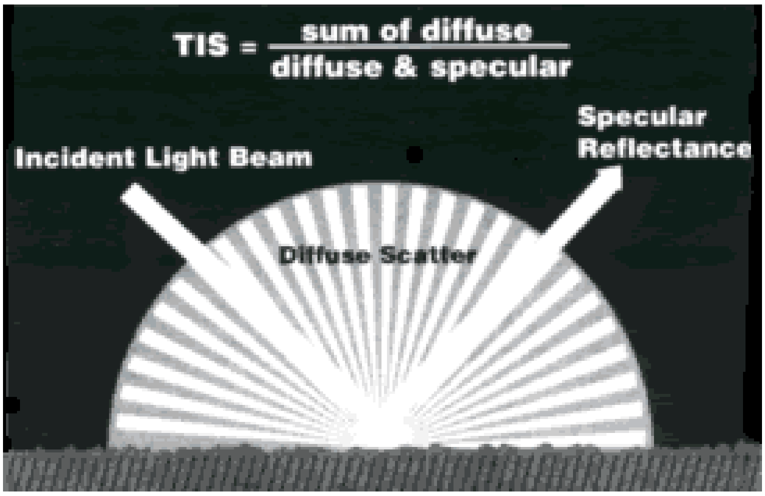

Figure 10 Principle of photogrammetry. Light is being projected on a surface and the reflection is captured (Tec13)

This method gives an accurate representation of the surface, and collected data can be used for detailed and accurate analysis. However, there are some weaknesses. In order to digitalize a surface many individual images have to be assembled. To make the software able to do this, reference points must be glued to the surface, which is very time consuming.
This type of measurement also creates a huge amount of data to be processed, which requires a high computer processing capacity in order to keep the time consumption as low as possible. Such equipment is also sensitive to vibrations and ambivalent light. This does that there

sometimes are necessary to perform several measurements of the same surface to get good results. After completing the digitalization, data has to be analyzed. There is a relatively high threshold to learn how to use this type of equipment, making this method much more demanding compared to manual linear profiling equipment.

2.3.2 Roughness parameters

When evaluating ice abrasion of concrete it is of interest to investigate how, or if, the rate of abrasion changes with the roughness of the abraded surface. This section presents a few ways to characterize surface roughness.

Roughness parameters are a way to express the texture or topology of a surface. Initial surface texture depends on factors like type of material and pretreatment. Surface roughness can influence the functionality of a product for either better or worse. A rough surface might be preferred in coating technology where good adhesion is wanted. A surface can be characterized as rough when deviations from the ideal or average line are large and correspondingly as low if the deviations are small.

There are many different ways to express roughness of an object, and when characterizing a surface more than one parameter should be calculated (Sedlacek et al., 2012). What they all have in common is that they basically are a statistical interpretation of the distribution of surface deviations. NS-ISO 4287 describes terms, definitions and surface texture parameters. Table 1 shows an overview of some selected surface parameters.

Table 1 Summary of some roughness parameters

Parameter	Name
Ra	Roughness Average (Ra)
Rq	Root Mean Square (RMS) Roughness
Rt	Maximum Height of the Profile
Rv, Rm	Maximum Profile Valley Depth
Rp	Maximum Profile Peak Height
Rpm	Average Maximum Profile Peak Height
Rz	Average Maximum Height of the Profile
Rmax	Maximum Roughness Depth
Rc	Mean Height of Profile Irregularities
Rz(iso)	Roughness Height
Ry	Maximum Height of the Profile

In this review the focus has been on amplitude parameters. There are also area roughness parameters which are defined in the ISO 25178 series. Linear roughness parameters are written with a capital R and area parameters use capital S.

All parameters are calculated from deviations of the measured surface, and there is a close connection between the different parameters. This means that determination of one parameter almost automatically leads to the determination other ones (Gorlenko, 1981). This is illustrated by the fact that R_q (Formula 2) is a part of the formula calculating R_{sk}, skewness (Formula 3). The most common parameter to use is according to Sedlack et al. (2012) is Sa and S_q in addition to skewness and kurtosis. These four parameters are therefore described in more detail.

$$R_a = \frac{1}{l}\int_0^l |y|\,dl = \frac{\sum_{i=1}^{i=n} y_i}{n}$$

Formula 1 R_a where l is the sampling length and y is the ordinate of the profile

R_a is the arithmetic average roughness parameter (Formula 1) and is defined as the area between the roughness profile and the mean line over the sampling length. Figure 11 shows a graphical illustration of R_a which is one of the most common used roughness parameters (Talati, 2013, 2013c).

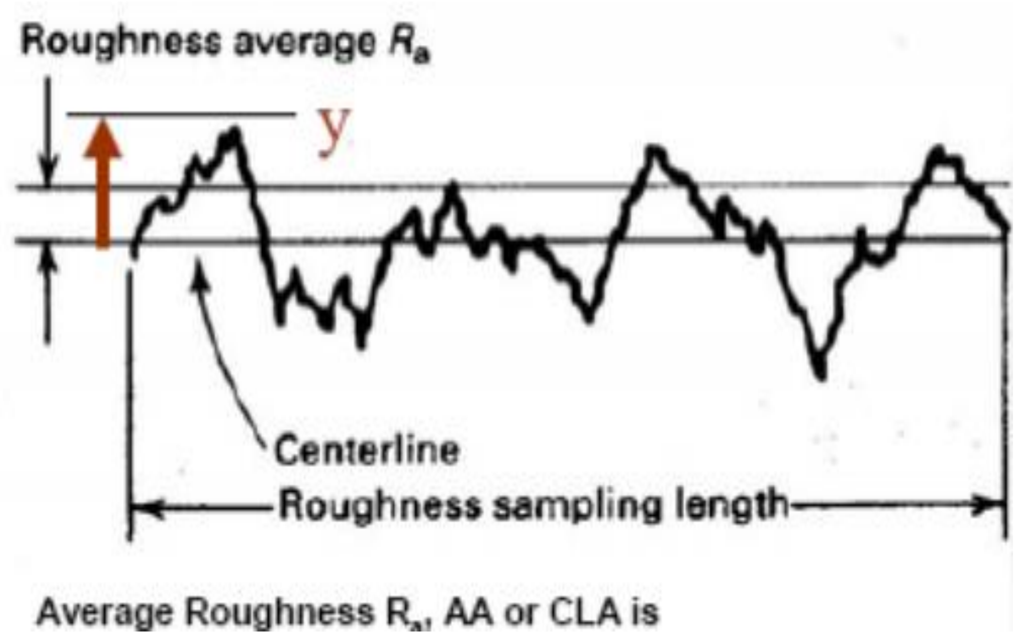

Figure 11The picture shows a graphic presentation of R_a (Talati, 2013)

R_a can be useful as a guideline to the general roughness of a surface but is often proven to be too general for detailed analysis (Zeccihino, 2013). This is because Ra does not make any consideration to if it is a valley or a peak. It also gives little information about the spatial variation of the measurements.

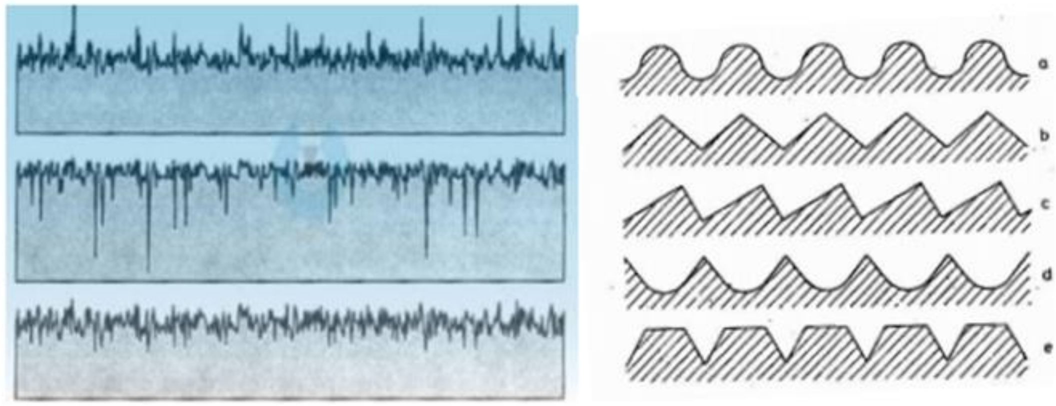

Figure 12 Surfaces with same R_a but very different surface profiles (Talati, 2013)

Figure 12 shows different surfaces with the same measured average roughness, and as seen they have very different surface profiles. From the picture it is clear that even if R_a is a good indication, also other parameters should be assessed when evaluating and comparing roughness of different surfaces to each other. Different profiles may give different behavior in relation to for instance wear, even if R_a is the same. For surfaces with large deviations and a generally “complicated” profile, a more detailed parameter, taking both peaks and valleys into account should therefore be used. In other words Ra gives a good overall description, but is not sensitive enough to all types of profile changes.

$$R_q = \sqrt{\frac{1}{n}\sum_{i=1}^{n} y_i^2}$$

Formula 2 R_q Root mean square deviation

R_q (RMS) is the root mean square parameter of the peak heights (Formula 2). This parameter is more sensitive to the occurrence of occasional high and low points compared to R_a (Kepconic, 2013). R_q contains square terms and large deviations from the average line are therefore more heavily weighted than those close to the average line. Using only R_q can be deceiving according to (Bloomfield, 2006).

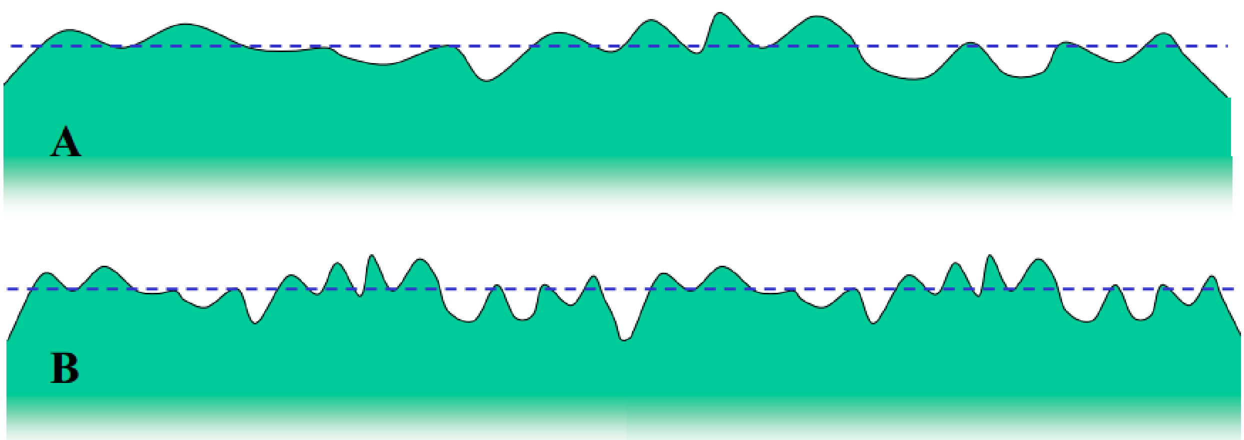

Figure 13 Two surface profiles with the same Rq (Bloomfield, 2006)

Figure 13 shows to surfaces with the same RMS. Both surfaces deviates the same amount from the average line but Surface B has a quicker variation in the vertical level and can therefore seem rougher than surface A. This is not the case, at least not according to R_q calculations.

$$R_{sk} = \frac{1}{N \cdot R_q^3} \sum_{i=1}^{N} z_i^3 = \frac{1}{L \cdot R_q^3} \int_0^L z(x)^3 dx$$ Formula 3 R_{sk} Skewness

Asymmetry of the surface profile may be characterized by *skewness* (R_{sk}) (Formula 3). Skewness is a dimensionless parameter where the heights are raised to the third power. Negative skewness indicates a surface with a large amount of valleys, while a positive skewness indicates an over-representation of peaks. Thus a symmetrical distribution of peaks and valleys on a surface gives a skewness of 0.

$$R_{ku} = \frac{1}{N \cdot R_q^4} \sum_{i=1}^{N} z_i^4 = \frac{1}{L \cdot R_q^4} \int_0^L z(x)^4 dx$$ Formula 4 R_{ku} Kurtosis

Kurtosis (Formula 4) measures the peakness or sharpness of the surface height distribution, characterizing the spread of the height distributions. Surfaces with high kurtosis tend to have a peak near the mean. Figure 14 shows the relationship between some different skewness and kurtosis values. In Figure 15 relationship between surface profiles and skewness and kurtosis values are illustrated.

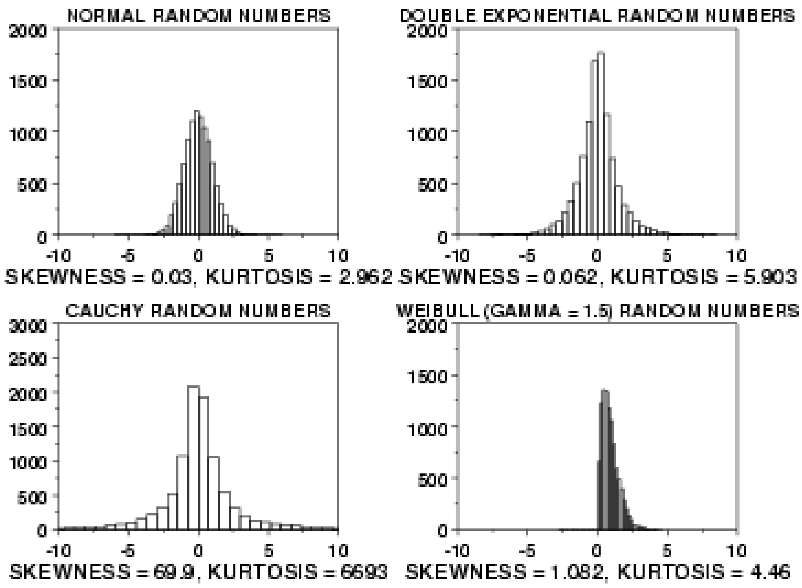

Figure 14 Distributions of different data sampling and the relationship between kurtosis and skewness (NIST, 2013)

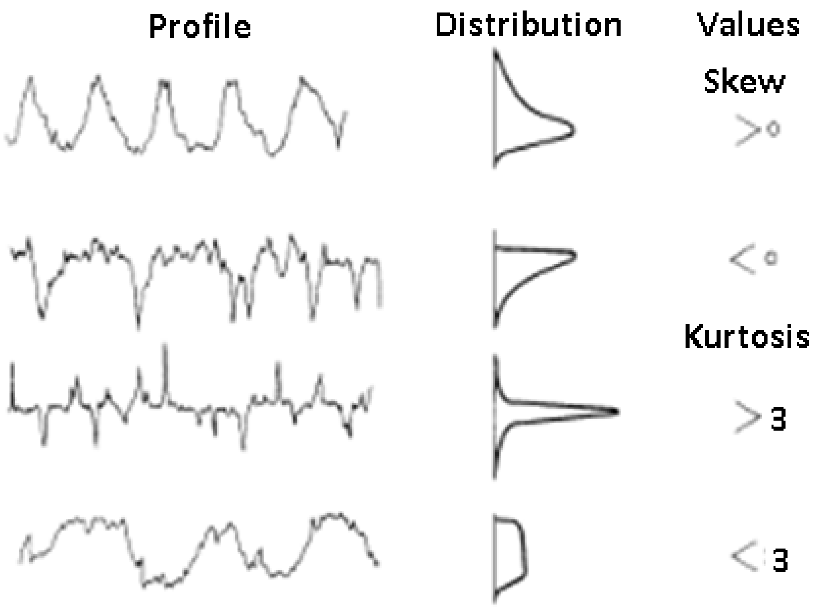

Figure 15 Profiles and their associated height distribution showing the effect of skewness and kurtosis (Thomas, 1981).

2.3.3 Surface roughness and friction/abrasion

The previous sections have given an overview of some ways to measure and characterize roughness. This section includes a short review of publications and papers where wear /abrasion due to roughness and or friction have been evaluated. Since it is the general correlation that is of greatest interest, other materials than just concrete has been included.

In "Influence of surface preparation on roughness parameters, friction and wear"(Sedlaeck et al., 2006) steel specimens were given different initial surface roughness by using different types of finishing methods. Abrasion was found to be the main wear mechanism regardless of the initial surface preparation. Increased roughness increased the sliding distance to reach a steady-state abrasion. It was also observed that sliding velocity did not have any influence on the coefficient of friction, except on the roughest surfaces where higher sliding velocity tended to reduce friction and wear. For specimens with low S_a it was observed that a high S_{ku} gave lower friction. This effect was reduced by increased sliding velocity. Low S_{sk} and high S_{ku} gave the lowest friction at low velocities and the more negative the S_{sk} the lower the friction was observed to be.

(Mitjan, et al., 2002) was a study undertaken to evaluate surface roughness impact on abrasive wear of hydroxyapatite (simulating tooth enamel). Grinding was used to produce different surface roughness. In general the wear volume increased with increased R_a. Results is presented graphically in Figure 16.

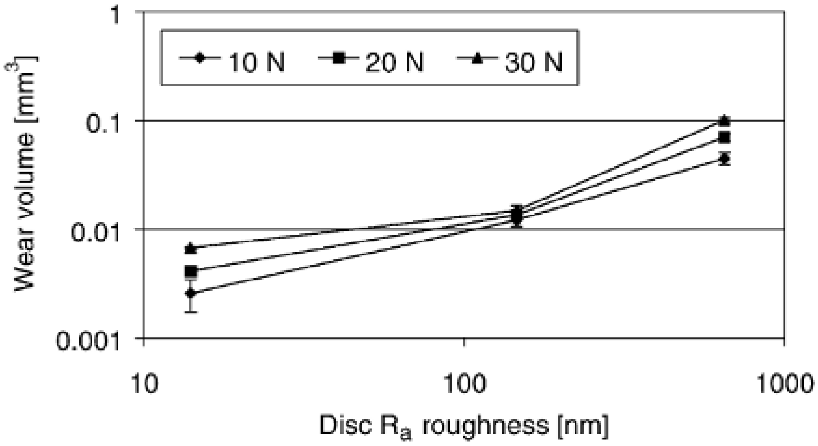

Figure 16 Wear volume of Hydroproxite for different R_a values (Mitjan, et al., 2002)

In "Wear characterization and degradation mechanisms of a concrete surface under ice friction "(Fiorio, 2004) it was focused on the small scale effect of friction induced wear of concrete due to ice. The paper is a part of a larger study whose objective was to study ice on concrete friction laws and the involved physical mechanisms. Initial roughness of the concrete specimens was controlled by molding, R_a=0.28 mm for rough profiles and R_a=0,11 mm for smooth surfaces. Figure 17 shows typical geometry of the surface of the smooth and rough concrete plates.

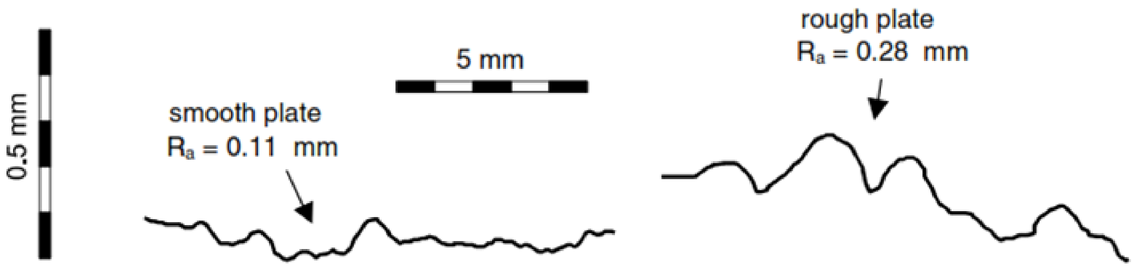

Figure 17 Typical geometry of the surface of the smooth and rough concrete plates (Fiorio, 2004)

Fresh water, columnar and deionized ice was used in the testing procedures. Concrete wear appeared to be a result of two general phenomena. A gradual and uniformly distributed general wear and a much faster time and space localized catastrophic wear. General wear corresponded to erosion of cement paste and small aggregate particles as a result of the friction from the ice moving against the concrete. Catastrophic wear is a result of general wear creating a weakened bond between paste and aggregate making the aggregate fall out, the same principal is also described by (Huovinen, 1990). Figure 18 illustrates general and catastrophic wear.

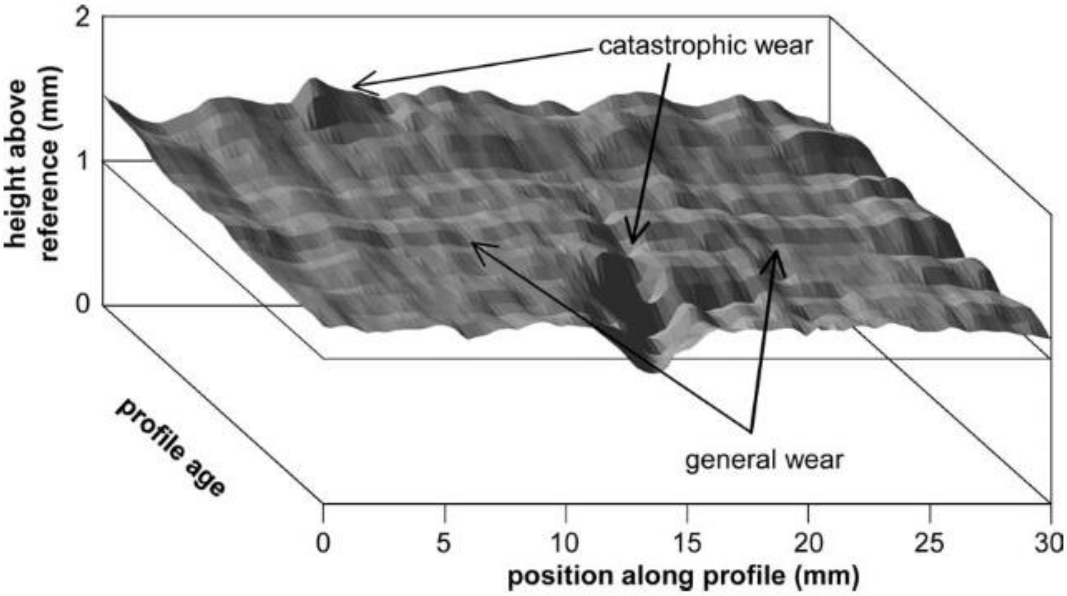

Figure 18 Graphic illustration of catastrophic and general wear (Fiorio, 2004)

Abrasion was divided in two stages. One initial stage were superficial layers of cement is abraded, characterized by a high and roughness depended abrasion rate. The permanent stage was characterized by a lower mean, and maximum, abrasion compared to the initial stage. It was also found that the rate of abrasion in the permanent state didn't depend on the initial roughness of the concrete plate. Findings are illustrated in Figure 19.

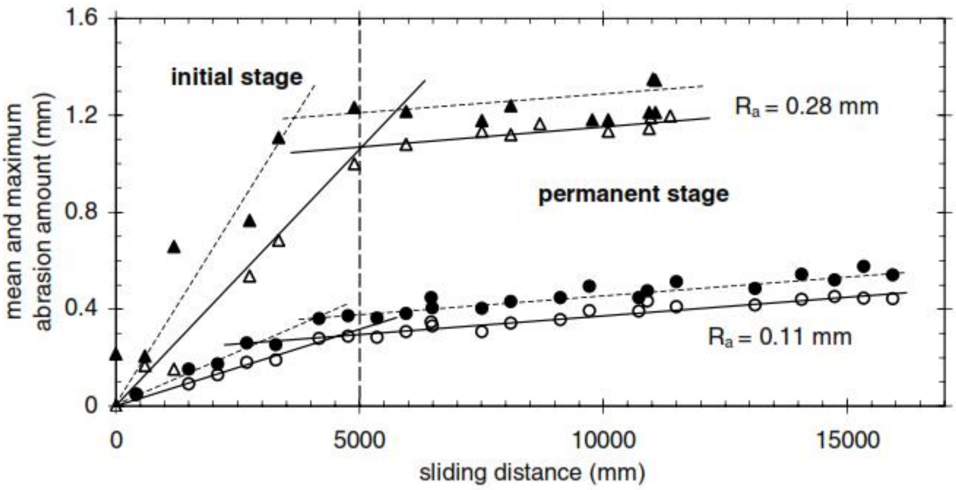

Figure 19 Abrasion for different R_a as a function of sliding distance (Fiorio, 2004)

As seen on the picture the rate of abrasion is much higher for the rougher (R_a) surfaces compared to the smooth one in the initial stage. In the permanent stage this effect seems to disappear and the rates of abrasion are almost the same.

2.4 Bond strength of concrete

Offshore concrete structures offer challenges in regard to repair and maintenance. It is complicated, expensive, time consuming and possibly dangerous work. When maintenance or repair is required, it is therefore important that performed improvements protect the structure for the remainder of its life time. For ice abrasion repair and/or protection, abrasion resistance of the repair products is important. However, also the bond between the substrate concrete and the repair product can easily become a weak link, and for a repair to be successful it is important to achieve sufficient bond strength between substrate concrete and the chosen repair product.

Bond properties are mainly influenced by boundary properties and surface roughness/friction. For the substrate concrete, surface roughness and general material properties are important. For repair products casted on the existing (substrate) concrete it is mainly the material parameters deciding the bond strength.
Good curing conditions and pretreatments like sandblasting (Júlio, et al., 2004) of the substrate concrete are measures that generally are assumed to improve bond/adhesion (Garbacz, et al., 2006). For concrete casted on old a substrate concrete, some of the most important parameters are low water to cement ratio and addition of silica fume (SF), which also ordinarily improves the strength. In (Morgan, 1996) it is showed that 7% SF increase the bond strength with 15-20% depending on type of measurement. This study also shows that a rough substrate concrete improves bond strength with approximately 9 % compared to a smooth surface. Table 2 shows how the relationship between different parameters in the repair mortar (R) and substrate concrete(C) should be to achieve good bond strength.

Table 2 Relationship between properties of substrate concrete (S) and repair product (R) for bond strength (Morgan, 1996)

Property	**Relationship of repair mortar (*R*) to concrete substrate (C)**
Strength in compressive, tension and flexure	$R \geq C$
Modulus in compressive, tension and flexure	$R \approx C$
Poisson's Ratio	Dependent on modulus and type of repair
Coefficient of thermal expansion	$R \approx C$
Adhesion intension and shear	$R \geq C$
Curing and long term shrinking	$R \geq C$
Strain capacity	$R \geq C$
Creep	Dependent on whether creep causes desirable or undesirable effects
Fatigue performance	$R \geq C$

As showed in Table 3 both tensile and compressive strength should be higher for the repair product than for the substrate concrete. Repair products should have better fatigue properties, and thermal expansion should be equal. Bond coatings are also a possible measure to improve adhesion, but in (Garbacz, et al., 2006) there is mentioned that some studies recommend to avoid this type of pretreatment because it can create an extra plane of weakness. It could also limit a good interlocking effect between substrate and repair concrete.

2.5 Literature review ice abrasion

In the last decades a number of studies and research project on ice abrasion has been performed, both as laboratory tests, field investigations, field experiments and computer simulations. In many of these studies the purpose has been to identify which parameters to include and create models to explain and predict the ice abrasion of concrete. Table 3 is a summary of some reviewed studies and their observations.

Table 3 Summary of reviewed studies

Study	Findings:	Estimated abrasion
Nawwar and Malhotra (1988)	Increased pressure →increased abrasion. Surface abrasion is larger than the steady state abrasion. Ice growth on concrete surfaces is reducing the abrasion. Observed abrasion rates: 0,03-0,05 mm/km	
Hanada(1996)	Abrasion [mm] is proportional to sliding distance. Minerals with higher strength experienced lower abrasion compared to lower strength minerals.	$S = S_r \cdot \sigma_v \cdot L\,[mm]$ S = Total abrasion depth S_r = Abrasion rate of material [mm/km/MPa] σ_v = Contact pressure [MPa] L= Relative abrasion distance
Hara (1995a, 1995c)	Almost equivalent and constant abrasion for sea and fresh water ice T>-10 °C. At lower temperatures the abrasion increased more with sea ice. Relation between increased pressure and abrasion. Sand particles in the ice increases abrasion.	$S = 0.0012 \cdot \sigma_v\,[mm/km]$ $[0 < T[°C] \geq -10]$ σ_v = Contact pressure
Itoh (1995, 1994)	3 phases with decreasing abrasion towards a stable steady state region. Increased pressure and reduced temperature increased the abrasion. Sea ice gives larger increase in abrasion rate T≤ 10 °C compared to fresh water ice. Ice with sand particles gives increased abrasion. Increased sliding speed reduced friction and abrasion. Abrasion is proportional to ice sliding distance.	$S_r = p(9.708T2 + 129.57) \cdot 10^{-6}\,[mm/km]$ (for sea ice) p = Contact pressure T = Ice temperature
Janson (1989b, 1988a)	Ice conditions are more important than concrete strength. Lightweight aggregate concrete has lower abrasion resistance than ordinary concrete. Largest abrasion on the sides parallel to the direction of ice movement.	$S_r = \int 0.0015 \cdot v \cdot s \cdot dt\ mm/år$ v = Ice speed s = Ice thickness t = Days of exposure
Kim (2012)	Increased pressure →increased abrasion. Increased abrasion with increasing temperature.	
Huovinen (1990, 1993)	Increased compressive strength and a low water-cement ratio gives increased abrasion resistance. Silica fume and blast furnace slag increased abrasion resistance. Increased aggregate size → increased abrasion resistance.	$ABR = \sum a_i \frac{\lg n_s}{\lg n_i} \cdot R_i + (1 - \sum a_i) \cdot b$ and $b = \frac{3}{f_c} \cdot s$ a_i = The proportional amount aggregate with radius i n_s = number of ice impacts during ice sheet movement n_i =Number of ice impacts when L/R = 1 b = abration rate of cement paste [mm] L = Crack length[mm] R = Aggregate radius[mm] s = Ice sliding distance [km] f_c= Concrete compressive strength [MPa]

Different studies and methods have given partly contradicting results, indicating that there still are some uncertainties when it comes to understanding ice abrasion. This part of the report contains a presentation of laboratory test methods and their strengths and weaknesses followed a summary of how different parameters are found to affect ice abrasion of concrete.

2.5.1 Test methods and equipment

This section is a review of the development of different laboratory test methods and is based on Hara et al. (1995). In the report, which to a large extent describes the development of testing equipment for ice abrasion, Hara et.al has defined which parameters testing equipment should be able simulate. Based on these parameters it has been evaluated how the results from different methods can be expected to represent realistic abrasion conditions. According to the report the parameters in Table 4 should be fulfilled in order to classify a test method as good.

Table 4 list of parameters with demands for ice abrasion test methods (Hara, et al., 1995)

Demands to test methods	
1.	Allowing the use of different ice temperatures
2.	Average ice pressure should be possible to change, and held constant.
3.	Sliding speed must be variable
4.	Both static and kinetic friction has to be accounted for
5.	An easy and simple method of measuring abrasion should be used
6.	Measures to prevent frictional heat and ice melting has to be taken
7.	Ice and abraded concrete on the surface should be removed from the surface
8.	The obtained results must be able to say something about the actual abrasion and possible to use to evaluate measures to avoid or reduce abrasion
9.	Result can be used as a representative material index, characterizing the abrasion resistance for the tested material.

Test methods were divided into four groups based on the principle the methods is developed from: «Relative abrasion test», «revolving disc test», «tumbler abrasion test » and «sliding contact abrasion test».

The *Relative abrasion test*, (RAT) was a test method developed by ABAM Inc. in cooperation with other companies. The main principle of this method is that a circular concrete specimen is rotated between to ice blocks. Figure 20 shows a principle sketch of the RAT. In (Hara, et al., 1995) the following weakness of this method is mentioned:

1) Only kinetic friction occurs because the cylinder only rotates in one direction with a constant speed.
2) Rotation speed is to large compared to actual ice speed.
3) Frictional heat is melting the ice and leads «adfreeze» on the concrete surface, creating a protective ice film.
4) Contact surface between concrete and ice increases during testing. This is not accounted for, and the test equipment is therefore unable to keep a constant pressure.

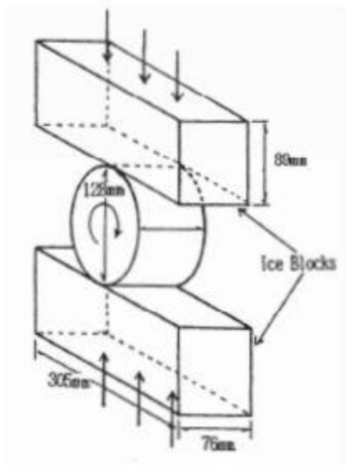

Figure 20 Relative abrasion test (Hara, et al., 1995)

Revolving disc test (RDT), illustrated in Figure 21 was the second phase of the project where the relative abrasion test was developed. A hollow concrete cylinder with an outer diameter of 300 mm and internal diameter of 190 mm and height of 100 mm is placed on a disc rotating with a speed of 60 RPM. Then an ice sheet is pressed against the concrete surface.

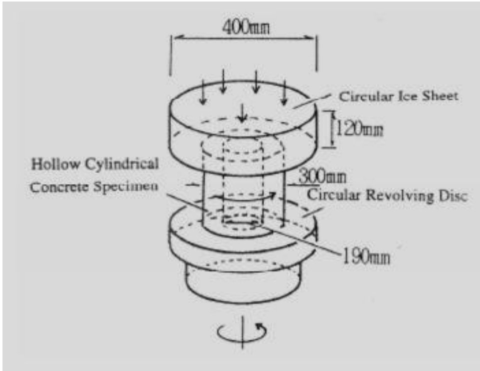

Figure 21Revolving disc test (Hara, et al., 1995)

Mentioned weakness with this method:

- Only kinetic friction due to one way rotation.
- Variations in relative speed over the concrete section
- No measures to avoid adfreeze on the concrete surface.

There also exist other test methods based on this principle, named revolving disc test II and III that are mentioned in the report (Hara, et al., 1995). However, none of these are intended for ice abrasion and is therefore not described further in this report.

Like RDT and RAT the *tumbler abrasion test* was developed by ABAM. Fresh water ice is put into a cylinder shaped container. Concrete specimens are mounted on the inside of the cylinder and the container is rotated. This method does not give any information about contact pressure, ice speed or accumulated distance of abrasion and was therefore found useless as a laboratory test method. Figure 22 shows the principal of the method.

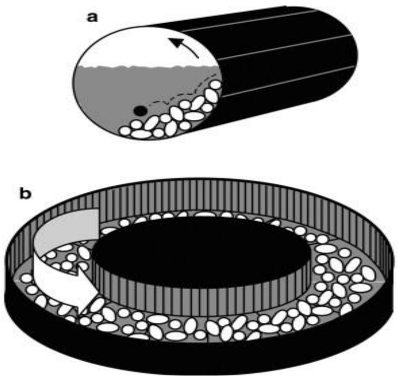

Figure 22 Tumbler abrasion test. (Hara, et al., 1995)

Sliding contact abrasion test (Sliding test 1) also has its origin in ABAM. The principle for this method is to move the concrete relative to the ice. A cylinder shaped concrete specimen is placed on an ice block and put under constant pressure. The test specimen is then put into a pendulum motion. A principle sketch can be seen in Figure 23 . According to (Hara, et al., 1995) this method represented the actual abrasion better than the previously described methods. However a number of weaknesses were pointed out:

- At high contact pressure the concrete penetrates the ice. Creating a “bulldozer” force, cutting the ice.
- The pendulum motion gives different relative velocity and therefore also variations of the surface abrasion.
- There are no points on the surface that can be used as reference points to measure the abrasion since the whole surface is in contact with the ice. Good abrasion measurements is therefore difficult to obtain
- Cold air is pulled in when the pendulum motion is reversed and this area is cooled down, increasing the risk of ad-freeze.

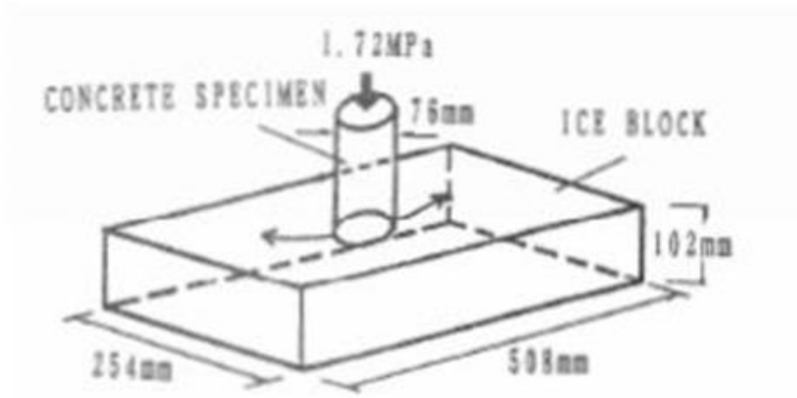

Figure 23 Sliding test 1(Hara, et al., 1995)

Saeki et al. developed their own version of the sliding test method (Sliding test 2). A concrete specimen with a trapezium shaped section was moved horizontally over the ice. As seen in Figure 24, concrete section was wider than the ice making it possible to use the unabraded zone as reference when measuring the abrasion. Unlike other test methods there was not found any large weaknesses to this method except for the risk of the ice block cracking due to fatigue, demanding huge amounts of ice.

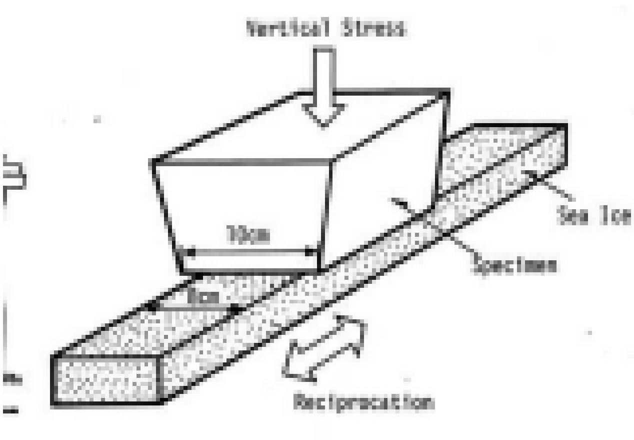

Figure 24 Sliding test 2 (Hara et al., 1995b)

In the report (Hara, et al., 1995), the described test methods are evaluated in respect to the requirements an ice abrasion test method should fulfill, see Table 4 at page 22. The methods were then given grades from A-C:

A: Excellent for ice abrasion testing
B: Results can be used as an indication to measure the relative abrasion resistance.
C: Not suited for ice abrasion testing

The numbers 1-9 in Table 5 refers to Table 4 containing the suggestions to which parameters to be included in ice abrasion test methods.

Table 5 Evaluation of ice abrasion test methods. O =Satisfying, Δ = partly satisfying, X = Not satisfying. (Hara, et al., 1995)

	Nr:	**(1)**	**(2)**	**(3)**	**(4)**	**(5)**	**(6)**	**(7)**	**(8)**	**(9)**	**Evaluation**
Relative abrasion test		O	X	O	X	Δ	X	O	Δ	O	B
	(1)	O	Δ	Δ	X	Δ	X	X	Δ	O	B
Revolving disc test	(2)	O	?	?	X	O	X	Δ	Δ	O	B
	(3)	O	X	X	X	Δ	X	X	X	Δ	C
Tumbler abrasion test		O	X	X	Δ	X	X	X	X	O	C
Sliding contact test	(1)	O	Δ	Δ	O	O	O	Δ	O	O	A
	(2)	O	O	O	O	O	O	O	O	O	A

Sliding contact test 2 was concluded to be the most optimized test. By using this test method important parameters such as sliding speed, contact pressure and temperature can be controlled at the same time as it is fairly easy to measure the abrasion.

2.5.2 Review of Ice Abrasion Studies

There has been performed laboratory experiments, field studies and fields investigations on ice abrasion in many different studies all over the world. In this section the research summarized in Table 3 is reviewed. First there is a short description of the papers/studies followed by a presentation of different parameters influencing ice abrasion.

In the report “Development of a test method to determine the resistance of concrete to Ice abrasion and/or impact” (Nawwar and Malhotra, 1988) the development of testing equipment to estimate ice abrasion resistance of concrete is described. The method falls into the relative abrasion test category. To avoid surface ice growth the concrete specimen was lowered half way down in a salt water solution. Used ice had a salinity of 3-5 ppm.

In the papers “Estimation Method for abrasion of concrete structures due to sea ice movement” and “The mechanism of the abrasion of concrete due to the movement of sea ice sheets” (Itoh et al., 1994, Itoh et al., 1995) experiments were used to study the abrasion mechanism of concrete and a method to estimate ice abrasion of concrete is proposed. Normal density and lightweight concretes were tested in a sliding contact machine

In the report “Abrasion rate of various materials due the movement of Ice Sheets” (Hanada et al., 1996) abrasion rate for different materials was investigated and is included to set ice abrasion of concrete in relation to other materials. A constant temperature of -10° C was used to reduce possible differences to if the ice is made of sea- or freshwater ice.

In the report “Prediction of the degree of abrasion of bridge piers by fresh water ice and the protective measures” (Hara et al., 1995a), ice abrasion was studied in experiments, field investigations and field studies.

In the two reports ”Long term resistance of concrete offshore structures in Ice Environment” and “Results from the winter season 1988-1989, conclusion after three winters 1986 -1989” (Janson, 1988b, Janson, 1989a) ice abrasion was studied. The reports describe results from field investigations of lighthouses and field experiments in the Golf Bothina.

“Abrasion of concrete by Ice in Arctic Sea Structures”(Huovinen, 1990) is the PhD thesis of Huovinen where field studies, field experiments, laboratory experiments and computer simulations were used to study ice abrasion. In the laboratory a mechanical cutter was used to test the abrasion for different types of concrete and field experiments were performed by mounting concrete specimens on an ice breaker which, while sailing, exposed concrete to 40 km of ice sliding.

The reviewed literature gives no definitive answer to which extent the different parameters contribute to the ice abrasion of concrete.

According to observations by Itoh et.al (1994), ice abrasion can be divided there stages. Figure 25 shows the relation between sliding distance and mean abrasion depth for the different stages.

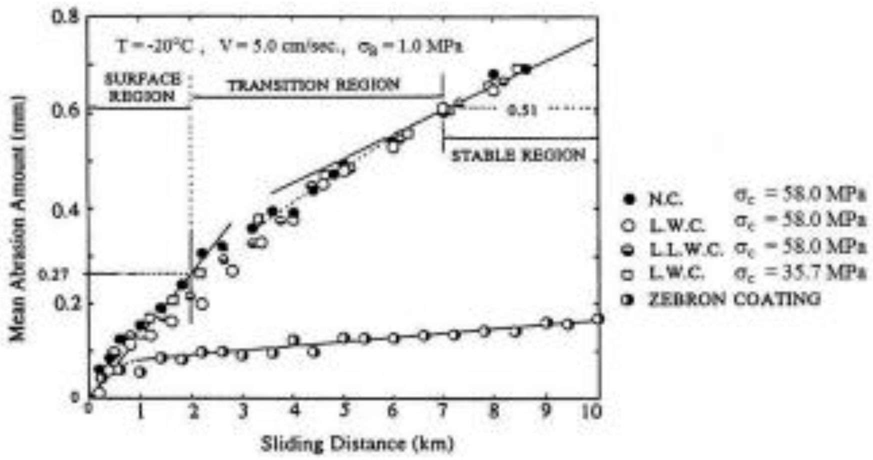

Figure 25 Average abrasion [mm] for tested concretes plotted against sliding distance (Itoh, et al., 1994)

The stages were named "surface region", "transition region" and "stable region". In the surface region only cement paste was visible and the rate of abrasion was measured to 0,137 mm/km. In the transition zone, aggregate started to be visible on the surface and rate of abrasion decreased to 0,07 mm/km. The reduction in abrasion rate continued as more aggregate became visible until it stabilized at a rate of 0,05 mm/km in the "stable region". Observations were verified by cutting of 6-10 mm of the concrete surface, leaving an aggregate exposure of 45-60% on the surface. Observed abrasion rates were equal to the rates in the stable region of the initial experiments and are illustrated in Figure 26.

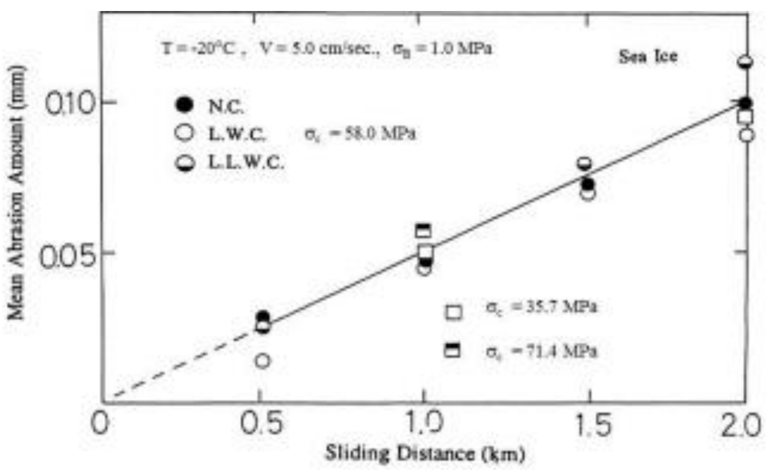

Figure 26 Abrasion of cut surface (Itoh, et al., 1994)

Other reviewed studies seem to agree on a linear relation between abrasion and sliding distance.

Reviewed literature also seems to agree on a close relationship between abrasion and contact pressure. Figure 27 from Itoh et al. (1994) indicates a linear relationship between increased contact pressure and abrasion rate. Observations in (Nawwar, et al., 1988) and (Hara, et al., 1995) supports this theory.

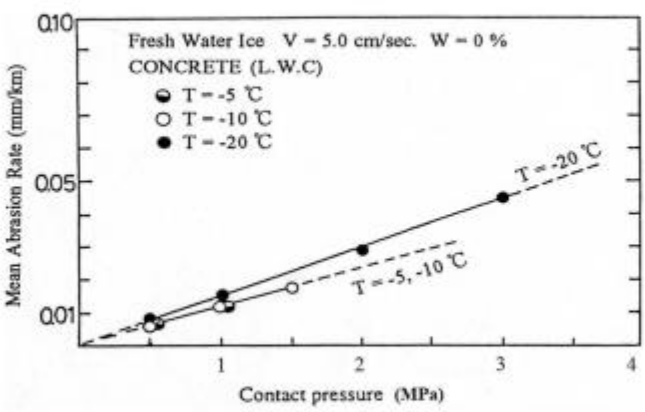

Figure 27 Abrasion rate for increased contact pressure (Itoh et al., 1994)

The effect of temperature on sea- and freshwater ice, and its effect on ice abrasion is also a fairly thoroughly investigated parameter. Results from both Itoh et.al and Hara et.al indicates that abrasion rate for seawater- and freshwater ice are almost the same for T>-10 ° C. For lower temperatures separation of chlorides participates to increase the abrasion from seawater ice compared to freshwater ice. Figure 28 from (Itoh et al., 1994) shows the observed relationship between ice temperature and abrasion rate. Abrasion rate for sea ice was found to more or less constant for temperatures > -10° C. For temperatures below -10° C abrasion rates increased considerably. In addition to Hara and Itoh, also Janson reports about increased abrasion for reduced temperatures. Adding sand particles in the ice is also found to increase abrasion.

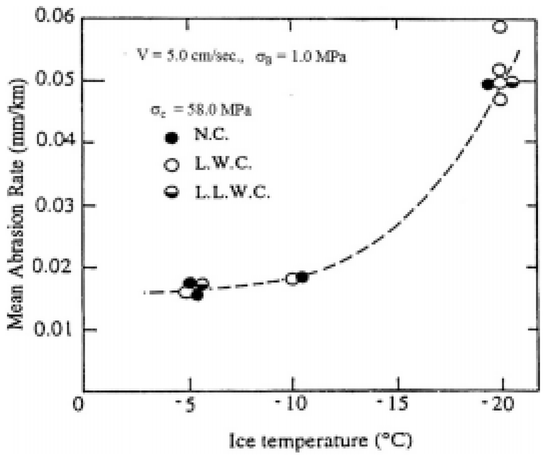

Figure 28 Abrasion rate for changing temperatures (Itoh et al., 1994). Sea ice

(Kim et al., 2012) is the only of the reviewed papers with a different observation. As seen in Figure 29 abrasion is highest at -5°C and lower at -10°C and -20°C. .

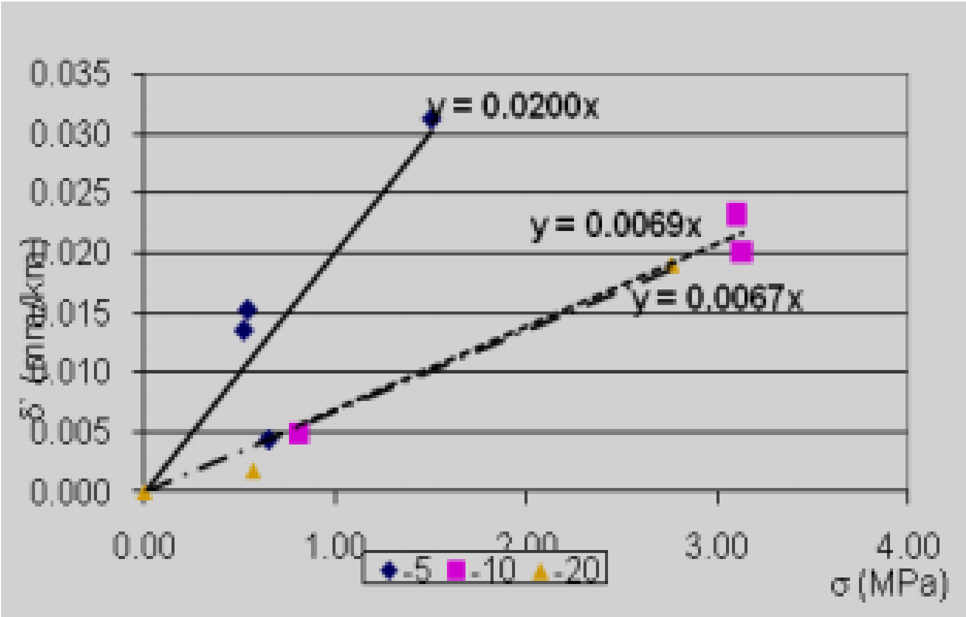

Figure 29 Abrasion rate for different temperatures (Kim et al., 2012)

Comment: As showed in Figure 29 abrasion rates are similar for T=-10°C and – 20°C. To explain this is difficult, but it might be because of a protective ice film on the surface, that was not able to form at -5° C. Nawwar and Malhotra (1988) observed that ice growth and a protective ice film on the surface almost removed abrasion completely, as ice was sliding on ice instead of concrete.

Influence of sliding velocity is another investigated parameter. According to (Itoh, et al., 1994) abrasion is reduced by increasing the sliding speed. This effect was found decline for velocities higher than 10 cm/sec.

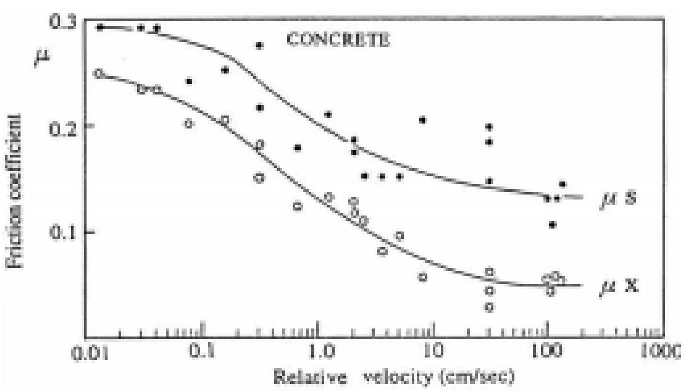

Figure 30 Friction as function of velocity. Increasing friction for low velocities (Itoh, et al., 1994)

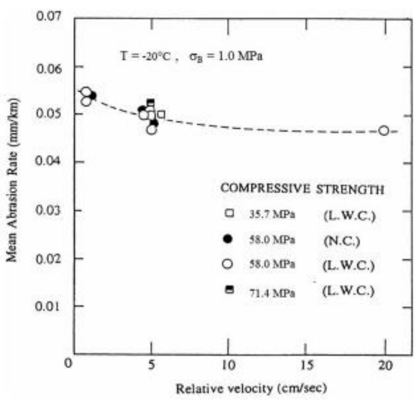

Figure 31 Abrasion as a function of relative velocity (Itoh, et al., 1994)

Figure 30 and Figure 31 shows how friction and abrasion was affected by the sliding velocity. Reduced velocity was found to increase both friction and rate of abrasion. Abrasion rate stabilized when the sliding velocity reached approximately 10 cm/sec. The coefficient friction also seems to stabilize for velocities higher than ≈10 cm/sec.

These results open up for the possibility of using higher sliding velocities in experiments and thus reduce the time of testing. However, results from the project thesis (Kirkhaug, 2012) on which this study is based, indicates that tests performed with the NTNU abrasion rig may encounter different abrasion rates for velocities of 16 cm/sec and 25 cm/sec.

A correlation between direction of movement and abrasion rate was found both by Janson and Hara. They observed increased abrasion on surfaces parallel to the direction of movement compared to surfaces were the ice movement/collision was perpendicular to the surface. This seems reasonable given that the ice gets a more crunching effect sliding along the surface and thus provides greater risk of abrasion.

Compressive strength is an important parameter when it comes to concrete, and is investigated in many of the reviewed papers. Results published in Huovinen, Hanada and Nawwar and Malhotra indicates a correlation between increased compressive strength and increased abrasion resistance. Hanada did not examine concrete strength specifically, but studies of different materials indicate that increasing strength also increases the abrasion resistance. Observed abrasion rates are presented in Table 6. Given the thorough assessments of strength as a parameter by Huovinen, it seems likely that compressive strength is an important parameter. Huovinen collected his findings in an illustration, Figure 32, showing abrasion for the different concrete compressive strengths. Abrasion also increases for lower compressive strengths. Itoh chose to ignore strength as a parameter in his investigations and Janson found it to be an irrelevant parameter. Janson only tested concretes with compressive strength around 40 MPa and his results are therefore only valid for concretes with equivalent strength. Reduced abrasion for higher compressive strength is also supported by findings in studies of general concrete abrasion (Dhir et al., 1991, Sonebi and Khayat, 2001).

Table 6 Abrasion rate of various tested materials Hanada

Materials	**T= -10 °C, σ=1MPa Abrasion rate (mm/km) for Sea ice**
Concrete	0.0178
Steel	0.0030
Polyurethane	0.0030
Zebron	0.0078
LPDE	0.0022
Sandstone	0.0049
Tuff	0.0251
Pyroxeneandesite	0.0084
Dacite A	0.0065
Dacite B	0.0177
Granite	0.0216

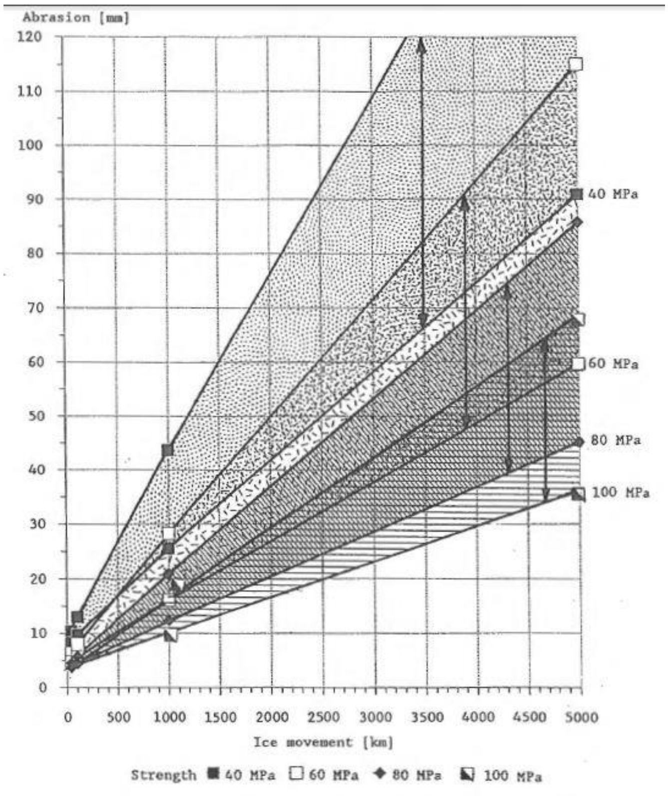

Figure 32 Abrasion of concrete with different compressive strengths (Huovinen, 1990)

Density and additives like blast furnace slag and silica fume are parameters found to have an effect on the abrasion resistance of concrete. Huovinens research indicates that addition of silica fume and blast furnace slag in the concrete improved the abrasion resistance. Lightweight concrete was also found to be more abraded compared to normal density concrete. Janson also found some correlation between increased abrasions of lightweight concrete compared to normal weight concrete. This indicates that although the strength of concrete is important also density of concrete should be considered. This is also supported by general abrasion tests described in (Sonebi and Khayat, 2001). Table 7 and Table 8 shows observed abrasion for different types of concrete.

Table 7 Abrasion for different types of concrete (Huovinen, 1990)

No	Material	f_c	w/b	Exposure	Abrasion
1	**ND Concrete**	**60**	**0,27**		**6,2**
2	**ND Concrete**	**60**	**0,28**		**5,4**
3	**ND Concrete**	**60**	**0,31**		**9,3**
4	**ND Concrete**	**40**	**0,41**		**10,8**
5	**ND Concrete**	**40**	**0,36**		**9,1**
6	**ND + Silica Concrete**	**60**	**0,31**	**Freeze – thaw (50 cycles)**	**2,6**
7	**ND + Silica Concrete**	**60**	**0,31**	**+ abrasion (mechanical)**	**4,8**
8	**LW Concrete**	**30**	**0,35**		**11,2**
9	**LW Concrete**	**30**	**0,35**		**11,5**
10	**ND Slag Concrete**	**60**	**0.29**		**4,5**
11	**ND Slag Concrete**	**60**	**0,29**		**7,1**

A concrete with silica fume will thus have more positive effects in repair products as it also improves adhesion.

Aggregate diameter also seems to be of importance. Huovinen found that reduced aggregate diameter reduced the abrasion resistance (Huovinen, 1990). An increase of the maximum size of aggregate has also shown to increase the compressive strength (Meddah et al., 2010).

Table 8 Abrasion results Ice breaker study (Huovinen, 1990)

Concrete	Compressive strength	Maximum abrasion[mm]	Mean abrasion [mm]
Light-weight concrete	30	30	15
Ordinary cement concrete	50	8.5	3.5
Blast furnace cement concrete	60	7	2

In other words the abrasion resistance of concrete depends on several parameters and it is difficult to predict the abrasion resistance to a specific concrete without doing some sort of testing. The results from the studies and experiments in this literature review shows that an abrasion rate in the range of $x*10^{-2}$ [mm/km] is too be expected. In the experimental part of this study, these parameters, together with roughness and friction are used to evaluate ice abrasion of concrete.

3 Experiments and research plan

This chapter describes the tested materials, test conditions, test equipment and how measurements and calculations have been performed, both for ice abrasion- and bond tests.

3.1 Materials

Tested products of this master thesis and the project thesis last semester are:

- Densit Wearflex 2000 (repair mortar) (Densit)
- Reforcetech (repair mortar)
- B60 reference concrete (B60)
- B70 reference concrete (B70)
- Rockbond (repair mortar)
- Polyurethane (rigid epoxy)
- MapeCoat CFS (elastic epoxy)

All three repair mortars are commercially available products which are supposed to be strong and durable. It has chosen to test these products as they are considered being used for repair of ice abrasion damaged structures in the future. The concretes are standard concretes proportioned to fulfill standard requirements. The two tested epoxies are Mapei products, and included to measure abrasion rate and behavior of coatings.

Densit is a high-strength and dense cement-based mortar which is supposed to provide high protection against wear. It has a high compressive- and flexural strength (150 MPa/20 MPa). The average particle size is low, and the density is 2850 kg/m^3.

The Reforcetech mortar is a high strength mortar with addition of basalt fiber composite reinforcement. Basalt fibers are corrosion free and have low density in addition to high tensile strength. Density of the tested product is 2640 kg/m^3.

Rockbond is a mortar made from a premixed, ready to use, cementitious powder. The compound contains stainless steel fibers and a combination of admixtures. The compressive strength is only 51 MPa, but the steel fibers are increasing the flexural strength considerably, 91 % increase in flexural strength at 30% fiber content by weight of cement (Cox, 2012).

The B70 concrete is reference concrete designed according to ISO 19906, Clause A.12.4.1.4.2, "Abrasion Tests" and is a part of the test program as it is supposed to have acceptable abrasion properties (Kværner Engineering, 2012). The B70 concrete is therefore used as a reference to evaluate the properties of the other products. Volume fraction 0/8 mm and 8/16 is 48/52 %.

The B60 concrete is a typical reference for concrete on offshore structures. This concrete represents a typical concrete of already built offshore structures. The abrasion resistance of the repair products should therefore be better than the B60. B60 is also used as substrate concrete for bond tests to get an indication on how the repair mortars will bond to existing structures. Volume fraction 0/8 mm and 8/16 is 49/51 %.

MapeCoat CFS from Mapei is a flexible epoxy for use as a coating. It has been applied on a sandblasted substrate concrete.

Polyurethane is a self-leveling polyurethane coating, which is supposed to be suited for use on surfaces exposed to high mechanical wear. The coating used in this study is a Mapei product.

3.2 Ice abrasion Experimental Equipment and Procedures

In this section there is first a description of test conditions and ice abrasion test procedures. Then there is a description of equipment used for ice abrasion testing.

3.2.1 Ice Abrasion Test Conditions and Procedures

As previously described, the main purpose is to evaluate abrasion resistance. In total there are performed 42 ice abrasion tests. Table 9 shows the setup and test conditions for these tests. A summary of the ice abrasion test procedure is included on page 34, and a more detailed description on how to use and operate the ice abrasion rig can be found in appendix 4.

General test conditions:

- Ice of frozen tap water
- Surface temperature of concrete:≈ 0^{0}C
- Sampling rate: Once each cycle

Table 9 Test setup and conditions. Number of tests for different test conditions and products

Temperature	**-10^{0}C**				
Sliding speed	**16 cm/sec**			**25 cm/sec**	
Contact pressure [MPa]	**1**	**0,5**	**1**	**1**	**1**
Sliding distance	**2500 m**	**2500 m**	**2500 m**	**2500 m**	**7500 m**
Sandblasted surface(Yes/No)	**No**	**No**	**Yes**	**No**	**No**
Reforcetech	2	2	-	2	-
Densit	2	2	2	2	2
Rockbond	2	2	-	2	-
Polyurethane	2	-	-	-	-
MapeCoat	2	-	-	-	-
B70	2	2	-	2	2
B60	2	2	2	2	-
Total	14	10	4	10	4

Summary of ice abrasion test procedure:

1 Make ice
2 Perform pre-abrasion surface measurement
3 Decide test conditions; ice contact pressure, sliding velocity, sliding distance, temperature of ice, laboratory and copper bedding.
Testing:
4 Mount test specimens on the copper bedding and pretension the concrete specimens.
5 Calibrate vertical and horizontal load cells.
6 Insert ice in the ice specimen container.
7 Make sure concrete specimens are located directly under the ice specimen.
8 Make sure there is a gap between ice specimen container and concrete specimen
If not: Loosen the screws holding the ice container and level it so that there is a gap.
9 Hit Run/stop button in Labview.
10 Push the "apply vertical load" button in Labview.
11 The rig now runs automatically to wanted sliding distance is reached or ice has to be changed.
12 The ice abrasion rig is entering maintenance-mode, adjusting horizontal velocity to 400 RPM and the piston is reset to its top vertical position.
13 Stop horizontal movement by hitting the run/stop button.
14 Before removing ice, open the gauge on the heating circulator to the ice container circuit for approximately 30 seconds before closing it again.
15 Use a mallet to give the ice a stroke. This makes the removal faster.
16 Insert new ice.
17 Reset vertical and horizontal velocity.
18 Hit run/stop button and continue testing by performing step 5-17 until wanted distance is reached.
19 Remove concrete specimen from the bedding.
20 Measure abrasion.
21 Obtain log file. Log files should be obtained immediately and archived in a well-organized system for each specimen.

3.2.2 Plane cutting of surfaces

To get a representative aggregate exposure of the test surface, all specimens were grinded/plane cut. If abrasion tests are performed at surfaces cut too close to the original molded surface, the abrasion will be done on a surface where the paste content is higher than on a surface deeper into the concrete body that better reflects the real volume fraction of aggregate. Most of the test specimens, used for the tests in this study, were too high to fit in the ice abrasion rig. The height had to be reduced to avoid contact between the ice specimen container and the concrete specimen. The bottom side was also grinded a little bit to make it parallel to the top side. Uneven specimens can give uneven abrasion over the surface. Grinding/plane cutting was done with the plane cutting equipment seen in Figure 33. A high speed rotating blade is cutting the surface. Horizontal position can be adjusted with a manual handle. One rotation on the handle equals 0,4 mm height change. Densit and Reforcetech specimens were cut up to 2 mm and Rockbond and B70 were cut up to 4 mm. How much the specimens were grinded depended on their initial height and they were grinded so that the gap between surface and ice container was the same for all specimens. Figure 34 shows pictures of typical test surfaces for the different products, where the aggregate/particle exposure can be seen.

Figure 33 Plane cutting device used to plane cut specimens to increase aggregate exposure at the test surface

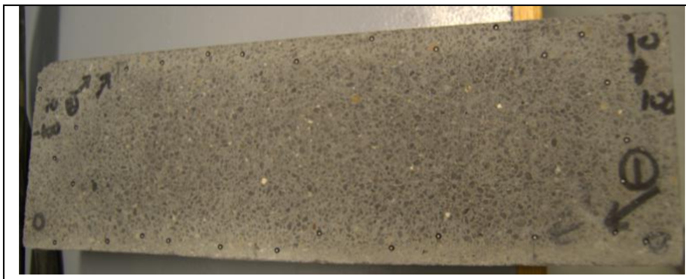	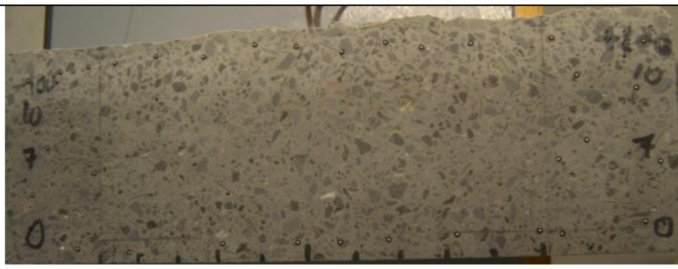
Densit	Reforcetech
	
Rockbond	B70 concrete
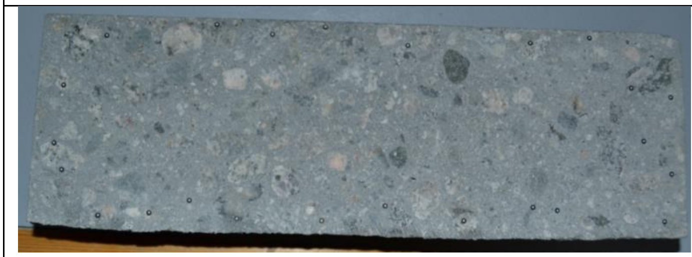	
B60 concrete	Polyurethane (Rigid epoxy)
	
MapeCoat (Elastic epoxy)	

Figure 34 Typical surfaces of tested products after being plane cut, ready for ice abrasion testing

3.2.3 Sandblasting

In order to test the effect of surface roughness, two specimens of Densit and B60 were sandblasted prior to the abrasion testing. Specimens used as substrate for MapeCoat was also sandblasted. Sandblasting is performed manually in the NTNU laboratory. Compressed air, with a pressure of 4 bar, and sand are mixed to roughen the surface.

Figure 35 Sandblasting equipment

Gaffer tape was used as protection to keep area used for reference measurements unaffected of the sandblasting, Figure 36 illustrates this.

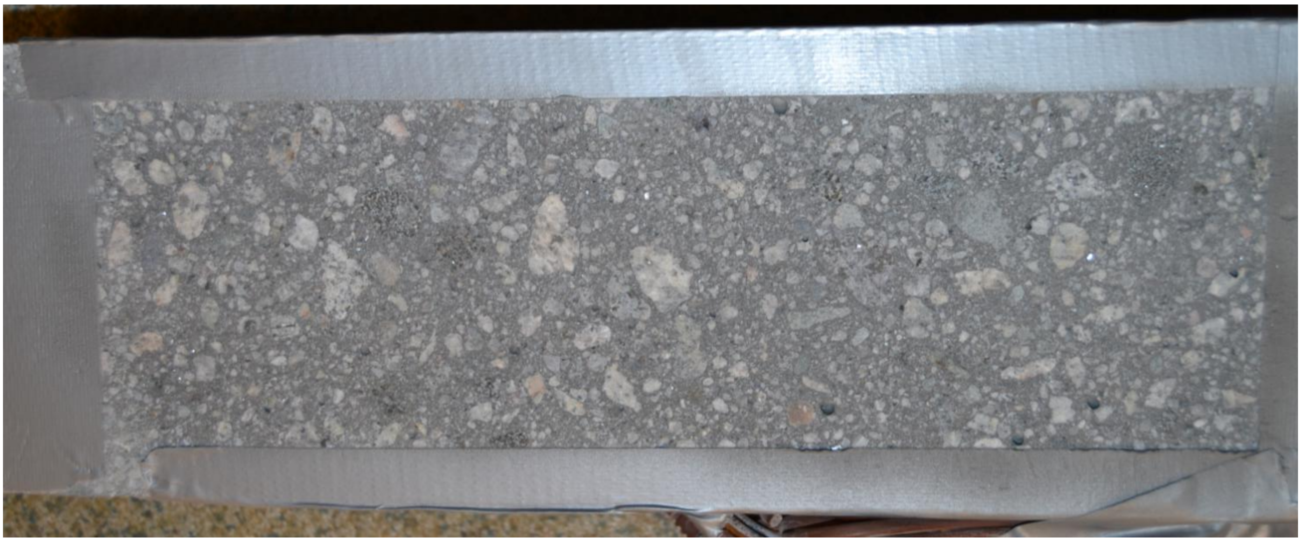

Figure 36 Gaffer tape is used as protection of the reference point zone when sandblasting

3.2.4 Ice Abrasion rig

NTNU has built its own ice abrasion laboratory test rig, and based on (Hara, et al., 1995) it can be classified as a sliding contact type. This section contains a description of the rig and a short description on how to use it. The NTNU ice abrasion rig is not a product purchased in the store with a complete user manual. After performing this study, and experienced what can fail and/or go wrong, there is also included a more detailed description on how to use and maintain the rig in appendix 4. Hopefully future study can reduce chances of unwanted downtime and unforeseen events.

The ice abrasion laboratory test rig is placed in a cold-storage room and consists of three main parts; the ice abrasion rig, a heating circulator and a control unit. Temperature of the storage room is regulated by a refrigerating system, controlled by a *Pego 2000 Expert* control unit, making temperatures as low as -20^{0}C possible.

In the ice abrasion rig, a stationary concrete specimen is placed below the ice specimen container. The ice specimen container is supposed to be ≈ 1-2 mm above the concrete surface to ensure that the ice is the only part in contact with the test surface. The container can be seen in orange in Figure 37. Ice specimens are placed inside the container before testing.

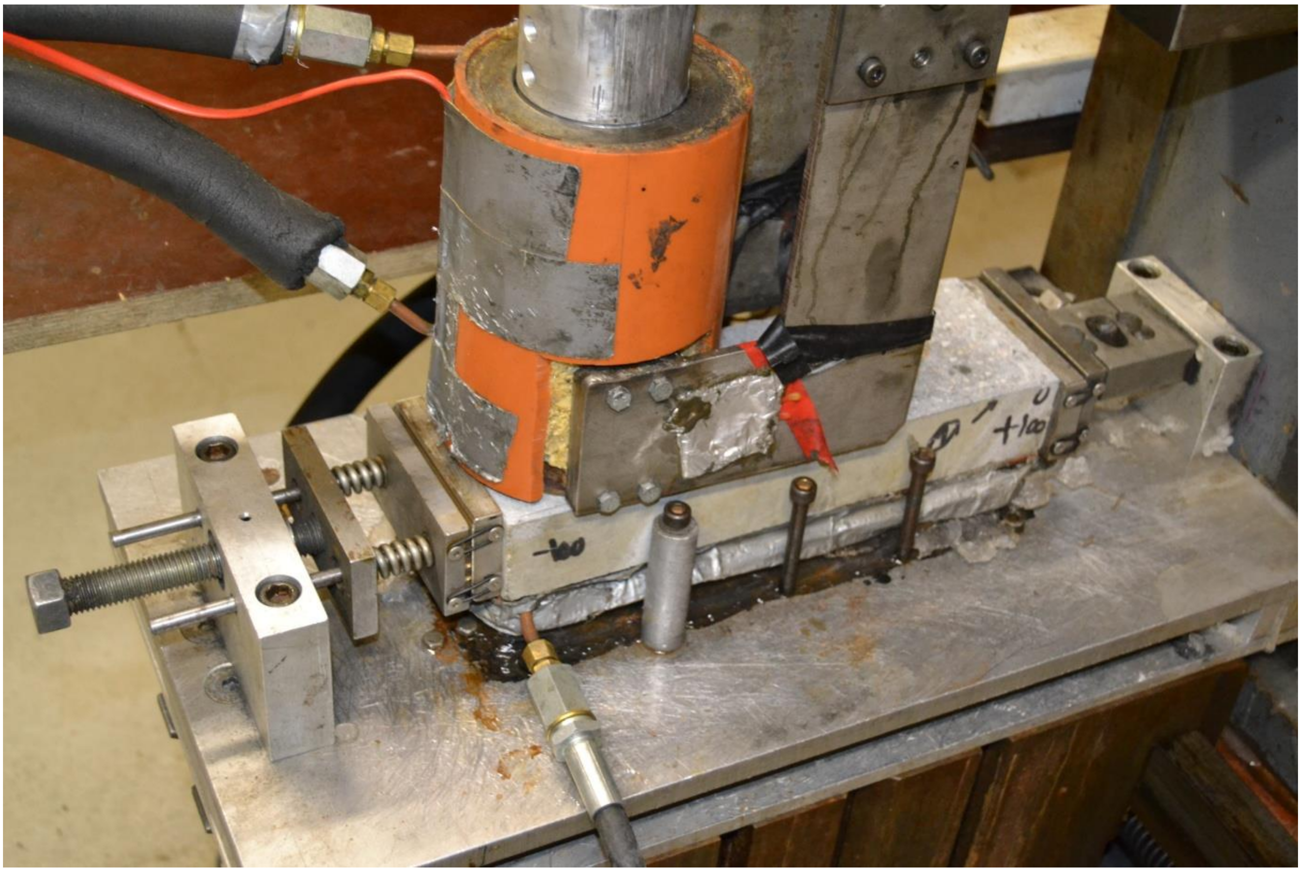

Figure 37 Ice abrasion rig. Ice container located centrically over the concrete specimen to be tested. The screw in the bottom left is used to tension the concrete specimens. The horizontal load cell can be seen on the right side. Illustration.

The rig applies load in [N], and desired contact pressure is calculated by multiplying the surface area of the ice specimen with desired pressure. Surface area of ice specimens are 4299 mm^2. Load is controlled by a piston pushing ice down towards the concrete surface. Two vertical load cells records the load and sends it to a Labview written program on the laboratory computer. Then the Labview program automatically adjusts the vertical position of the piston to obtain and maintain desired load on the concrete surface. Vertical gain and speed ("vertikal turtall") controls how fast the piston is adjusted. All settings are controlled in Labview. For the test in this study vertical speed was set to 600 RPM and vertical gain to 0,02 mm. In Figure 38 the piston can be seen over the orange ice specimen container. On the top, in green, it is possible to get a glimpse of the engine controlling the piston.


Figure 38 The piston which is adjusting the applied load is seen over the orange ice specimen container

A standard horizontal shaping machine with a stroke length of 200 mm is creating the horizontal movement. A stroke length of 200 mm gives a total ice sliding distance of 400 mm for each cycle. When the concrete specimen is placed in the rig, on a copper plate, it has to be tensioned. This is done by tightening the screw seen on the left side of Figure 37. Friction forces (horizontal load) are being registered with a horizontal load cell as seen on the schematic drawing in Figure 41 and in the right edge of Figure 37.

The copper plate is placed on sliding bearings. Both the copper plate and the ice specimen container are connected to the heating circulator (*Julabo 2000*). The circulator uses alcohol as circulating media which will not freeze for the temperatures in the performed experiments. The heating circulator has two purposes. By using concrete specimens with temperature sensors casted inside, it is possible to regulate the temperature on the heating circulator so that freezing of water on the concrete surface is avoided. Freezing is unwanted because it has a protective effect on the concrete, resulting in ice sliding against ice (Nawwar, et al., 1988). In

Figure 39 the copper plate and its connection to the heating circulator can be seen. The heating circulator is seen in Figure 40. For the concretes tested in this study a temperature of $\approx 12^{0}$C was necessary.

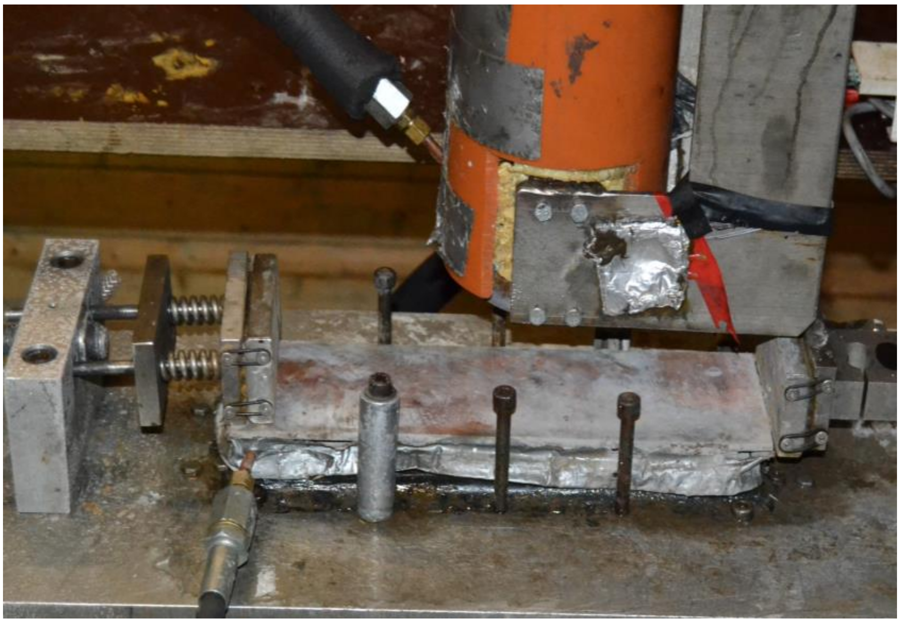

Figure 39 Copper plate. In the left corner the connection to the heating circulator can be seen.

Another useful application for the heating circulator is when changing the ice specimens. By opening the gauge on the circuit connected to the ice container, the ice inside starts to melt making it possible to remove and replace it with a new cylinder. It can also be used to cool down the ice in cases where the tests are performed in high room temperatures. The ice container and the copper plate circuit is connected to the same device, but is connected separately with individual gauges.

Figure 40 Julabo heating circulator

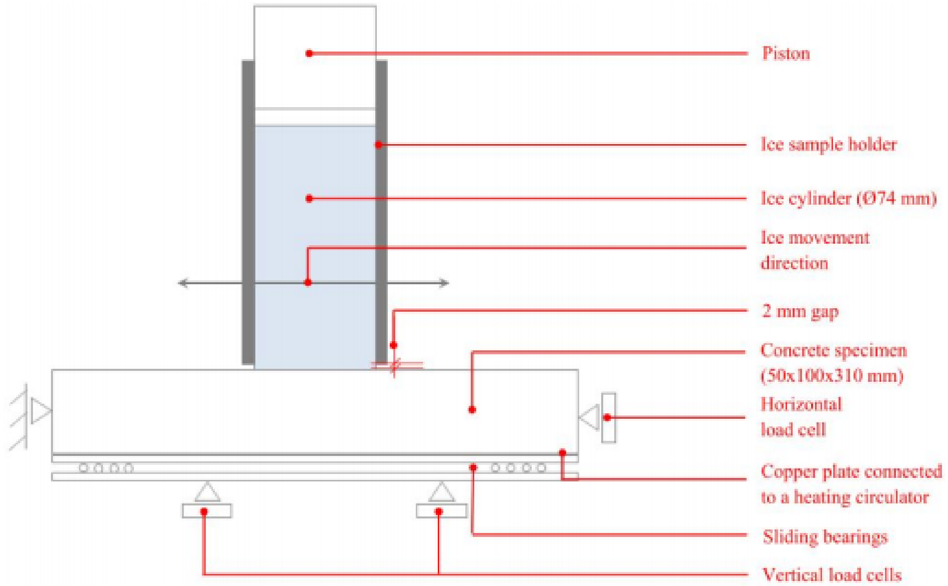

Figure 41 Schematic drawing of ice abrasion rig by Egil Møen (Kværner Engineering, 2012)

In Labview all data from the load cells and temperature sensors are being recorded during testing. Contact pressure, sliding velocity, sampling rate and vertical speed of the contact pressure adjustment are controlled in Labview. Table 10 is a modification of table 4 in (Bøhn, 2012) and shows how parameters are controlled and which data is being logged in Labview.

Table 10 Controllable and logged parameters and variables for ice abrasion testing

Function	Controlled by	Logged by Labview
Horizontal sliding velocity	Labview	Yes
Vertical load (contact pressure)	Labview	Yes
Velocity of vertical pressure adjustment	Labview	Yes
Automatic adjustment to keep constant pressure	Labview	Yes
Automatic stop when ice has to be changed	Labview	Yes
Ambivalent air temperature	Pego refrigerating control unit	Yes
Concrete surface temperature	Julabo 2000	Yes*
Ice cylinder temperature	Julabo 2000/ Room temperature	
Pretension of the concrete specimen	Manual	Yes
Horizontal force, friction	--	Yes
Automatic stop after given ice sliding distance	Labview	Yes
Horizontal position (trace) of the ice cylinder	Labview	Yes

*** If temperature sensors are casted in the concrete specimen**

All logged files from this study are stored in E:\Is-abrasivmaskin\V3\Masteroppgave at the laboratory computer for potential future use.

For sliding velocity, vertical load, horizontal load and friction Labview is recording both average per cycle values and the current value for the horizontal position where the data is being logged. As Labview is also recording time, average sliding velocity is calculated based on the time and sliding distance between two consecutive recordings.

3.3 Ice abrasion specimens

All the concrete and repair mortar specimens, except from Rockbond, have been casted by SINTEF in Trondheim. Rockbond repair mortar specimens are prepared by “Rockbond SCP LTD,UK”. Specimens used in the ice abrasion rig at NTNU are 300*100*50 mm. However, the actual size and shape of the specimens were subject of minor variations. All specimens are casted as individual single piece specimens, except from the B60 specimens (Figure 42) that were casted in double sizes and saw-cut in the NTNU laboratory.

Figure 42 Uncut B60 specimen. Later cut in two to create two specimens for ice abrasion testing

MapeCoat was applied on sandblasted specimens from the same batch of w/c= 0,6 std concrete with air used in the experiments of (Bøhn, 2012).

Polyurethane specimens were made at NTNU a few years back by placing a half cylinder shaped concrete piece in a formwork before polyurethane was casted around the concrete. Figure 43 shows a cross section profile of a polyurethane specimen.

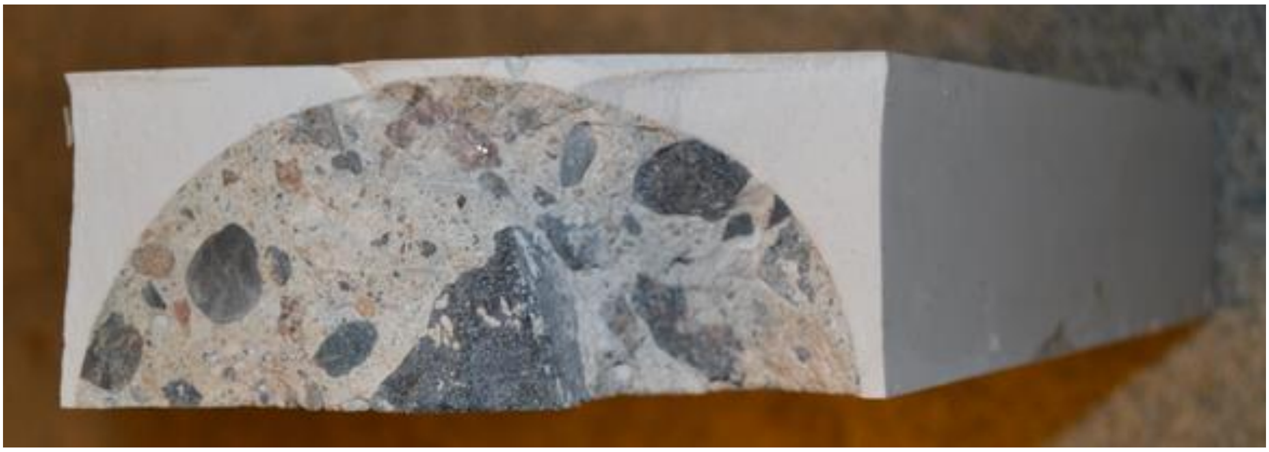

Figure 43 Cross section of Polyurethane specimens. Polyurethane is casted on a half cylinder shaped concrete specimen

All specimens have been freeze-thaw tested. The exposure includes 300 cycles according to ASTM C 666 (-20^{0} C $+20^{0}$C). Due to time limitations, Rockbond specimens were exposed to only 200 cycles before abrasion testing. Remaining cycles is completed afterwards. As previously mentioned all specimens have been grinded/plane cut to remove the surface layer before ice abrasion testing. This to ensure a representative test surface were abrasion should start directly in the steady-state region as described by (Itoh, et al., 1994).

Specimens for ice abrasion testing of Rockbond were casted in two different series. In one series Rockbond were casted on top of a substrate B60 concrete, and in another series specimens were consisting of only Rockbond. One specimen from the batch where Rockbond (Figure 44) was cast on substrate concrete delaminated during the freeze-thaw testing. Therefore specimens consisting of only Rockbond were chosen; this is also believed to reduce the chance of cracking during testing and abrasion the rates should be the same.

Figure 44 Delaminated Rockbond specimen

All specimens were stored in water when not being tested or measured.

3.4 Ice

The NTNU ice abrasion test laboratory uses cylindrical ice specimens with a diameter of 74 mm and height up to ≈ 180 mm. Ice for this study is made of regular tap water in the laboratory. Results from both (Hara et al., 1995c) and (Itoh et al., 1994) found small difference in abrasion from sea ice and fresh water ice for temperatures T>-10C. Ice containing salts could also give unwanted corrosion on the laboratory equipment. Ice cylinders used for these experiments is made by filling plastic cylinders with water and place them in a freezer. After being in the freezer for a minimum 20 hours the plastic cylinder were placed in room temperature for approximately 30 minutes (Figure 45). This made the ice melt enough on the boarder to the plastic so that it could be removed from the cylinder. After being removed, ice was stored in the ice abrasion laboratory (Figure 46).
This method of making ice means that it freezes from all directions at the same time, resulting in what can be classified as granular ice. Another option is to use ice from an ice growth laboratory where water is deionized and the freezing process can be controlled to freeze water from top to bottom. Ice cores can then be drilled out from the ice sheets. This should give a more homogenous and stronger ice.

In order to get some knowledge of the properties of the ice, density was measured by the principal of Archimedes. First the weight of the ice specimen was found. Then the volume was found by submerging the ice into a measuring cup with water and observing the increased water volume. To reduce sources of error due to melting of the ice to a minimum, cold water with a measured temperature of 0,8 °C was used. The ice cylinders had a temperature of ≈-9 °C when density was measured. In total 30 cylinders have been measured during the testing period. The measured average density was found to be 0,913 kg/m^3 with a standard deviation of 17 kg/m^3. Compared to the theoretical density of ice (917 kg/m^3) this indicates that there is some air and weakness in the ice.

$$\rho_{ice} = 913 \pm 17 \; [kg/m^3]$$

Figure 45 Plastic cylinders used to produce ice

Figure 46 Storage of produced ice specimens in the laboratory

3.5 Abrasion measurements

For the tested specimens a Mitutoyo 543-250B digital indicator from Mitutoyo Corp. has been used to measure the surfaces. This device has an accuracy of 0,003 mm and can measure deviations in the range of 0-12,7 mm with a load of 0,9 N (Mitutoyo Corp., 2013). The principal of this method is described in the chapter "Measuring techniques".

Figure 47 Surface measurement setup. Concrete specimen is placed on a coordinate table and moved in a predefined grid under the indicator.

Concrete specimens were placed on a coordinate table under the digital indicator, as is illustrated in Figure 47. Surfaces were then measured in a predefined grid. The grid was chosen with measuring points also outside of the abrasion zone to be used as reference points. The measuring grid and the used coordinate system can be seen in Figure 48, the abraded zone is colored in blue. The concrete specimens are measured before, during and after testing and the abrasion was determined as the difference between these measurements, and by using the reference points.

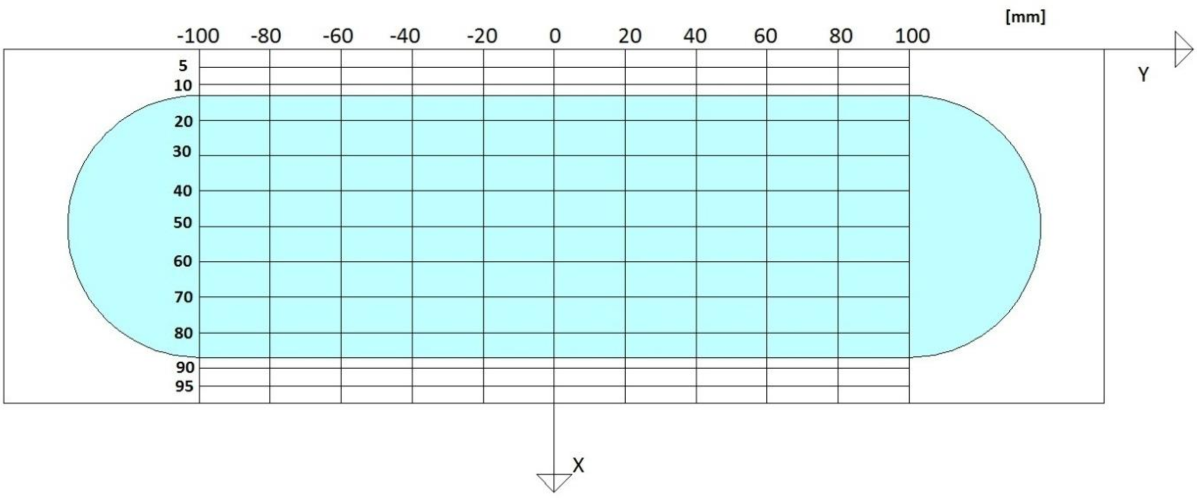

Figure 48 Measurement coordinate system, grid and measurement points. The part of the surface exposed to abrasion is colored in blue.

Figure 49 shows the scheme where the individual surface measurements taken with the digital indicator was written down. After testing, all the measurement schemes were entered into an excel sheet to calculate the abrasion.

x/y	-100	-80	-60	-40	20	0	20	40	60	80	100
5											
10											
20											
30											
40											
50											
60											
70											
80											
90											
95											

Figure 49 Scheme for recording of measured surface profiles.

In addition an ATOS III optical scanner from GOM Optical Measuring Techniques is used to create digitalized 3D images of the concrete surfaces (Figure 50). However, this device was first made available long after the ice abrasion testing had started, therefore such scans could not be made for all specimens. The contrast of some of the concrete surfaces also made it very difficult to perform good measurements. This device is also found to be very demanding to use, at the same time as the experiments itself was very time consuming. Therefore these measurements are only used as illustrations to visualize measurements from the digital indicator. Still many measurements are performed and all data is saved at the ATOS computer in the folder: Joakim/overflateskanninger for potential future use. Appendix 5 contains a short quick guide on how to use this device.

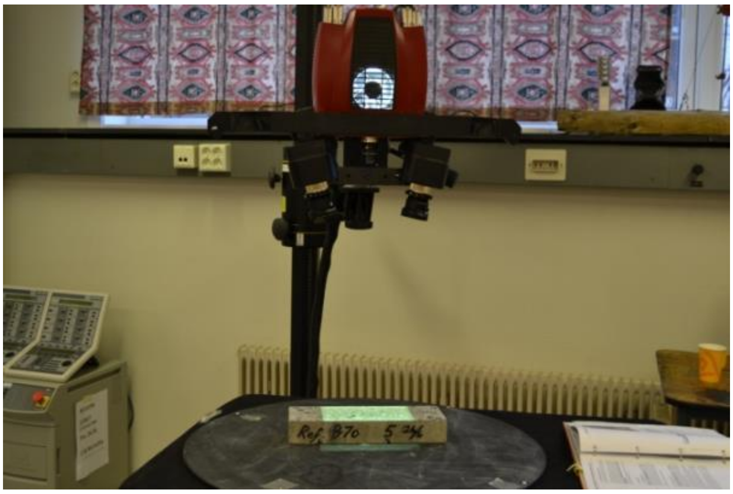

Figure 50 ATOS optical scanner. Two cameras is photographing the disorientation of the projected light

3.6 Roughness calculations

For all specimens the R_a, R_q, R_{sk} and R_k roughness parameters are calculated. Formula 1 and Formula 2 is used to calculate R_a and R_q. Skewness and Kurtosis is calculated with the built-in formulas in "Microsoft Office, Excel 2010". Roughness parameters is calculated with the same measurements as the abrasion depth along the lines of x=20-80 mm (abrasion zone). This means that the roughness parameters are calculated for each x-coordinate with 11 measuring points (y-coordinates).

3.7 Measurement calibrations

In Labview the total accumulated horizontal distance is logged. Because the ice cylinder has a diameter 74 mm and the shaping machine has a stoke length of 200 mm it is necessary to calibrate measured values to get the effective sliding distance. By dividing the ice cylinder diameter with the stroke length the effective ice exposure at a given point of the surface is found: $\frac{D}{l} = \frac{74}{200} = 0{,}37$. 1 m accumulated sliding on a given surface point equals 0,37 m effective ice sliding, meaning that for each complete cycle the machine exposes the concrete to 148 mm of ice sliding while Labview is registering 400 mm.

The effective exposure would actually only be valid for the concrete under the center of the ice cylinder, at x= 50 mm. Calculated abrasion values should therefore also be calibrated for the cylinder shape of the ice specimens. The further way from the center of the ice cylinder the smaller the chord is. 30 mm from the center the chord has just 58% of the length in center (diameter). To get comparable abrasion rates these calibrations are performed. Chord calibration factor is easily found by the theorem of Pythagoras. Calculations are illustrated in Figure 51. Table 11 shows both chord calibration factors and the total calibration factor for each measuring point along the x-axis.

d(x) :distance from the centerline to the chord
k: length of half the chord
R= Radius
D= Diameter = 74 mm
C(d)= Cord length as a function of d(x)

$$R = Radius = \frac{Diameter}{2} = \frac{74}{2} = 37\ mm$$

$$k = \sqrt{R^2 - d(x)^2}$$

$$C(d) = 2 * k = 2 * \sqrt{R^2 - d(x)^2} = 2 * \sqrt{37^2 - d(x)^2}$$

$$Calibration\ parameter, chord = \frac{C(d)}{D}$$

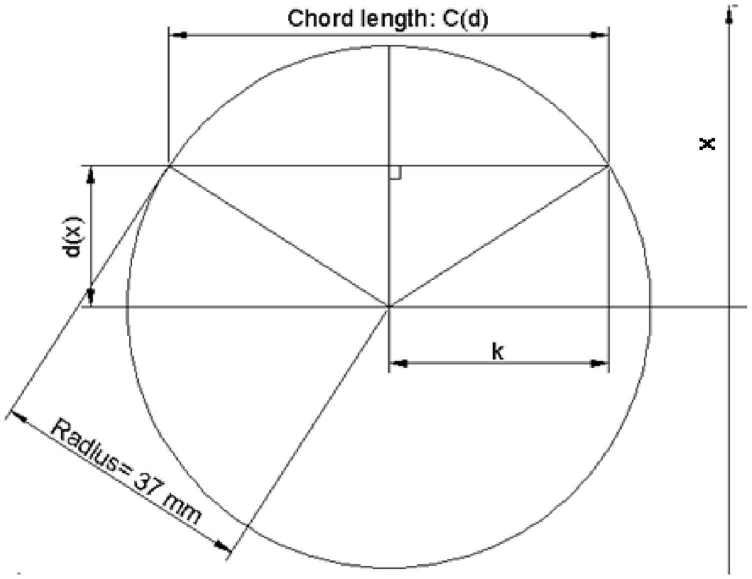

Figure 51 Illustration for the chord calibration factor

Table 11 Calibration factors for accumulated distance

X-Coordinate	Distance from center	Calibration parameter, chord	Calibration parameter, accumulated distance	Total calibration parameter
5	45	0	0,37	0
10	40	0	0,37	0
20	30	0,59	0,37	0,22
30	20	0,84	0,37	0,31
40	10	0,96	0,37	0,36
50	0	1,00	0,37	0,37
60	-10	0,96	0,37	0,36
70	-20	0,84	0,37	0,31
80	-30	0,59	0,37	0,22
90	-40	0	0,37	0
95	-45	0	0,37	0

3.8 Bond tests

Bond tests are performed on Densit, Reforcetech and Rockbond repair mortars with B60 as substrate concrete. Pull-out tests are preformed according to NS-EN 1542 (1999). This includes that the substrate concrete is sandblasted before application of the repair mortar. SINTEF (Trondheim, Norway) has prepared the Densit and Reforcetech specimens, while Rockbond is prepared by *Rockbond SCP LTD (Suffolk, UK).*

Figure 52 Steel discs are glued to the surface with two-component epoxy glue. Wooden pins are used to center the disc and avoid getting glue between core and panel

Figure 53 Pull-out test blocks after drilling of the 55 mm cores

On each panel 5 cores with diameter of 55 mm were drilled out, as shown in Figure 53. This procedure has been performed by the NTNU and SINTEF laboratory staff.
Steel discs were then glued to the concrete with two-component epoxy glue (Figure 52).
Testing was performed in a pull-out machine (Figure 56) set to use a load rate 0,05MPa/sec.
The load was applied centric trough a “friction” free hinge (Figure 55) and the failure load was recorded and read from the control unit (Figure 54).

Figure 54 Pull-out machine control unit

Figure 55 Test panel mounted in pull-out machine

Figure 56 Pull-out test machine

4 Results

In this chapter results from the performed ice abrasion and bond tests are presented. Densit and Reforcetech were tested in the project thesis last semester (Kirkhaug, 2012) and the prolonged testing of 7,5 km sliding distance and testing of sandblasted surfaces of Densit specimens is performed as a part of this master thesis. Since this study is a continuation of the project thesis, these results are also included in this report. In total 42 ice abrasion tests and 25 pull-out bond tests were performed, resulting in large amount of data to analyze. The intention of this chapter is to present the most relevant and important results in a structured manner, giving a good overview of the performed tests.

The labview program reports average cycle values for load, sliding velocity and friction in addition to the actual value for the different parameters at the horizontal position used to calculate the average. This makes it possible to evaluate both average values and the influence of horizontal position.

Presentation of ice abrasion results starts at page 50, followed by roughness values (page 57), observed friction (page 64) and observations of test conditions and parameters of the ice abrasion tests/rig (page 66). Results from bond tests are presented at the end, starting at page 75.

While working on the experiments in the laboratory, a great deal of obstacles and unforeseen events occurred. This is especially the case for the ice abrasion rig, but also the other equipment used in the laboratory. The ice abrasion rig experienced an overheated engine, parts falling out, water freezing on the load cells, blown fuses, electrical failure, etc. Neither did the large number of broken plastic cylinders contribute to improve the situation. First of all this made the experiments much more time consuming than originally planned, as time had to be spent on repairs and waiting for new parts. For Reforcetech it was also necessary to restart one of the tests, with one of the spare test specimens, because the load history of the specimen tested first was uncertain. Secondly, precautionary measures and improvements had to be found continuously to prevent problems for reoccurring. This is described in more detail together with the short user manual in appendix 4.

4.1 Ice Abrasion

4.1.1 Abrasion rates

Measured average abrasion rates [mm/km] for the abraded surface are presented in Table 12 and Figure 57. Table 13 shows a summary of abrasion rates for different test conditions. More detailed presentations of abrasion rates are presented in appendix 1 and 2.

Appendix 1 contains average abrasion rates along x-axis for all tested specimens

Appendix 2 contains average abrasion rates along y-axis for all tested specimens

Reported abrasion values are presented with the same number of decimals as have been used for the measurements. The results should give a good indication of the abrasion resistance for the different products.

Table 12 Abrasion rates [mm/km] for tested specimens.

Product	**Specimen nr**	**Contact pressure[MPa]**	**Sliding speed[cm/s]**	**Abrasion rate [mm/km]1,25 km**	**Abrasion rate [mm/km]2,5(5/7,5) km**
Reforcetech*	1	1	16	0,029	0,032
	3	1	16	0,026	0,033
	2	1	25	0,026	0,030
	4	1	25	0,022	0,028
	5	0,5	16	0,015	0,015****
	6	0,5	16	0,019	0,019
Densit*	9	1	16	0,024	0,026
	10	1	16	0,023	0,026
	13	1	25	0,017	0,015(0,016/0,016)
	14	1	25	0,011	0,014(0,017/0,017)
	11	0,5	16	0,09	0,011
	12	0,5	16	0,012	0,011
	8 (Sb)**	1	16	0,020	0,021
	39 (Sb)**	1	16	0,023	0,024
B70	15	1	16	0,052	0,052
	17	1	16	0,047	0,050
	19	1	25	0,030	0,032(0,032/0,034)
	20	1	25	0,045	0,047(0,047/0,048)
	16	0,5	16	0,026	0,024
	18	0,5	16	0,023	0,024
B60	33	1	16	0,089	0,090
	36	1	16	0,091	0,088
	34	1	25	0,070	0,071
	35	1	25	0,086	0,085
	31	0,5	16	0,027	0,025
	32	0,5	16	0,033	0,032
	37 (Sb)**	1	16	0,070	0,072
	38 (Sb)**	1	16	0,071	0,073
Rockbond	50	1	16	0,039	0,041
	51	1	16	0,042	0,039
	53	1	25	0,035	0,034
	55	1	25	0,033	0,036
	52	0,5	16	0,021	0,024
	54	0,5	16	0,025	0,024
MapeCoat	21	1	16		***
	22	1	16		***
Polyurethane	24	1	16		***
	26	1	16		***

***Tested autumn 2012 in project thesis**

**** Specimen surface sandblasted before testing**

***** No measurable abrasion. Measured max/min abrasion rate were ±0,004 with average 0,0001=0**

****** A summation error in the sheet used to calculate abrasion in the project thesis is corrected.**

Table 13 Summary of abrasion rates for different test condition after testing, ref. Table 9

Abrasion rates [mm/km]										
Temperature	-10°C									
Sliding speed	**16 cm/sec**						**25 cm/sec**			
Contact pressure [MPa]	**1**		**0,5**		**1**		**1**		**1**	
Sliding distance	**2500 m**		**2500 m**		**2500 m**		**2500 m**		**7500 m**	
Sandblasted surface(Yes/No)	**No**		**No**		**Yes**		**No**		**No**	
	1	**2**	**1**	**2**	**1**	**2**	**1**	**2**	**1**	**2**
Densit	0,026	0,026	0,011	0,011	0,021	0,024	0,015	0,014	0,016	0,017
Reforcetech	0,032	0,033	0,030	0,028	-	-	0,015	0,019	-	-
Rockbond	0,041	0,039	0,024	0,024	-	-	0,034	0,036	-	-
B70	0,052	0,050	0,024	0,024	-	-	0,032	0,047	0,034	0,048
B60	0,090	0,088	0,025	0,032	0,072	0,073	0,071	0,085	-	-
MapeCoat	0	0	-	-	-	-	-	-	-	-
Polyurethane	0	0	-	-	-	-	-	-	-	-

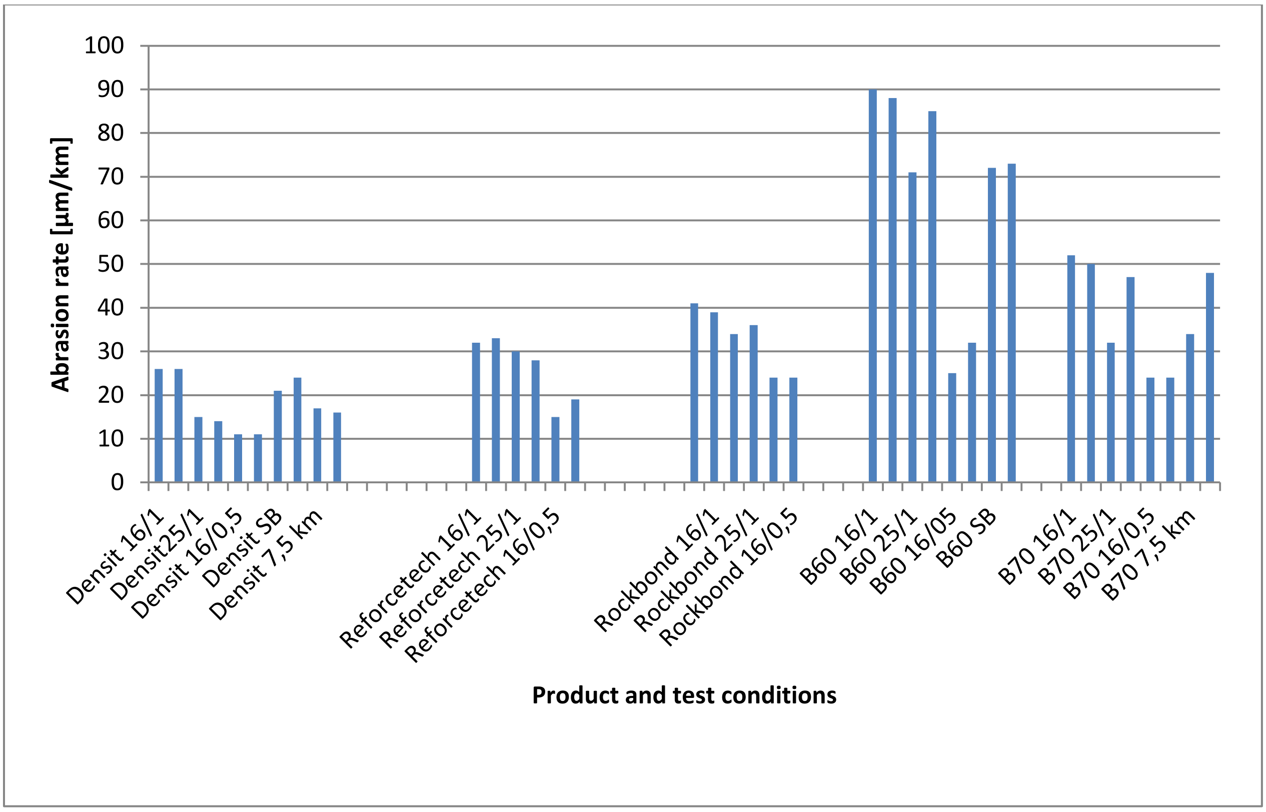

Figure 57 Total abrasion rates after complete test [µm/km]. Product/ sliding velocity [cm/sec]/ contact pressure [MPa]. There are two specimens for each variable, ref table 13. SB= Sandblasted surface

Table 14 shows an overview of compressive strength and density of the cement based products tested in the ice abrasion rig. Reforcetech, Densit, B60 and B70 are tested by SINTEF, while the Rockbond are tested by Rockbond SPD LTD.

Table 14 Compressive strength and density for tested cement based products

Product	**Compressive cube strength, 7 days[MPa]**	**Compressive cube strength, 28 days[MPa]**	**Density, 7 days [kg/m^3]**	**Density, 28days[kg/m^3]**
Densit	128.7	152.3	2850	2870
Reforcetech	67.5	85.2	2640	2660
Rockbond	-	61.0	-	-
B60	Not tested	74.7	Not tested	2350
B70	79.5	102.2	2460	2460

There is little difference of abrasion rates in relation to sliding distance. Most specimens have measured almost the same abrasion rate at all distances. Specimens exposed to 7,5 km of testing does not show any considerable change of abrasion rate compared to earlier measurements at 1,25 and 2,5 km. Figure 58 shows average abrasion rate development during testing for some selected specimens.

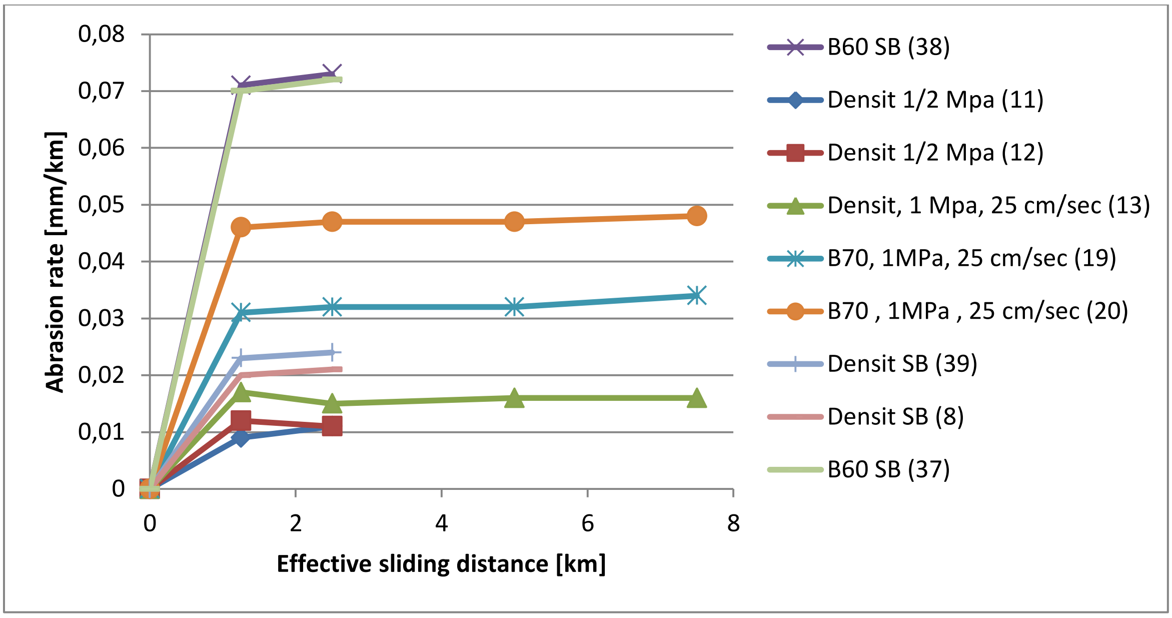

Figure 58 Average abrasion rate developments for some of the tested specimens. Numbers in the parentheses indicate the test specimen number according to Table 12.

All the specimens were tested according to the previously described test plan (Table 9). However, four B60 specimens, both polyurethane and one MapeCoat specimen cracked after ≈ 1200 m of effective sliding. Except from one specimen, they all cracked in what is described as the “common crack point” in (Bøhn, 2012). Cracking of the last specimen happened in the middle, where the temperature sensors were casted. The way the cracks developed suggests that tensile strength might have been too low. Most cracked specimens were measured once before they cracked, and a second measurement was performed after cracking.


Figure 59 Cracked B60 specimen

For all specimens, except the two epoxies, it was visible signs of abrasion, and sand grains could be observed as loosened from the surface. This effect was more visual thus higher the rate of abrasion. For the B60 this could be visually observed as pitting or what can be described as catastrophic abrasion (Fiorio, 2004). Based on the results in (Hanada, et al., 1996) where concrete was found to be abraded six times as much as Polyurethane the results from this does not seem unreasonable. Figure 60 shows an ATOS scan of a Polyurethane specimen, no signs of abrasion can be seen. The blank areas are white because the surface reflects the projected light in such a way that the cameras are unable to capture that part of the surface.

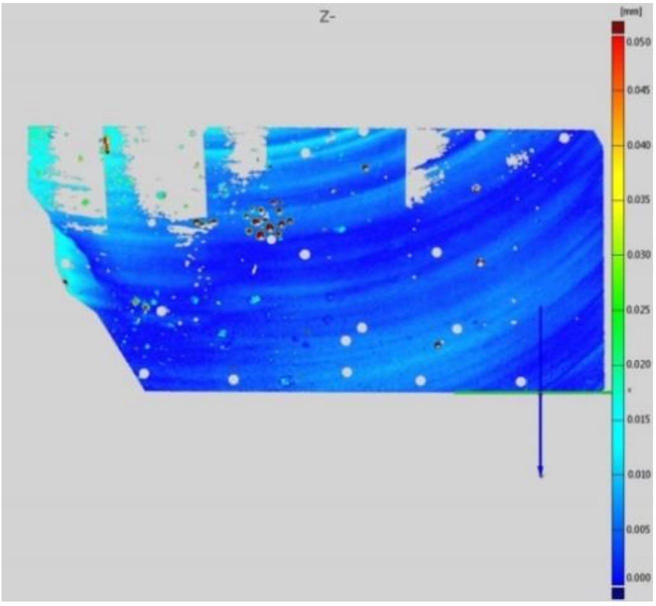

Figure 60 ATOS scan of cracked Polyurethane specimen after testing. Even with high resolution there is no sign of abrasion

Specimens tested with a contact pressure of 0,5 MPa has lower abrasion rates than the specimens tested with 1 MPa contact pressure. B60 specimens experiences three times as high abrasion rate at 1 MPa compared to 0,5 MPa pressure, while the same value for Densit is ≈2.

All specimens show a tendency towards lower abrasion for increased sliding velocity. However, it seem like the effect might be a bit higher for the tests performed in this study compared to results presented in (Itoh, et al., 1994). Increased sliding velocity also seems to have a greater impact on the Densit specimens than the other products.

In previous tests in the NTNU laboratory there has been found an increased abrasion at the outer edges of the abraded area compared to the center of the specimen.   For the tests performed in this study, this effect was more visible on the B60 and B70 concretes than at the repair mortars. Variation along the y-axis is illustrated by the images from the ATOS scans. Figure 61to Figure 67are showing some of these scans.

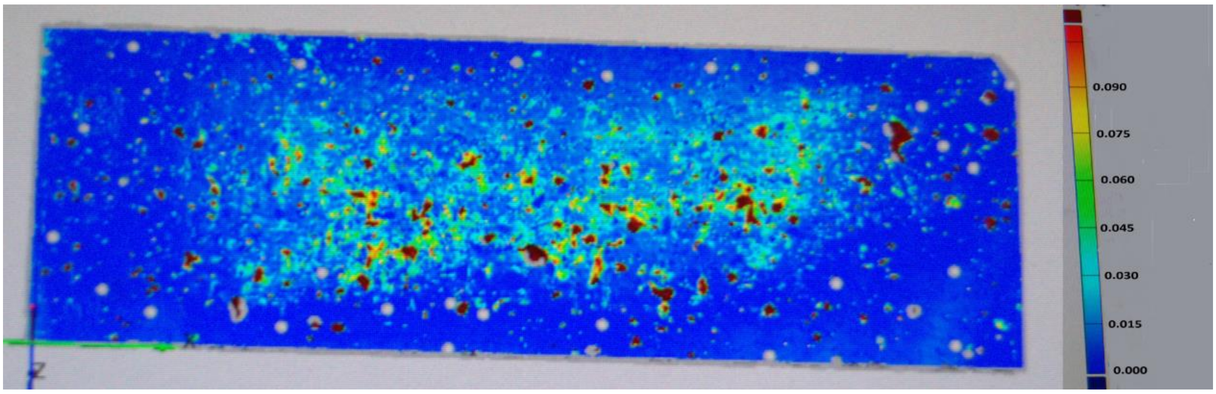

Figure 61 Reforcetech specimen after testing

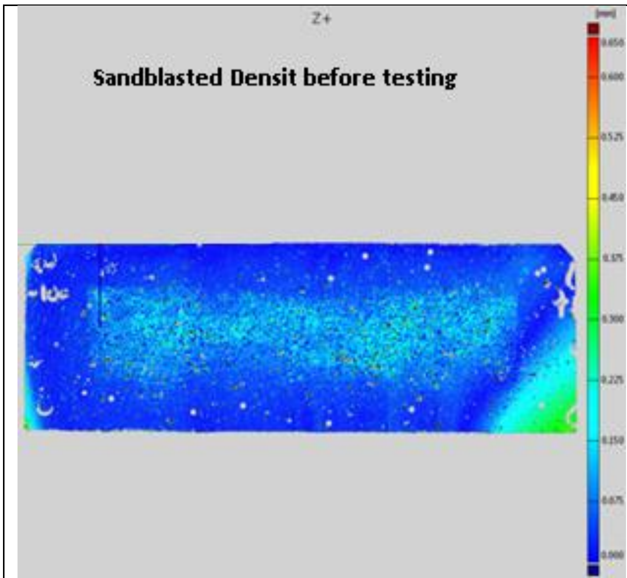

Figure 62 Sandblasted Densit specimen before testing

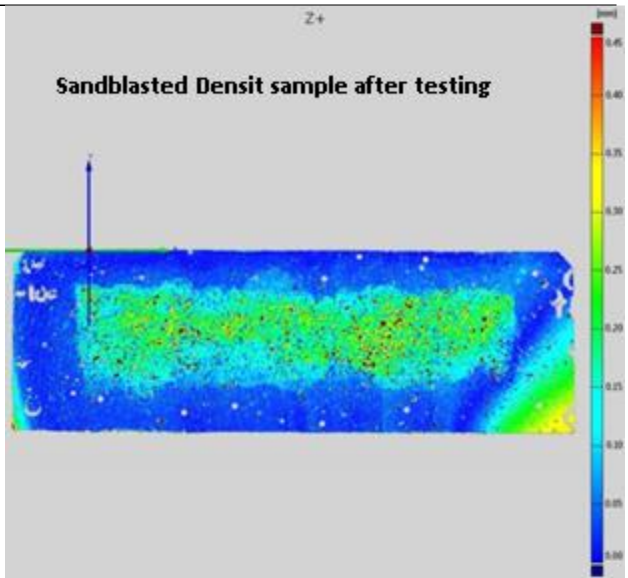

Figure 63 Sandblasted Densit specimen after testing

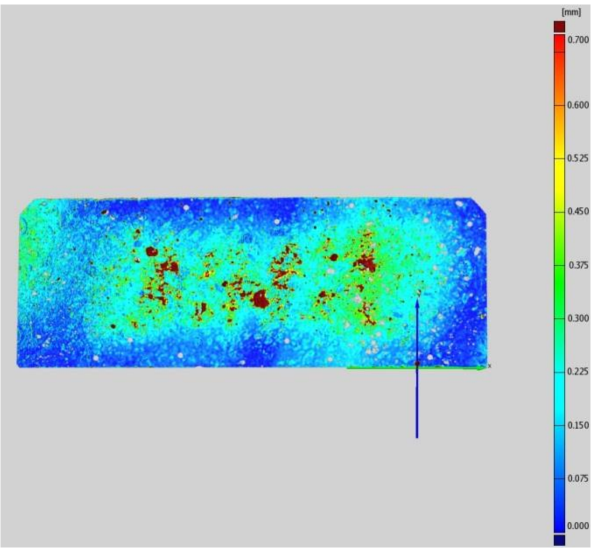

Figure 64 B70 after testing

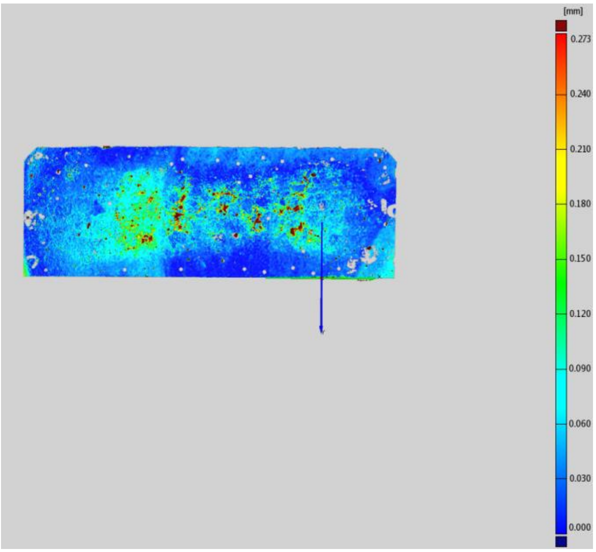

Figure 65 Rockbond specimen after testing

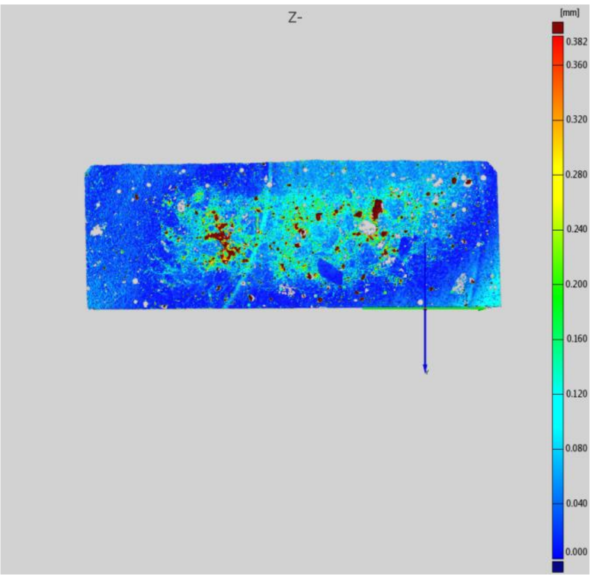

Figure 66 B70 specimen after testing

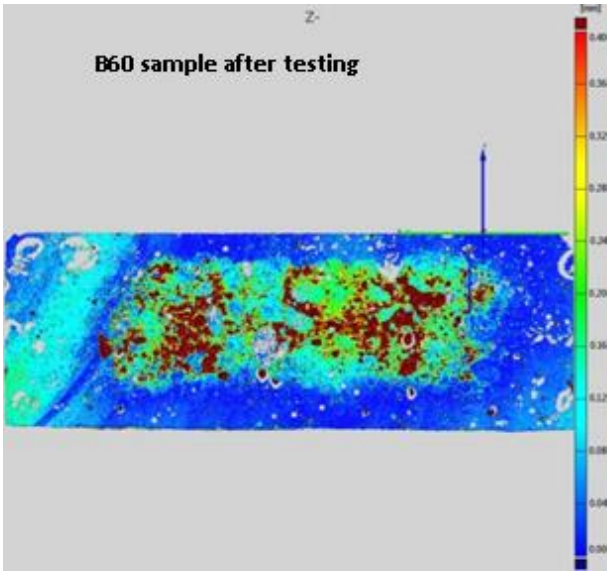

Figure 67 B60 specimen after testing

4.1.2 Roughness

A subtopic of this study is to look for any correlation between the surface roughness and the abrasion rates. In this section it is made an attempt to analyze the surface roughness of the test specimens.

The specimen surfaces have been measured before, during and after abrasion testing. In addition to calculate the abrasion, these data has also been used to calculate the surface roughness of the specimens. Abrasion rates are calculated as the difference between two surface profiles, and roughness is calculated from each of these profiles. All roughness parameters are basically a statistical interpretation of the surface topography. Average Roughness, Root mean square roughness, Kurtosis and Skewness is calculated. Development of investigated roughness parameters are presented separately for each of the tested products. Roughness parameters are calculated along the y-axis, for each x-coordinate. The presented values are calculated average values for the lines from x= 20→ x= 80 mm. This means that each parameter, of one line along the y-axis, is calculated from 11 surface points. The presented average values are then calculated as the average of the 9 calculated roughness values.

Standard deviations of the presented values are included in appendix 3.

Densit: Results of the calculated roughness parameters for Densit are presented in Figure 68. The two specimens used for testing with contact pressure of 0,5 MPa had the highest initial R_a and R_q values. With exception of the sandblasted specimens R_a and R_q seems to go towards the same value, independent of the initial roughness. In general the Densit specimens have a smooth surface after testing compared to for instance B60. Skewness tends to get close to zero after the test has been running for a while. This means that measured values go towards a uniform distribution of peaks and valleys.

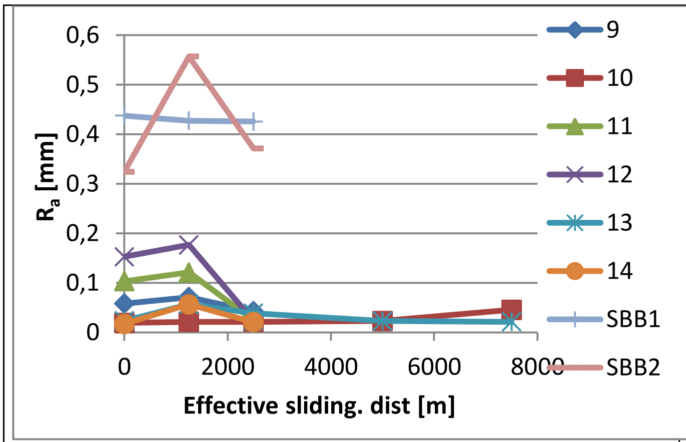	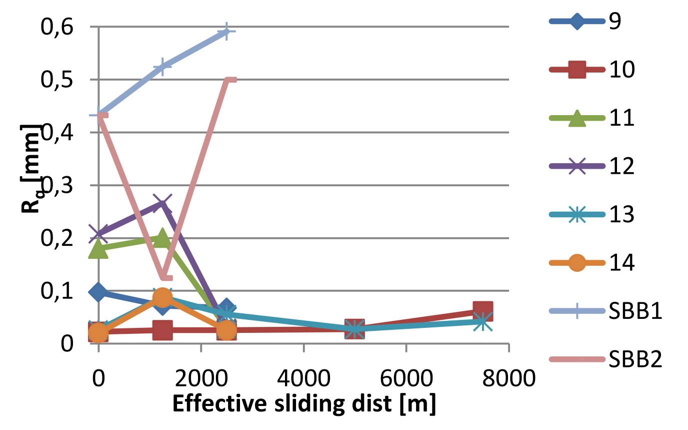
Densit: R_a [mm] as function of eff. dist. [m]	Densit: R_q [mm] as function of eff. dist. [m]
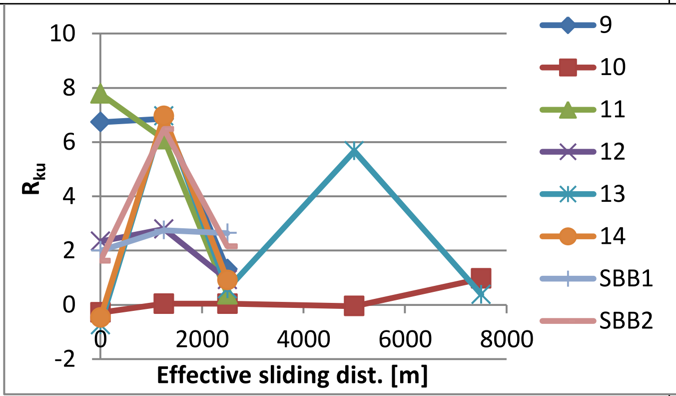	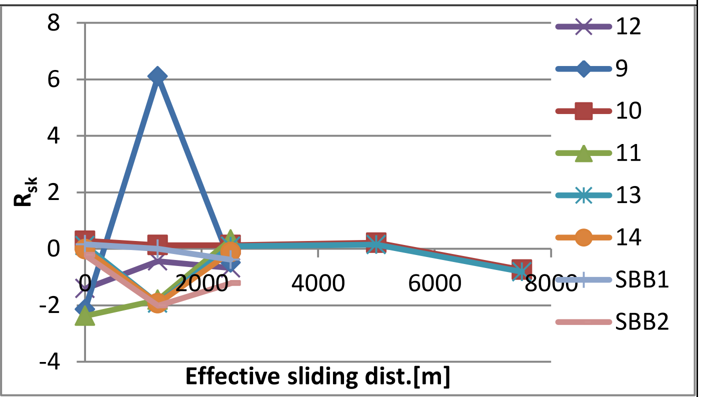
Densit: R_{ku}	Densit: R_{Sk}

Figure 68 Densit Roughness parameters.
-9/10: 1 MPA_16 cm/sec
-11/12: 0,5 MPa _25 cm/sec
-13/14: 1 MPa_25 cm/sec

Reforcetech: Figure 69 presents calculated roughness parameters for Reforcetech specimens. All Reforcetech specimens shows almost the same low initial R_a. Except from one specimen, there seem to be to a close to linear increase as a function of sliding distance. For the 0,5 MPa tests, the specimen with lowest abrasion have the highest initial Kurtosis. For the 0,5 MPa specimens (5 and 6) both R_{sk} and R_k is considerably higher for the specimen with lowest abrasion (5) after 2,5 km of ice sliding. Kurtosis also tends to be higher for the 1 MPa specimens with lowest abrasion, while R_{sk} is low.

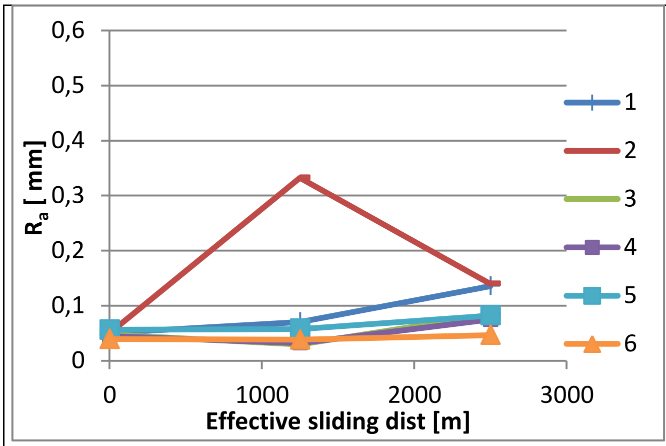

Reforcetech: R_a [mm] as function of eff. dist. [m]

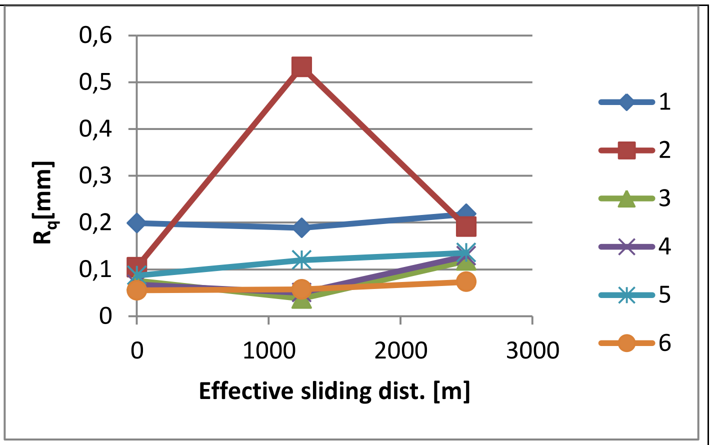

Reforectech: R_q[mm] as function of eff. dist. [m]

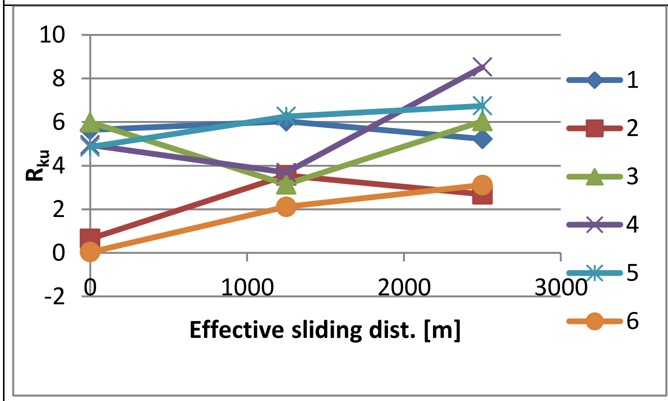

Reforcetech: R_{ku}

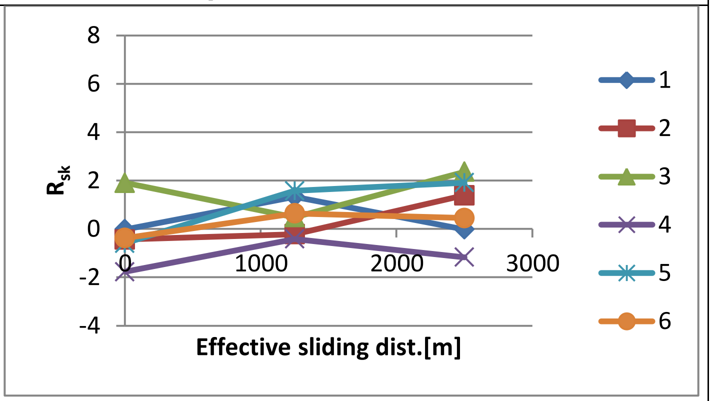

Reforcetech: R_{Sk}

Figure 69 Reforcetech Roughness parameters

-1/3: 16 cm/sec 1 MPa

-2/4: 25 cm/sec 1 MPa

-5/6: 16 cm/sec 0,5 MPa

Rockbond: In Figure 70 the calculated roughness of Rockbond specimens are presented. R_a increases for all specimens, but it is considerably lower for the specimens exposed for 0,5 MPa contact pressure. Development of R_a, for specimens tested under same conditions, seems to be very similar. Tests run with a velocity of 25 cm/sec and 1 MPa contact pressure have lower abrasion rate and higher R_a and R_q after testing compared to the 16 cm/sec specimens. Specimens with lower abrasion tend to have higher kurtosis at finish.
All specimens ended up with almost the same Kurtosis, except for specimen 53, which has almost twice as high R_k as the other specimens. This is also the specimen run at 1 MPa with the lowest abrasion rate. The same specimen also has the lowest R_{sk}.

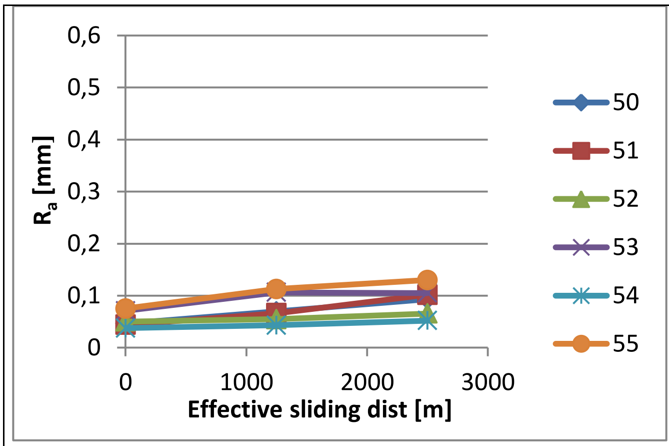

Rockbond: R_a[mm] as function of eff. dist. [m]

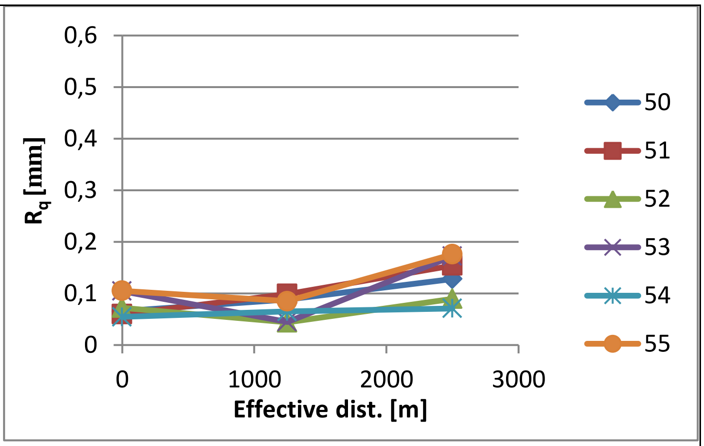

Rockbond: R_q[mm] as function of eff. dist. [m]

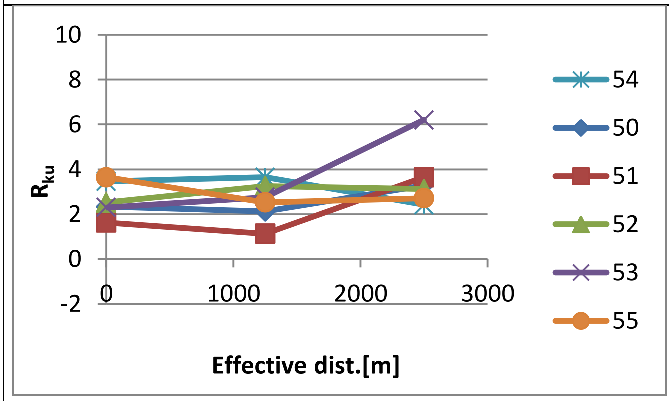

Rockbond: R_{ku}

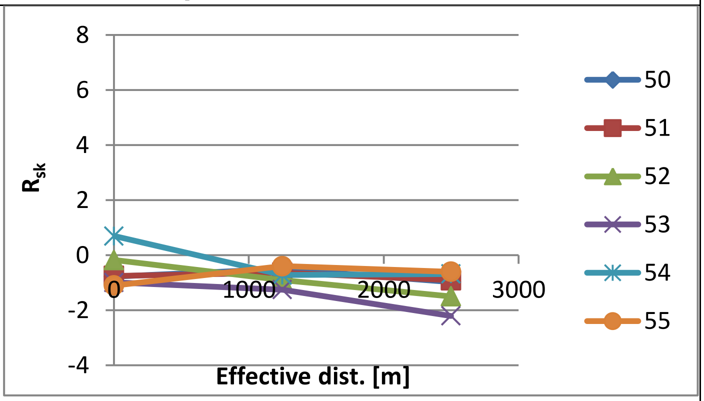

Rockbond: R_{Sk}

Figure 70 Rockbond Roughness parameters
-50/51: 16 cm/sec 1 MPa
-52/54: 16 cm/sec 0,5 MPa
-53/55: 25 cm/sec 1 MPa

B70 concrete: In Figure 71 calculated roughness parameters from B70 specimens are presented. Initial R_a and R_q values were low for all specimens. All specimens experienced an increase in both R_a and R_q . The two specimens tested with a contact pressure of 0,5 MPa has the highest Rq after 2,5 km of sliding and also the largest incline.
Specimen 19 which has the lowest abrasion rate of the tests performed at 1 MPa contact pressure has the highest R_{ku} and R_{sk} after 2,5 km of effective sliding. Calculated values for effective sliding distance of 7,5 km seem to move towards a stable value.

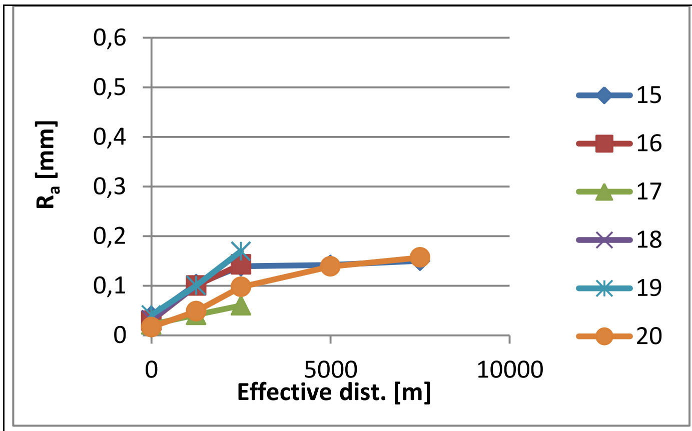

B70: R_a[mm] as function of eff. dist. [m]

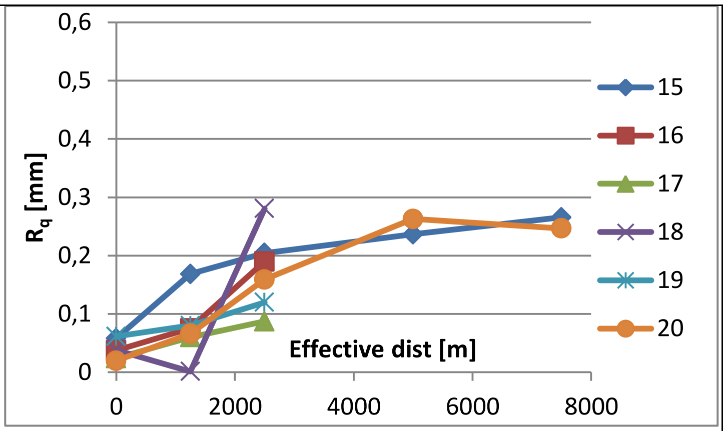

B70: R_q[mm] as function of eff. dist. [m]

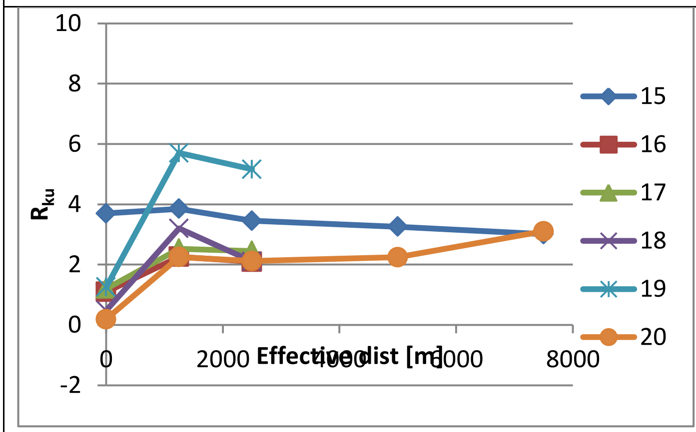

B70: R_{ku}

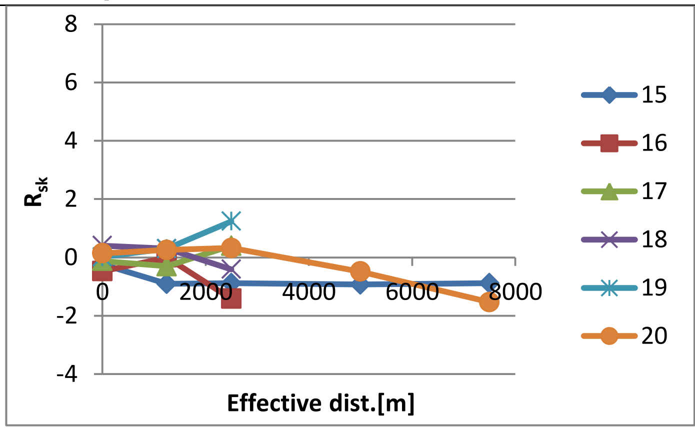

B70: R_{Sk}

Figure 71 B70 Roughness parameters
15/17: 16 cm/sec and 1 MPa
19/20: 25 cm/sec and 1 MPa
16/18: 16 cm/sec and 0,5 MPa

B60: In Figure 72 calculated roughness parameters for B60 specimens are presented. There is less data from the B60 tests, due to specimens cracking. Only two specimens are tested for 2,5 km , while the rest cracked after ≈1200-1500 m of effective sliding. All specimens were measured before start and once before cracking. In addition there is performed a measurement on those specimens where it was possible after they cracked. These measurements are performed in the same way as the other, but given that the specimen had cracked, the measurements can’t necessarily be said to be comparable to those performed on un-cracked specimens.
Initial R_a and R_q parameters are low for all specimens except for those who were sandblasted. The two specimens that didn’t crack both ran at 25 cm/sec and shows similar R_a and R_q development.

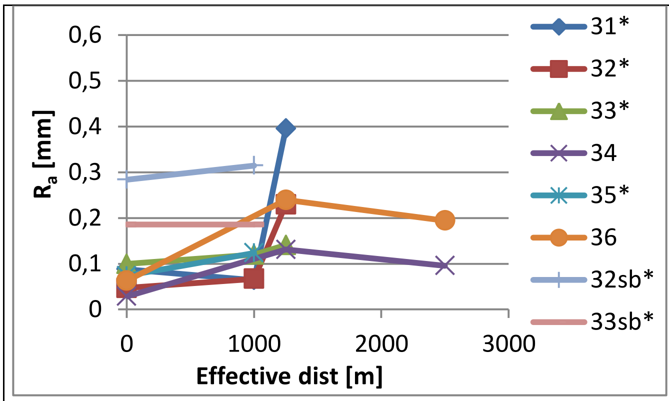

B60: R_a [mm] as function of eff. dist. [m]

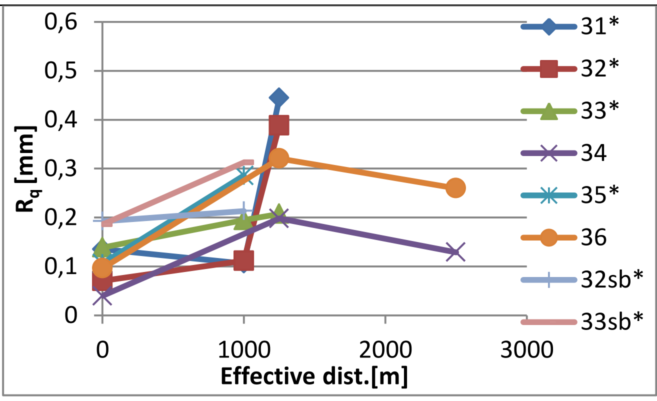

B60: R_q [mm] as function of eff. dist. [m]

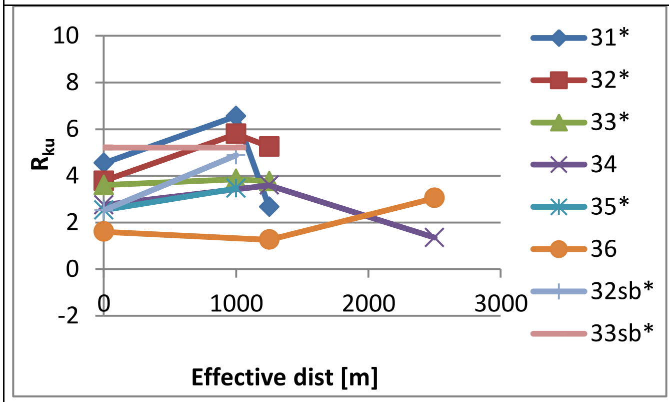

B60: R_{ku}

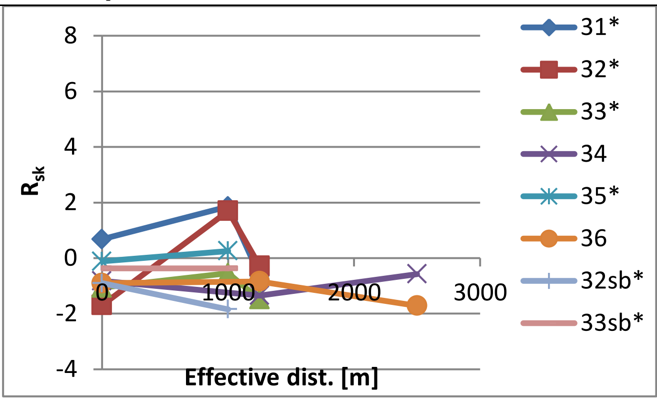

B60: R_{Sk}

Figure 72 B60 Roughness parameters. *Specimen cracked during testing.
- 32 sb/33 sb: 16 cm/sec and 1MPa, Sandblasted surface
- 33/36: 16 cm/sec and 1 MPa
- 34/35: 25 cm/sec and 1 MPa
-31/32: 16 cm/sec and 0,5 MPa

MapeCoat and Polyurethane: Even if there were no measurable abrasion for these products and all specimens except from one cracked at approximately the same distances as the B60 cracked roughness has also been analyzed for these specimens. Results are shown in Figure 73. These calculations can be used for two things. As there is no measured abrasion, the calculated roughness values should be the same for the before and after measurements. Deviation from measurements made before and after should give an indication of the error. Initial values can also be of interest.
As seen, all the surfaces are smoother for both R_a and R_q, than all the other tested products. R_k seem to be "high" while skewness tends to be close to zero. An interpretation of these calculations is that the surface is even, with a distribution of measured surface deviations close to average and small variations in size.

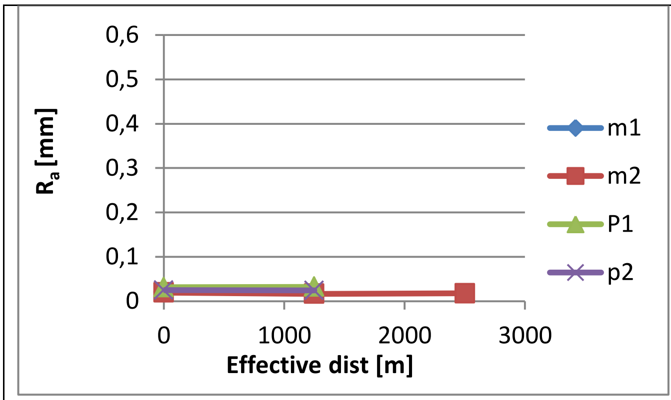

MapeCoat(m)/ Polyurethane(p) : R_a

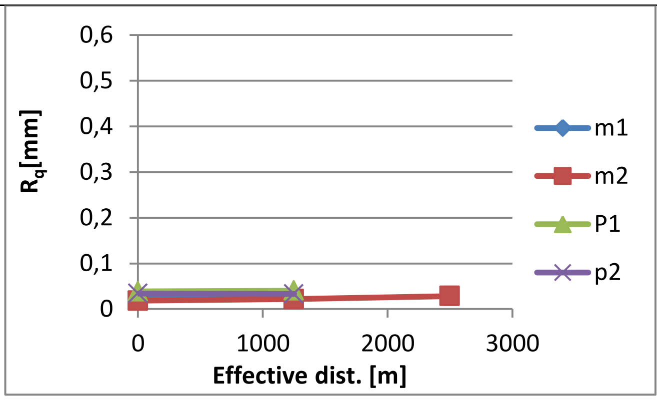

MapeCoat/ Polyurethane: R_q

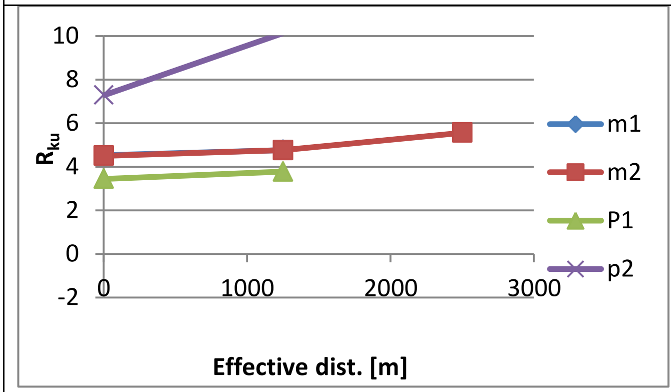

MapeCoat/Polyurethane(p): R_{ku}

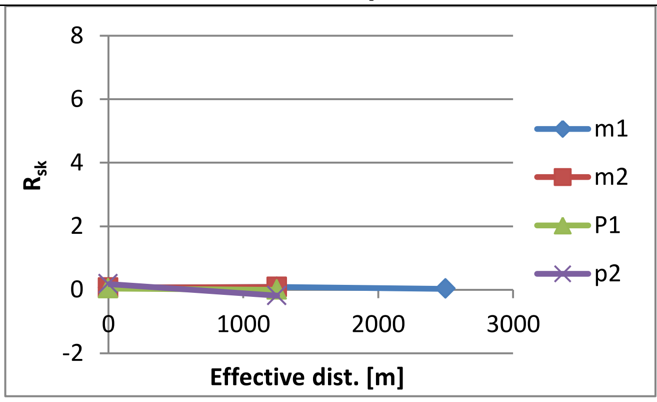

MapeCoat/Polyurethane(p): R_{Sk}

Figure 73 Roughness parameters for MapeCoat and Polyurethane specimens
- M1/M2: MapeCoat specimens, 16 cm/sec and 1 MPa
- P1/P2: Polyurethane specimens, 25 cm/sec and 1 MPa

4.1.3 Friction

The coefficient of friction has been analyzed for some of the tested specimens. The purpose has not been to perform a complete analysis, but to look into friction as a function of accumulated distance and horizontal surface position. It is unclear how average values are calculated and if both dynamic and static friction is included, therefore the presented values are the actual friction at the point the recordings are made.
Figure 74 shows what is found to be a typical development of friction in relation to accumulated distance.

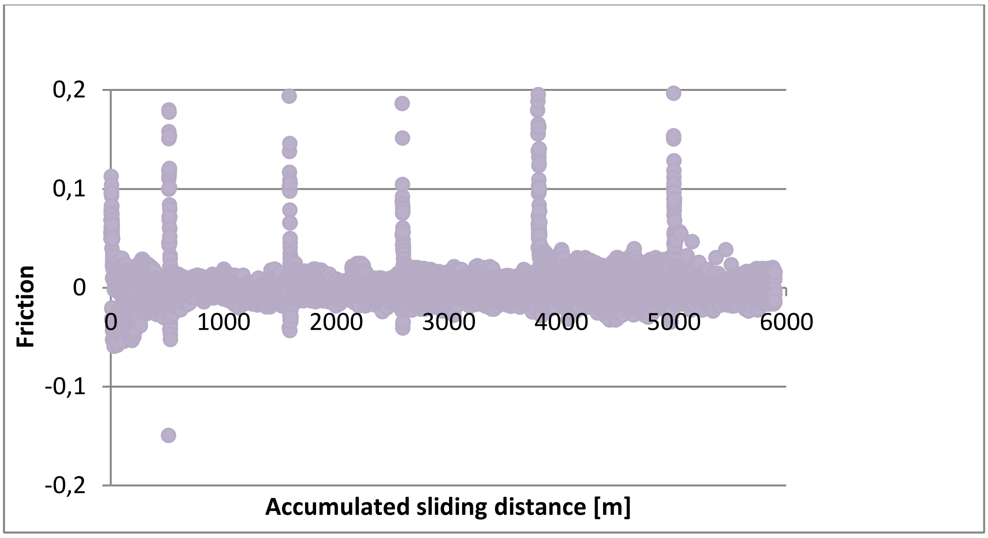

Figure 74 Friction coefficient as function of accumulated horizontal distance [m]. 1 MPa pressure (Rockbond) specimen

Figure 75 shows the same relation as Figure 74 but for a Rockbond specimen exposed to 0,5 MPa as average contact pressure.

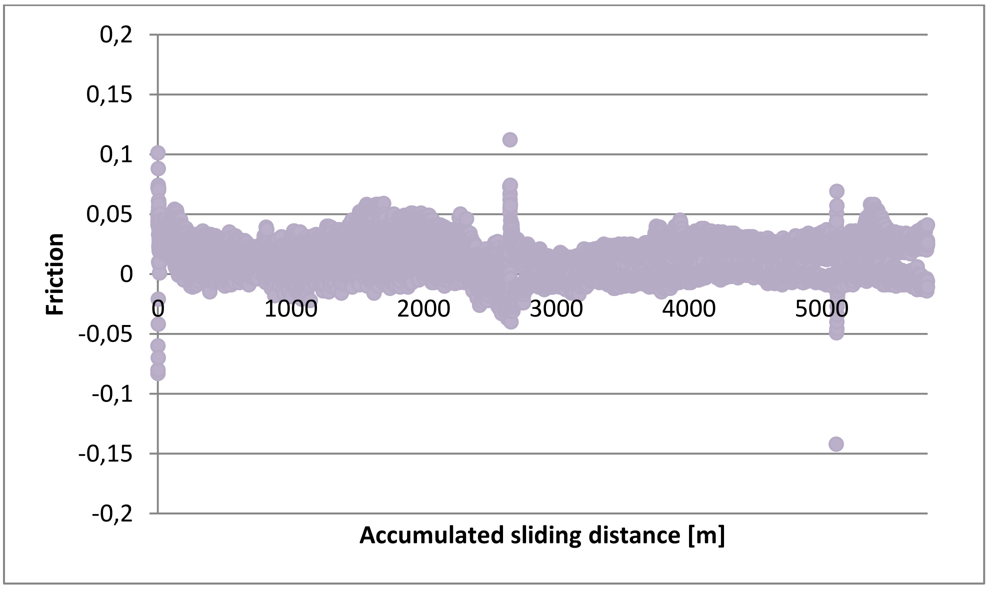

Figure 75 Friction as function of accumulated distance, ice contact pressure of 0,5 MPa. Rockbond specimen

There are only small differences in the friction coefficient of tested concrete products. Contact pressure and sliding distance is not found to affect the friction coefficient considerably. The tested cement based products is found to have an absolute average friction coefficient value in the range 0,045-0,055, calculated with absolute values in excel. For Polyurethane and MapeCoat average friction coefficient was ≈ 0,015.

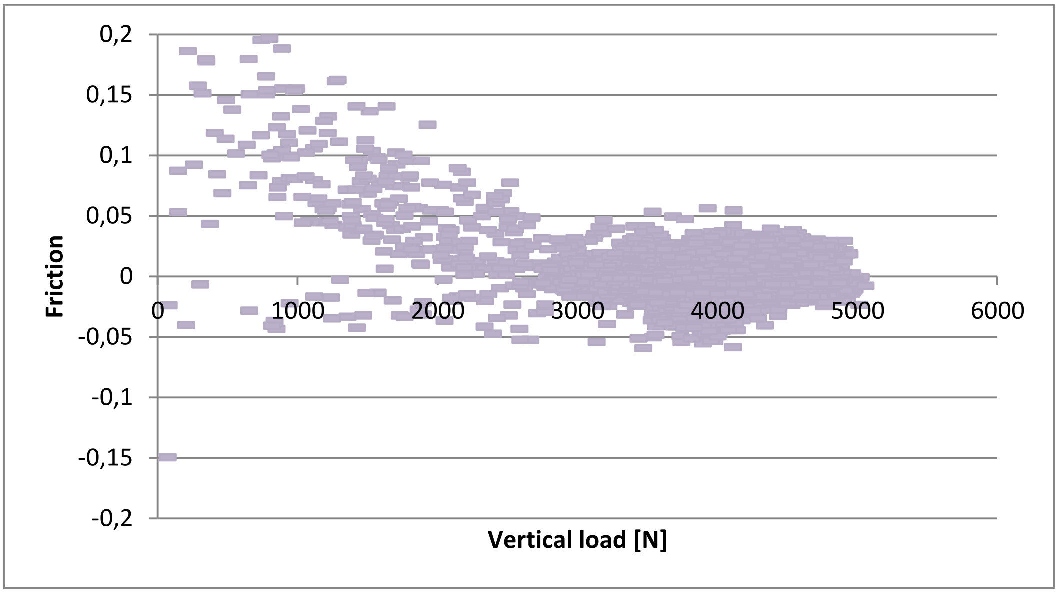

Figure 76 Friction as function of vertical load. Specimen with contact pressure =1 MPa = 4300 N. B70 specimen

On Figure 74 it seems like there are peaks occurring in regular intervals. This was found to correspond to recordings made just after ice is changed. The vertical load is small for a short period before the piston is able to apply sufficient load. Therefore the friction, which is the relation between horizontal and vertical load, is be going to high, even if the horizontal load is small. In Figure 76 the friction coefficient are plotted as a function of vertical load. As seen the friction coefficient decreases with increasing load until it is stabilizing around 2500 N.

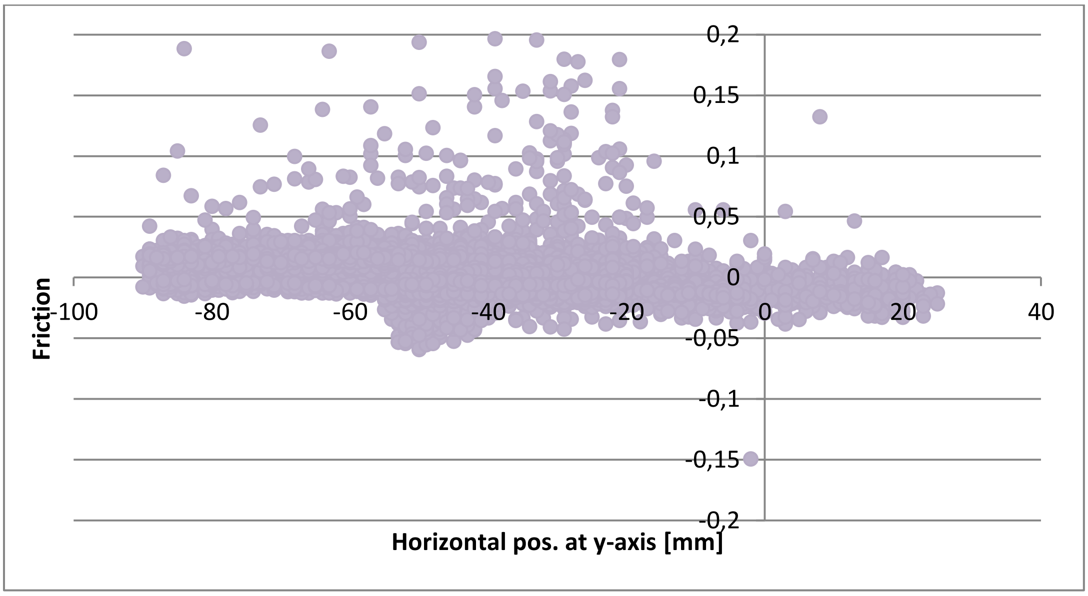

Figure 77 Friction as a function of horizontal position at y-axis [mm] B70 specimen. Contact pressure 1 MPa

Increased friction has been proposed as an explanation for increased abrasion at the edges of the test specimens. On Figure 77 friction is plotted against horizontal position. There seem to little or no difference in friction coefficient along the y-axis (ref. Figure 48), except for a weak decrease from y=-20. The gathering of high absolute values close to y=0 is the result of recording made just after ice is replaced and corresponds to the low loads in the beginning, see Figure 76. There is no logged friction between y=-90 and y=-100.

4.1.4 Ice abrasion rig and test conditions

In this section, data from the ice abrasion rig is presented to evaluate the reliability of different test parameters/conditions and the ice abrasion rig. Presented pictures and graphs are found to quite typical and representative for all tests, unless something else is stated.

For the ice abrasion tests, data has been recorded once each cycle. Figure 78 shows the horizontal position on the y-axis of recordings during testing.

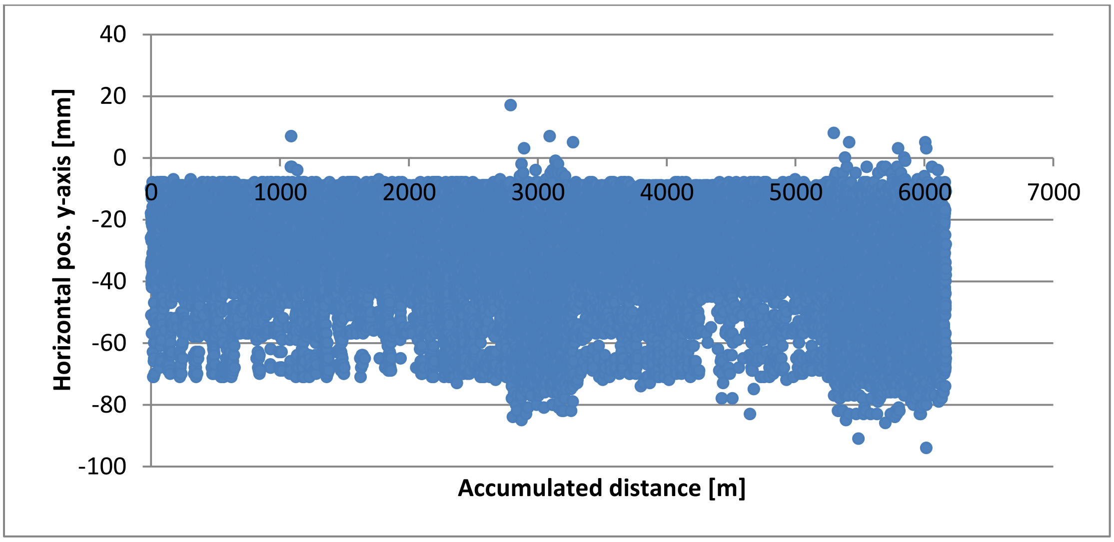

Figure 78 Horizontal position, at y-axis, for recordings plotted as function of accumulated sliding distance (ref. Figure 48). B70 specimen

Figure 78 shows that almost all recordings are made on the negative side of the y-axis (ref. Figure 48). Negative position values are on the same side as the horizontal load cell is placed.

In Figure 79 variation of average horizontal sliding velocity during the test is presented. Figure 79 is from a Reforcetech specimen where average velocity was 16 cm/sec and 1 MPa contact pressure. Velocity encountered some variations. From the figure it can be seen that the velocity varies in the range from 12-19 cm/sec with an average of 16 cm/sec.

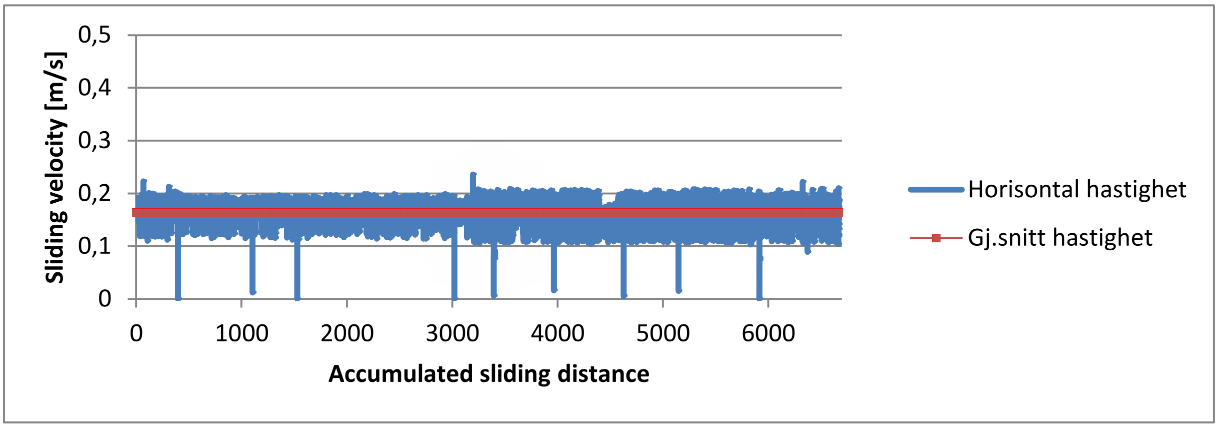

Figure 79 Average sliding velocity (cycle)(blue line) for test specimen 3, average velocity (red line)=16 cm/sec (Reforcetech)

Figure 80 shows recorded sliding velocity of a Reforcetech specimen test where average sliding velocity was 25 cm/sec. Average velocity was 25 cm/sec, but it is clear that the variations is larger at specimens tested with a sliding velocity 25 cm/sec tests compared to 16 cm/sec. In order to find a measurable difference, the standard deviation is calculated for three tests of 16 cm/sec and three 25 cm/sec tests.
Variation of velocity is presented as average values ± standard deviation:

- 0,16 ±0,016 [m/s] for the 16 cm/sec tests (10%)
- 0,25 ±0,045 [m/s] for the 25cm/sec tests (18%)

Standard deviation is 18 % of the average value for the 25 cm/sec tests and only 10 % for the 16 cm/sec tests. Whether the load was 1 or 0,5 MPa have not been found to influence this effect. Figure 80 (Reforcetech) and Figure 81 (B60) shows that average velocity development during testing is similar and independent of product type.

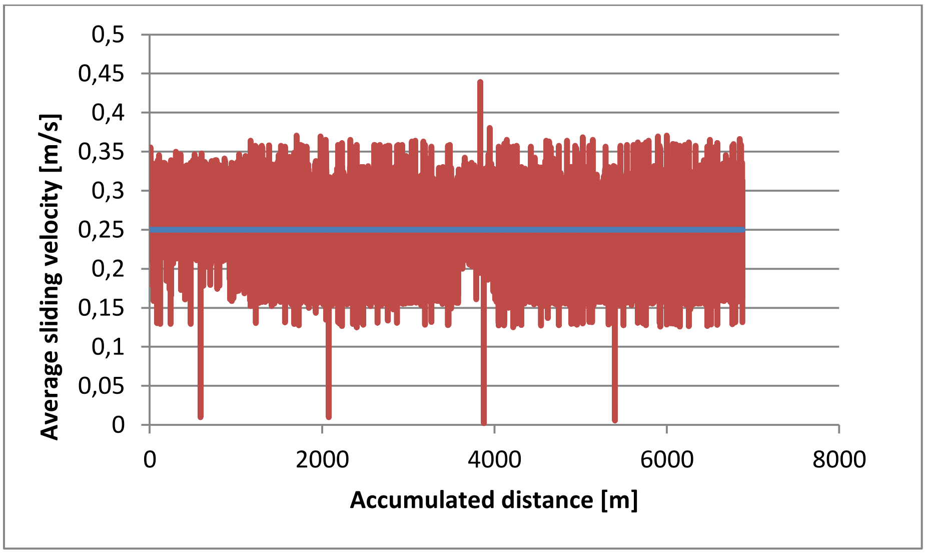

Figure 80 Average sliding velocity (cycle) for specimen 4 (Reforcetech). Average sliding velocity is 25 cm/sec. 1 MPa contact pressure

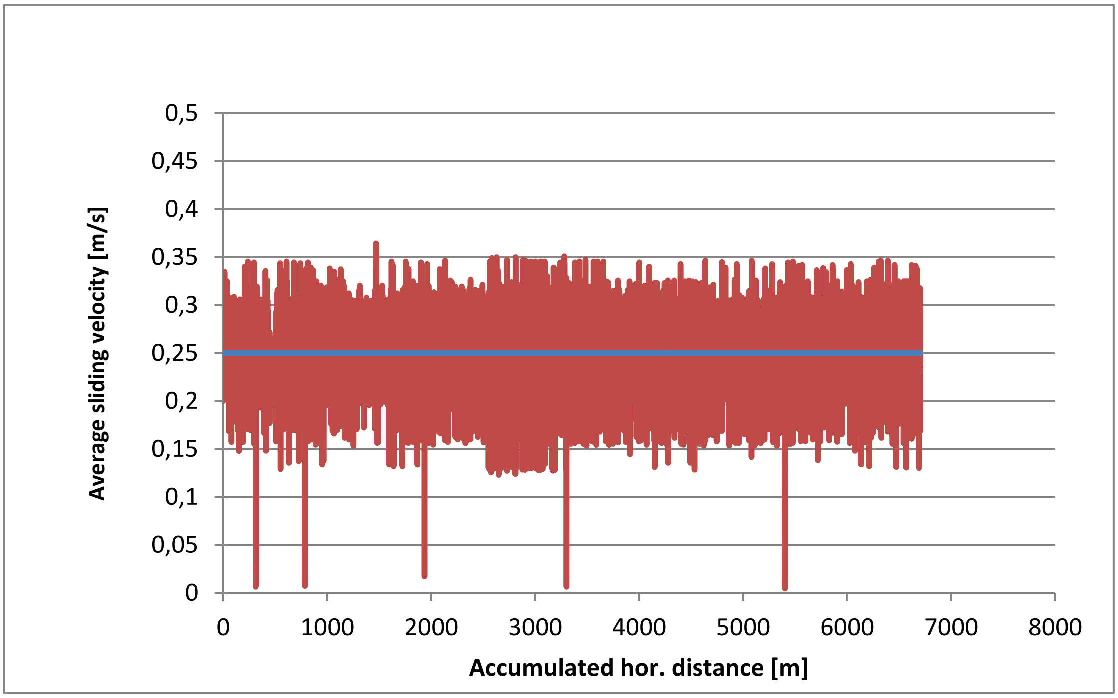

Figure 81Average sliding velocity B60 specimen with 1 MPa contact pressure and 25 cm/sec average sliding velocity

As shown in Figure 78 horizontal positions of the ice specimen are recorded. This makes it possible to analyze sliding velocity as a function of horizontal position. Logged average velocities have been analyzed to find if there are variations related to horizontal position. Figure 82 shows that there are no considerable differences in average velocity as function of horizontal position.

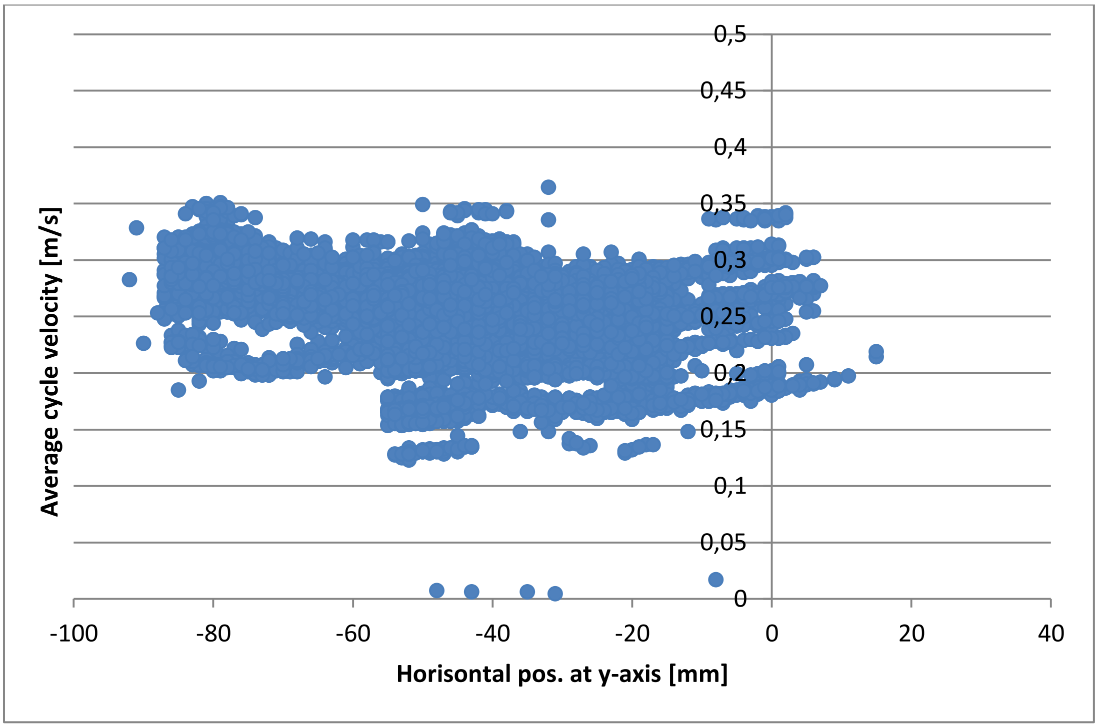

Figure 82 Average velocity as function of horizontal position. Average velocity = 25 cm/sec, 1MPa contact pressure

Figure 83 shows velocity as a function of horizontal position of the ice specimen, for B60 specimen 18 (1 MPa and 25 cm/sec). This is the velocity at a given position, not the average per cycle velocity.

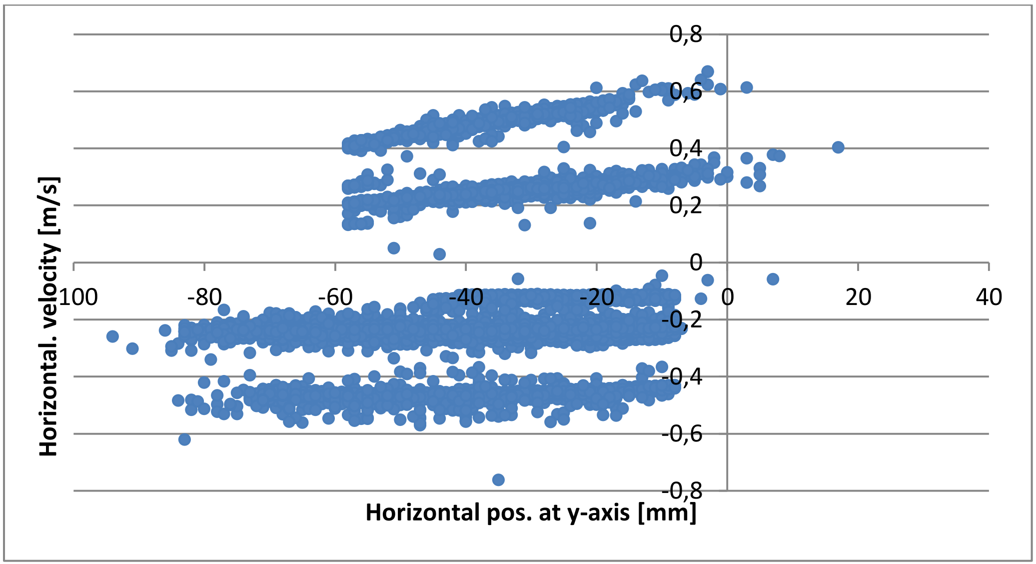

Figure 83 Horizontal velocity [m/s] as a function of horizontal position at y-axis [mm] for B60 specimen 18, average sliding velocity = 25 cm/sec and 1 MPa.

From Figure 83 it can be observed that negative velocity seem to be constant for negative coordinates, and that there is an acceleration when the ice is moving towards the center (y=0), after the ice has changed its sliding direction. From Figure 83 we can also say something about distribution of sampling. The lack of positive velocity values in the range from y= -100 to -60 indicates that there is more recordings when the ice is sliding in negative direction. As seen in Figure 84 variations in velocity occurs for the entire period of testing, and are therefore not depending of sliding distance.

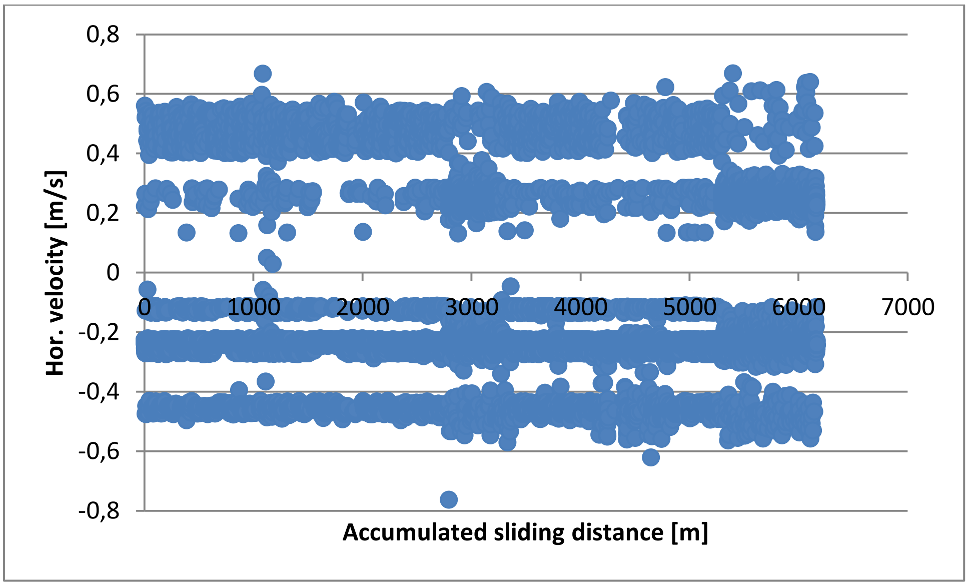

Figure 84 Horizontal velocity [m/s] as function of accumulated sliding distance [m]

Figure 86 is created from logged values of average vertical load [N] for a B60 test specimen with a contact pressure of 0,5 MPa. Figure 85 is from Densit specimen 13 where contact pressure was 1 MPa. These figures are found to be representative to present the average load variations. 1 MPa=4299 N and 0,5 MPa=2150 N. From the figures it can be seen that contact pressure is kept around the predefined values. As seen, load drops to zero on a regular basis. This happens when ice cylinders is worn out and have to be replaced. Labview starts recording data once testing is started/continued and the first logged values are small until desired load is obtained. It can also be used as a visualization of the distance before ice specimens has to be replaced for the different products. Ice consumption is found to correspond closely to the abrasion rate. B60 tests required an average of three times as much ice as Densit tests.

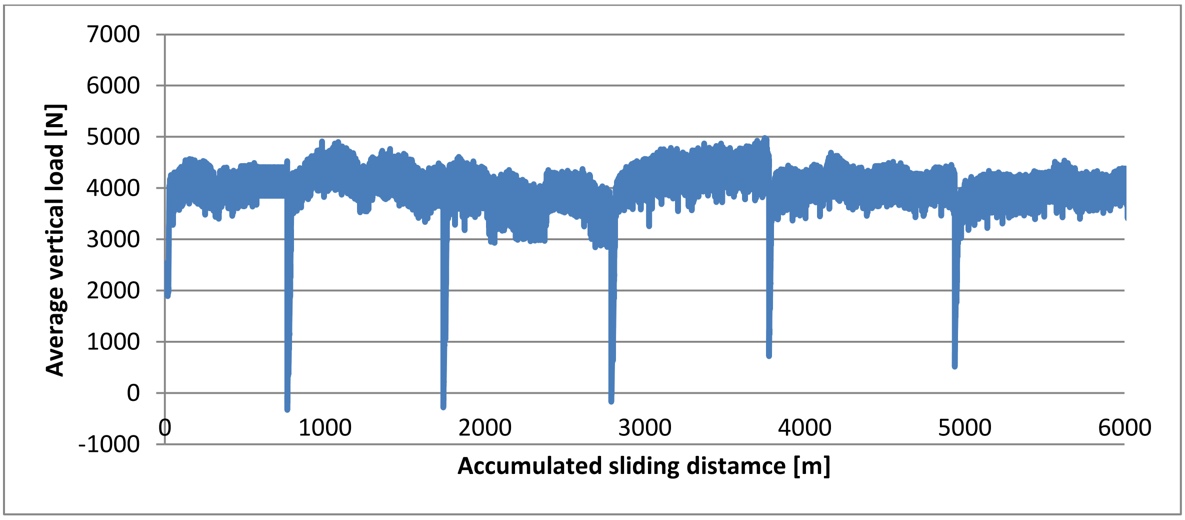

Figure 85 Average vertical load (cycle) [N] for test specimen 13 (Densit). Contact pressure = 1 MPa

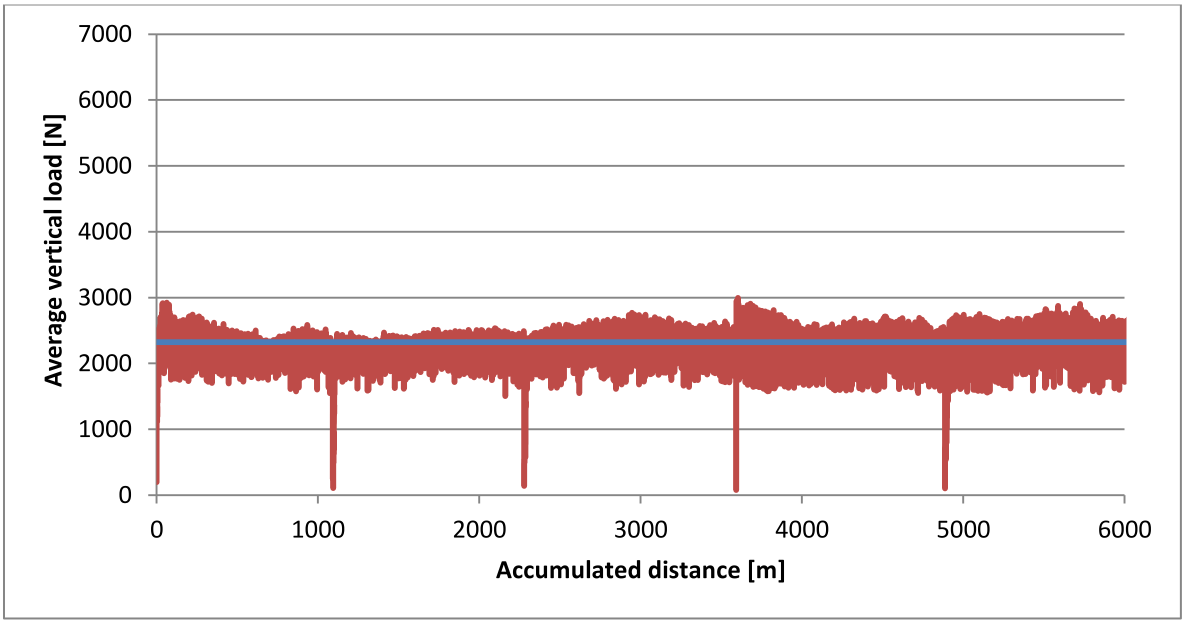

Figure 86 Average vertical load for a B60 specimen with 0,5 MPa contact pressure as function of accumulated distance

Vertical load as function of horizontal position can be seen in Figure 87, Figure 88 and Figure 89. Both for 0,5 MPa and 1 MPa tests there seem to be a decrease in registered load in the center of the test specimens.

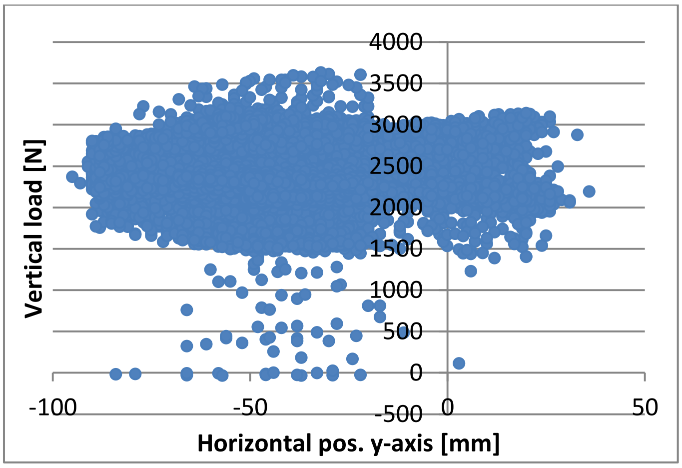

Figure 87 Vertical load as function of horizontal position for 0.5 MPa test. Rockbond. This is not the average cycle values

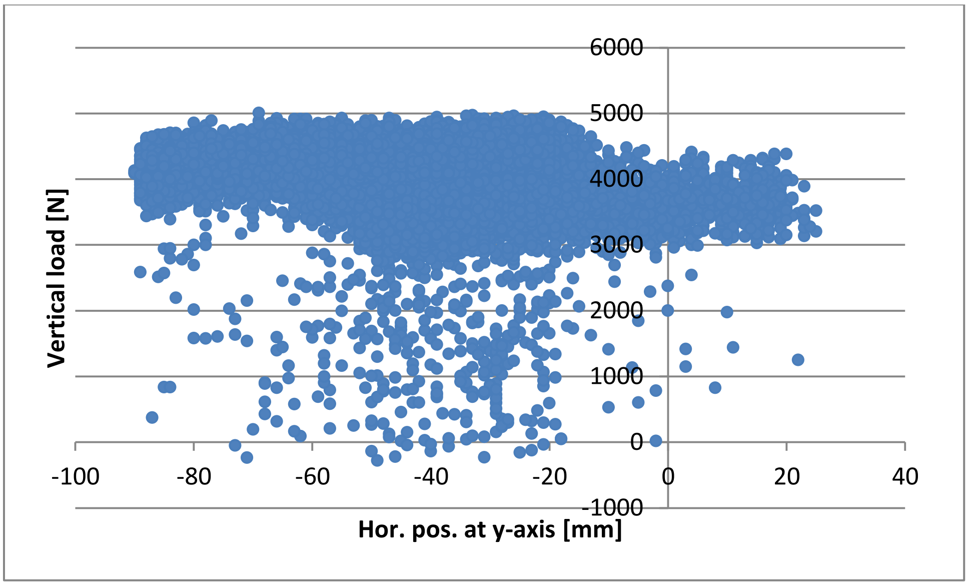

Figure 88Vertical load as function of horizontal position, B60 specimen 1 MPa contact pressure. Not average cycle values

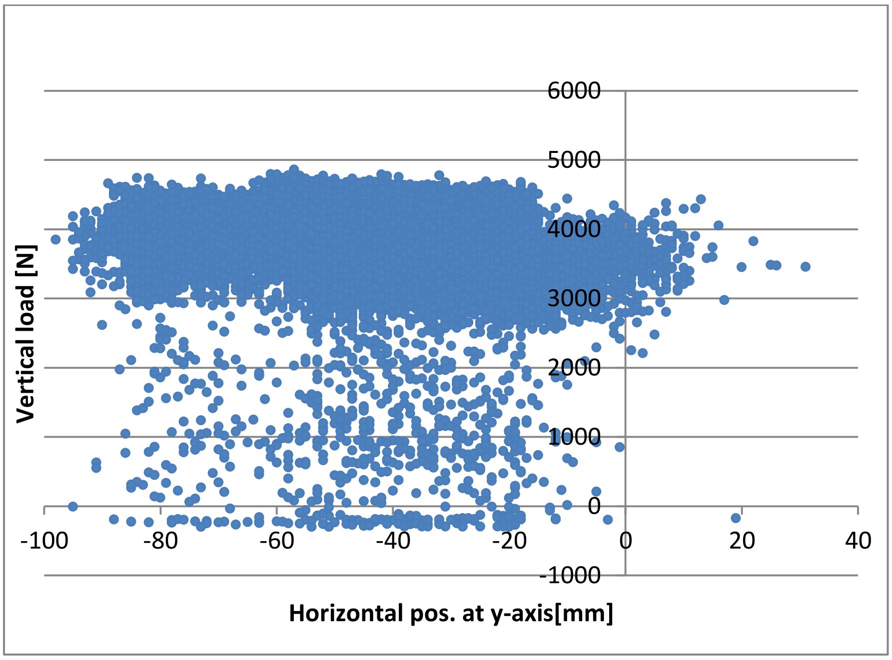

Figure 89 Vertical load as function of horizontal position, Densit, 1MPa contact pressure, 16 cm/sec

Figure 90 and Figure 91 shows temperature variations of the room temperature in the ice abrasion laboratory. The temperature has been found to change regularly in the range -8°C to -11^{0}C. It can also be seen that the temperature raises to almost -5^{0}C a couple of times. This is likely caused by opening of the laboratory door letting in hot air.

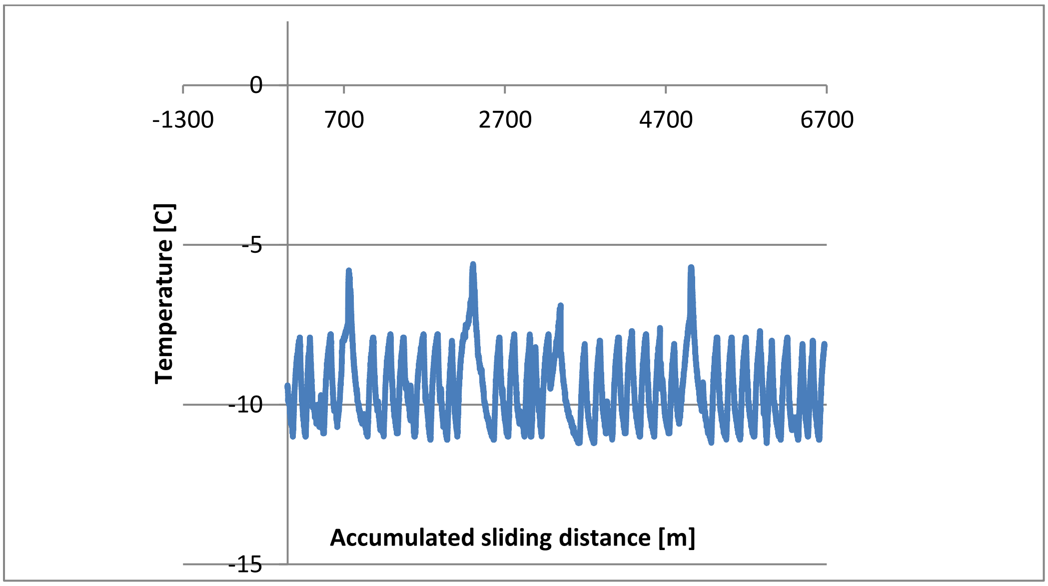

Figure 90 Temperature variations for test specimen 3 (Reforcetech) during testing. Temperature [°C]

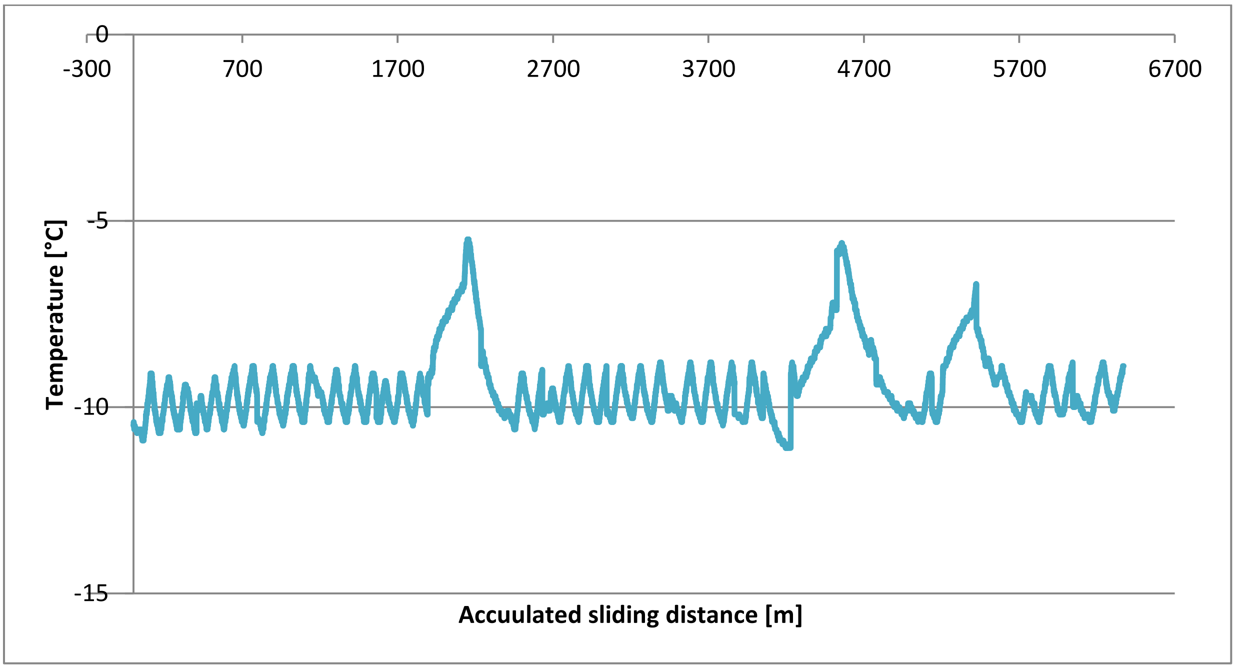

Figure 91 Temperature variations during testing for Specimen 15 (B70). T [°C]

Some specimens were casted with temperature sensors in the bottom, middle and top. These temperatures where recorded and Figure 92 shows the temperature history for one of these specimens. In addition to visual observations, temperature measurements was used to control the concrete surface temperature, and to keep it as low as possible without having water freezing   on the surface as described in (Nawwar, et al., 1988).

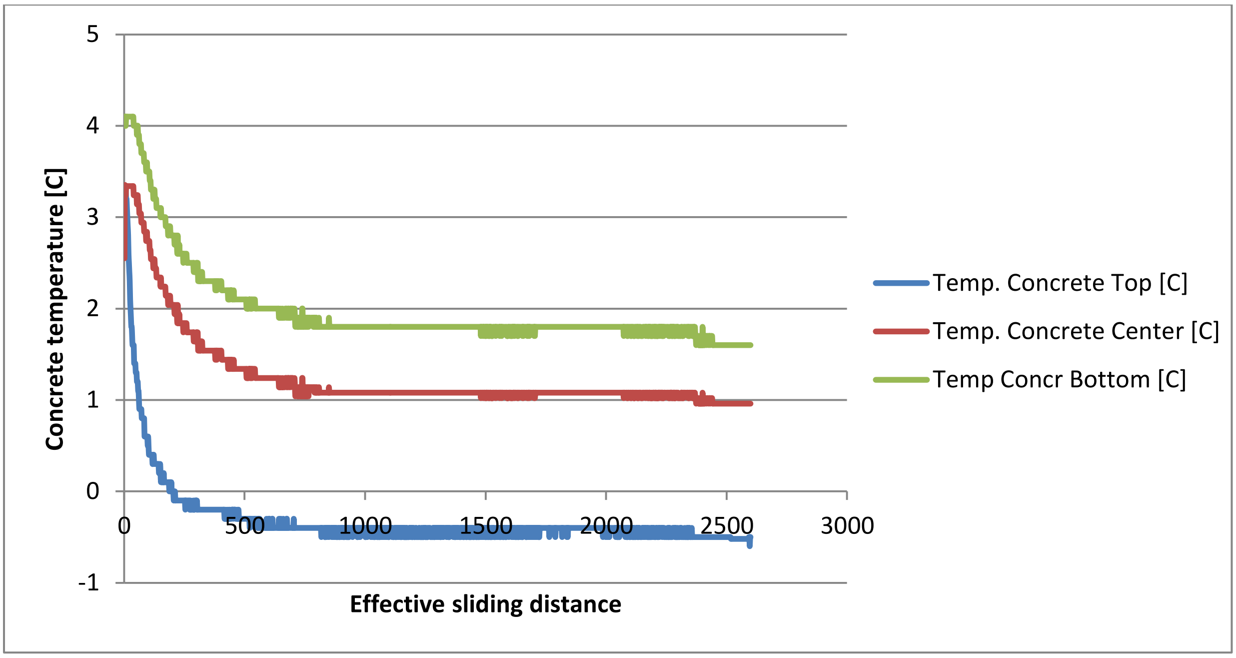

Figure 92 Concrete temperature at top, center and bottom [°C] as a function of effective sliding distance [m]

Figure 93 shows how vertical position of the piston, which creating the load, is changing during the tests. Since ice specimens are shorter than the container they are placed in, the piston has to be pushed down faster in the beginning, until the wanted load is obtained. From the figure it can be seen that there is an almost linear development from the point where the defined load is obtained. All specimens have this linear function.

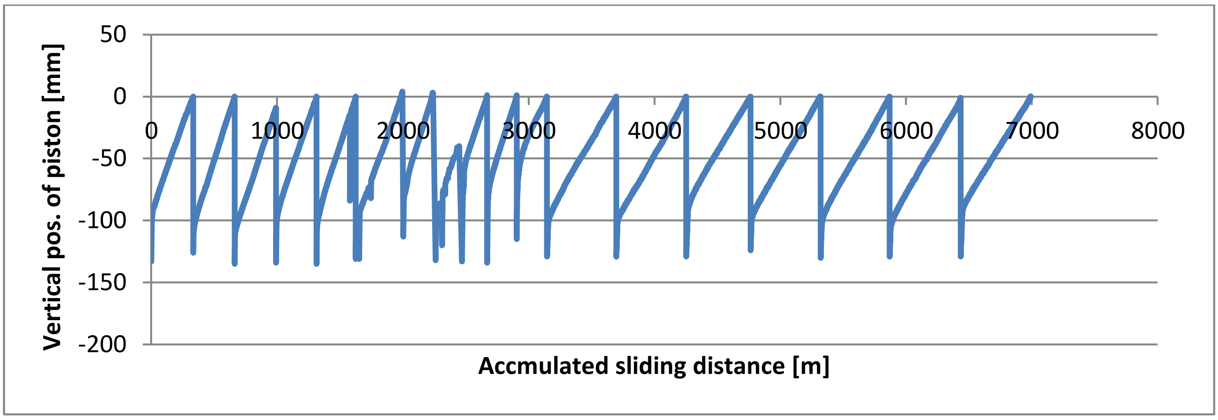

Figure 93 Vertical position of piston vs. accumulated sliding distance

To find an indication of the surface measurement precision, two specimens where measured twice with a couple of days in between. These measurements were compared to each other and the deviations between them were calculated. An average of 0,005 and 0,006 with a standard deviation 0,002 was measured. The calculated deviations are presented with the same number of decimals as the digital indicator uses to report deviations. The indicator is measuring in mm with a three decimal precision.

4.2 Bond tests

Bond strength test have been performed for Densit, Reforcetech and Rockbond according to NS-EN 1542. All tested products had a B60 as substrate concrete. In total 25 tests have been performed. The Densit and Reforcetech tests were performed as part of the project thesis last fall. Rockbond is tested in May 2013. For all products the thickness of the mortars was about 10 mm. For all tests a load rate of 0,05 MPa/s was used and the failure load was recorded by the test machine. Products and number of tests, number of test panels in the parentheses:

- Reforcetech: 10 (2)
- Densit: 5 (1)
- Rockbond: 10 (2)

Results are presented in
Table 15.

Table 15 Results pull-out tests [MPa]. Failure type according to NS-EN 1542.

		Test nr:	1	2	3	4	5	**Average**
Densit	Panel 1	Failure type	-	A/B	A/B	A/B	-	
		Bond strength [MPa]	-	0,78	3,19	2,42	-	**2,1**
Reforcetech	Panel 1	Load [kN]	A/B	A/B	A/B	A/B	A/B	
		Bond strength [MPa]	1,77	1,27	0,95	1,77	0,88	**1,3**
	Panel 2	Load [kN]	A/B	A/B	A/B	A/B	A/B	
		Bond strength [MPa]	2,11	2,69	2,28	2,27	2,19	**2,3**
Rockbond	Panel 1	Load [kN]	A/B	B/Y	A/B	A	A/B	
		Bond strength [MPa]	2,2	2,9	3	3,8	3	**3,0**
	Panel 2	Load [kN]	A	B/Y	B/Y	B/Y	A/B	
		Bond strength [MPa]	2,7	3,3	3,2	2,7	2,5	**2,8**

Results indicate that Rockbond has the best bond strength of the tested products. There is less data for Densit, but the results indicate that good bond strength is possible. Bond strength is presented as the failure strength [MPa] calculated from failure load [N] divided on surface area of the core.

Figure 94 Reforcetech panel after testing. The picture is illustrating the thickness of the repair mortars compared to the substrate concrete. Adhesion failure between substrate and repair mortar

Failure type is described according to NS-EN 1542:

- A: Cohesion failure in the concrete substrate (Figure 95)
- A/B: Adhesion failure between substrate and first layer (Figure 96)
- B:Cohesion failure in the first layer (Repair mortar in this case)
- B/Y: Adhesion failure between the last layer (B) and adhesive layer (Y) (Figure 97)

Figure 95 Failure of substrate concrete (A)

Figure 96 Adhesion failure between substrate and repair mortar (A/B)

Figure 97 Adhesion failure between repair mortar and adhesive layer

All failures occurred in the transition zone between substrate concrete and repair mortar for Densit and Reforcetech. Originally it was planned to test two Densit panels. However, all cores loosened from one of the panels when they were being drilled out.
For the Densit tests, which were performed, two cores loosened in the transition zone between substrate concrete and the repair mortar when preparing it for the pull-out test machine.

When testing Rockbond the first time, failure occurred in the zone between the mortar and epoxy-glue for all specimens. It was therefore decided to start over and glue steel dollies on the concrete once more and try again. To be safe, new and unopened araldite glue was used. As seen, there are four specimens with failure in the adhesive layer, four specimens with failure in the transition zone between mortar and substrate and two failures in the substrate concrete.

5 Discussion

5.1 Ice Abrasion

All repair mortars are found to have lower and more uniform abrasion than the two concretes. B60 and B70 surfaces can be characterized as more “catastrophic abrasion” (Fiorio, 2004) compared to the repair mortars, most likely due to the larger average particle/aggregate size. B60 is a standard offshore concrete, and all three repair mortars have considerably better abrasion resistance. Also B70, which according to ISO 19906 should have acceptable abrasion resistance, has better abrasion properties than the B60. All the tested products should therefore improve abrasion resistance if used to repair a structure casted with a standard B60 concrete. In new structures, it looks like it might be worth using B70 concrete instead of B60, as the results indicate that this will increase the abrasion resistance considerably. Densit is the product found to have the highest abrasion resistance, but also Reforcetech and Rockbond has good abrasion resistance. Pull-out strength tests also shows that it should be possible to get sufficient bond strength between tested repair mortars and the B60 substrate concrete.

Most previous studies have found a correlation between increased compressive strength and abrasion resistance. This is only partially confirmed by this study. Densit, which has the highest compressive strength, is also the product with the lowest abrasion for all test conditions. By just looking on the compressive strength, the B70 concrete should be the second best material. Abrasion tests shows that both Reforcetech and Rockbond have better abrasion resistance than the B70 concrete. There can be many explanations for this. Both repair mortars are fiber concrete products. Basalt fibers are used in Reforcetech and steel fibers in Rockbond. They also have a higher density than the B70 concrete. Houvinens finding indicates an increased resistance for higher densities. There is not enough data in this study to make a clear conclusion, but it is interesting results that should be investigated further. Tensile strength is closely related to compressive strength for unreinforced concrete, and the use of fiber reinforcement is increasing the tensile strength. It therefore seems more likely that abrasion resistance should be predicted as a function of the tensile strength rather than compressive strength, as Rockbond and Reforcetech has better abrasion resistance and tensile (flexural) strength than the B70 concrete.

Abrasion rate development is found to be stable, except for sandblasted specimens where abrasion rate is increasing for accumulated sliding distance. Steady abrasion rates are expected as the intention of plane cutting the specimens were to get straight to the stable-region abrasion described by (Itoh, et al., 1994). Results shows that the abrasion rates do not change considerably from 1,25 to 2,5 km. The tests run for 7,5 km also seem to confirm that the observed abrasion rates are representing steady-state abrasion. According to Itoh et.al (1994) abrasion rate in the surface- and transition region is higher than the steady-state abrasion (Ref. Figure 25). Because of this, the total abrasion of a structure exposed to a given distance of ice sliding is probably higher than the observed rates would indicate.

Abrasion rates of sandblasted specimens tend to get closer to the rates for the specimens who are not sandblasted and tested with the same sliding velocity and contact pressure. When sandblasting, it is mostly the cement paste that is being removed, making the surface rougher. Therefore, the reason for the lower abrasion on the rougher sandblasted surface could be due to higher volume fraction of aggregate on the surface. This could also explain why the abrasion rate seems to be increasing, as the removal of aggregates will give more abrasion of the paste for increased distances. Densit has lower D_{max} than B60, and it should therefore go faster to get to a more steady-state abrasion.

Aggregate usually has higher abrasion resistance than the paste. This is why specimens are grinded/cut to get a surface where the fraction between aggregate and paste reflects the average of the concrete. Since the volume fraction of paste is higher close to the surface, the abrasion rate will be higher down to a depth which better reflects the average distribution between aggregate and paste. Assuming a maximum particle size of 16 mm, this depth should be ≈> 5 mm, and for maximum particle size of 8 mm this depth should be ≈3 mm (Zheng, et al., 2002). Both the B60 and the B70 concrete have D_{max}=16mm, and the particle size of the repair mortars are definitely smaller, as seen at the pictures of representative test surfaces in Figure 34. The B60 specimens were saw-cut, and the tested surfaces would be approximately 50 mm from the original surface, and the surfaces should therefore be representative. This should also be the case for the repair mortars, assuming they have a maximum particle size of 8 mm or less. For the B70 the case is a bit different. It has only been cut a maximum of 4 mm and the fraction of paste might be higher than deeper into the specimen. B70 has however been tested for 7,5 km, without showing signs of a decrease in abrasion rate, indicating that the surfaces probably are representative. Repair mortars also seem to have stable abrasion rates. It cannot with complete certainty be said if the observed abrasion rates are values of the transition- or steady-state stage. However, 2,5 km of effective sliding with only small changes in abrasion rates indicates that it may be likely that the measured rates are steady-state rates. Anyways, the effect of having a surface which is not cut deep enough is that the observed abrasion rates can be higher than in a representative section of the concrete surface.

B60 seem to be a “weak” concrete that is cracking easily in the abrasion rig. Cracks is found to start develop in the bottom of the specimens, indicating that it is caused by tensile induced stress from bending moments. In his master thesis (Bøhn, 2012), Bøhn tries to give an explanation to why samples are cracking; *One or more of the components underneath the concrete specimen may not withstand the vertical load satisfactory. The result is that the concrete specimen is pushed down and given a small displacement*. This should mean that there are induced bending moments in the specimens.

To investigate this, a computer model with a moving concentrated load of 4,3 kN was created in *Robot Structural analysis* and *Focus konstruksjon*. The load was set to move within the stroke length of 200 mm and assumed to be concentrated in the center of the ice specimen. Figure 98 shows the statical system and the moment distribution for the possible load positions. The analysis shows that the bending moment is ≈ 0,19 kNm for the position where the concrete specimens tends to crack.

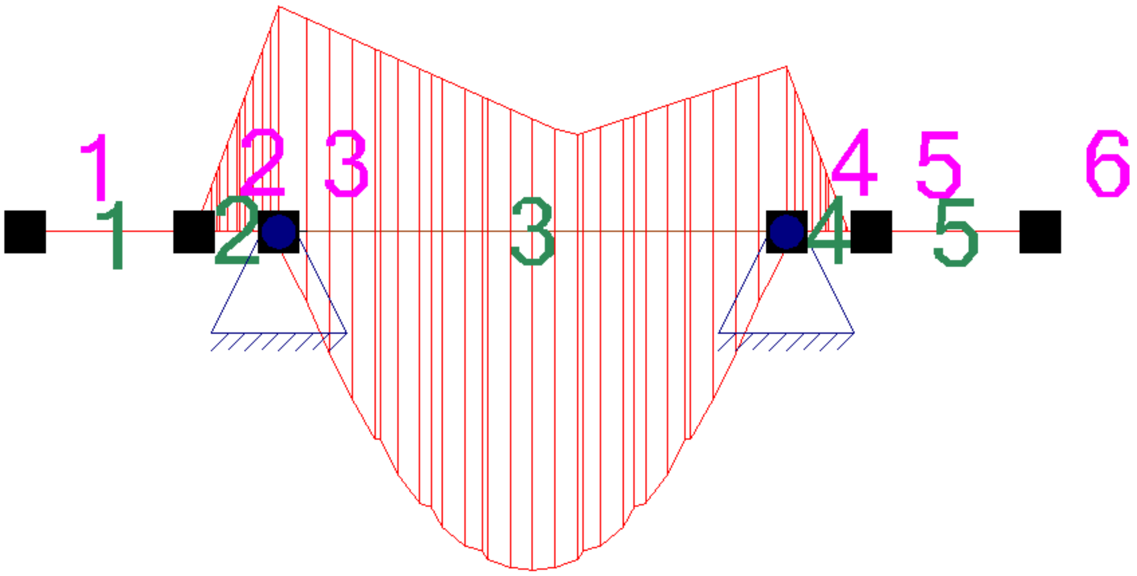

Figure 98 Statical system and moment distribution for the possible load positions

A critical parameter for concrete is tensile forces and the calculated bending moments are inducing tensile stress in the concrete.

F= Compressive and tensile force induced by support moment [N]
M: Calculated bending moment =0,19 kNm
h: height of concrete specimen =50 mm
b: width of concrete specimen = 100 mm
z: internal level arm = 34 mm
σ: Tensile stress [MPa]
$f_{ctm:}$ Tensile strength [MPa]
$f_{cm:}$ Compressive strength [MPa]

$$M = F * z$$

$$F = \frac{M}{z} = \frac{0,186}{0,034} * 1000[N]$$

$$F = \sigma_{.} * \frac{h}{2} * b * \frac{1}{2}$$

$$\sigma_{.} = \frac{4 * M}{z * h * b} = \frac{4 * F}{h * b} = \frac{4 * 5470}{100 * 50} = 4,37\ MPa\ [\frac{N}{mm^2}]$$

$$f_{ctm} = 2,12 * \ln\left(1 + \frac{f_{cm}}{10}\right) \quad \text{(Sørensen, 2009)}$$
$$\sigma_{.} = f_{ctm}$$

According to the made assumptions and calculations, the compressive strength to avoid cracking should be 72 MPa for concrete without reinforcement. According to NS-EN 1992-1-1:2004: Table 3.1 a B60 concrete is supposed to have $f_{ck,cube}$ = 75 MPa, which means that B60 seem to be a minimum quality for 1 MPa contact pressure. This seems reasonable considering that most of the B60 specimens cracked during testing. As showed in Table 14, B60 had an f_{cm}=74 MPa. Rockbond which has lower strength did not crack, which indicates that fiber steel reinforcement seem to have an positive effect on increasing tensile strength in addition to improving abrasion resistance and bond strength. According to (Cox, 2012) 30% fiber content by weight of cement is increasing the flexural strength with 91%.

One possible way to remove this problem is to use a stiffer plate under the sliding bearings. If the plate is stiff enough it will act as an elastic foundation and the chance for the concrete specimens to crack should be reduced. Addition of steel fiber reinforcement also seems to be an effective measure to avoid cracking. However, it seems like it also reduces the abrasion, which ordinarily is a positive effect. If an ordinary low strength concrete are to be tested, it is necessary to perform a test on a specimen where the abrasion properties is not affected by fibers, and this solution cannot be used. It could be considered to cast only the tensile zone with fibers or other reinforcement, leaving the abrasion zone at the surface with unchanged abrasion properties. Another option is to rebuild the ice abrasion rig and install an additional load cell. This gives three supports instead of two, and should therefore reduce the bending moments. An even better solution, if possible, is to measure the load in the ice specimen container, making it possible to remove the load cells under the sliding bearings.

There are of course uncertainties with these calculations and the purpose has only been to illustrate the possible effect of tensile strength as this seems to be a possible explanation.

Increase of contact pressure and following increased rate of abrasion are confirmed by many studies, also this one. The observed general trend is that all test run with a contact pressure of the 1 MPa has higher abrasion rates than the 0,5 MPa tests. Internal variations of abrasion rates for the specimens with the same test conditions are small, and when including possible sources of error in the measurement methods and equipment, and considering that there can be some variations in the quality of the specimens, results can be seen as reasonable.

Increasing the sliding velocity seems to decrease the abrasion rate. For the performed tests increased velocity gave lower abrasion rates for all specimens. As shown in Figure 30 (Itoh, et al., 1994) abrasion was found to change little for velocities in the range of 16-25 cm/sec. However, results from performed experiments in this study does show a noteworthy difference in abrasion for sliding velocity of 16 cm/s and 25 cm/s, which is much higher than could be expected when comparing to Itoh. One could say that increased velocity reduces abrasion, but the results do not give any good explanation why.

The abrasion tests have been performed by letting the ice slide parallel to the concrete surface. According to (Janson, 1988) parallel sliding is causing the highest abrasion. Thus the obtained results could be said to be conservative rates, making them more representative when choosing offshore concrete quality and thickness.

Roughness: The intention of calculating roughness was to look for a correlation between surface condition and abrasion rate. To make any distinctive conclusion from the analysis does however seem to be difficult. Calculated values are in general pointing in all directions, especially for Kurtosis and Skewness. In general there are high standard deviations, at the same time as the average abrasion rates for the different x-coordinates along the y-axis (Ref. appendix 1) does not change considerably. This might be explained by measurement errors, but calculated values for the areas unexposed for abrasion indicates that the roughness measurements should be valid.

Distance between each measurement is 2 cm along the y-axis. Roughness parameters will depend on the number of surface measurements they are calculated from. Shorter distance between measurements should be considered in the future to increase the reliability, and get more accurate calculations of the roughness parameters.

R_a and R_q seem to increase for all products, except Densit, for increased sliding distance. For Densit it seems as the roughness parameters are stabilizing quickly. A possible explanation is that the small average particle size of Densit compared to the other products is making the height difference between abraded particles and cement paste smaller than for other products. Or that "catastrophic wear" is smaller and more evenly distributed for Densit specimens. Therefore the surfaces profiles are experiencing less change, and the R_a and R_q will be more stable. If this is true, all the other products should experience similar stabilizing R_a and R_q if they are tested for a longer sliding distance.

Both (Fiorio, 2004) and (Mitjan, et al., 2002) points at increased wear for surfaces with higher initial R_a values. The variations in R_a for the tested specimens are small and the abrasion results indicate other parameters seem to be more important when abrasion rate is to be predicted. However, in the study of Fiorio the initial effect of Ra is found to disappear after 5 meters of sliding. Therefore this effect shouldn't be that important when sliding 2500 meters, something the results also seem to indicate, as specimens of Densit with high initial roughness values seems to get lower and similar to the low roughness to the other Densit specimens.

By looking a bit closer on the calculated roughness parameters there might be found a weak connection between surfaces with high kurtosis and lower abrasion. This can be seen for both Reforcetech and Rockbond. However, this relation is not found for all specimens with lower abrasion and no definite conclusion can be made. This does however corresponds to findings in (Sedlaeck, et al., 2006) and should therefore be looked further into.

Friction: Friction analysis indicates a couple of things. First of all, the average coefficient of friction seems to be independent on sliding distance, horizontal position and sliding velocity. There seem to have been registered only dynamic friction, as there are little or few measuring points on the outer edges of the specimens where static friction should be found. By looking on the results from Itho.et al (1994) the response to sliding velocity is to be expected. As can be seen on Figure 30, the friction coefficient is changing little for high velocities like those used in the experiments of this study. From the results there seem to a distinct correlation between friction and vertical load. As illustrated in Figure 76 the friction coefficient seems to stabilize for loads > 2500 N. As friction is the result of relationship between horizontal and vertical load this development is not that unlikely. Just a small change in horizontal loads increases the friction coefficient more at low loads compared to higher ones.

Lack of measurements for y=-90 to y=-100 in Figure 77 indicates that the static friction is not represented in the individual recorded values. As can be seen in Figure 77, there seem not to be any variation of dynamic friction as function of horizontal position at the surface, and the presentation of friction against sliding distance should therefore be valid and representative.

General test conditions:

The reliability of the ice abrasion rig and test conditions is important for two reasons. To compare results from the NTNU rig to other studies and real life conditions it is important to know the reliability test conditions and how they are varying. According to Table 4 (Hara, et al., 1995) there are certain parameters that should be fulfilled in order to obtain good and reliable abrasion results. Evaluated after these criteria the NTNU ice abrasion rig should give good results. However, analysis of test data shows that there are some uncertainties to consider. In this section ice abrasion rig and test conditions are evaluated.

Abrasion rates are presented as the average of the entire specimen, as wear per kilometer. There are many other ways it could have been presented, but for the purpose of this thesis it is found to be a sensible way of expressing the results. This is because the main purpose has been to evaluate abrasion resistance of different products and compare them to each other. The average values are calculated from 144 surface points and average values should therefore give a good indication of the variations between the different test specimens. Appendix 1 and 2 contains the average values along respectively x- and y-axis lines. It was considered to include a presentation of every single measured point. However, in this study a huge number of specimens have been tested, and abrasion is calculated at least twice for each of them. Therefore the average values have been found to give a good overview and be a good representation of total abrasion and difference between the various products and materials.

Average sliding velocity for each cycle corresponds to the values specified in the test program. Internal variations between tests run at same sliding velocity are found to be small. From the results it is clear that increasing the average sliding velocity from 16 cm/sec to 25 cm/sec influences the test conditions. Standard deviation of average velocity increased from 10% for 16 cm/sec to 18% for 25 cm/sec tests. The only parameter that can be changed in the Labview software in regard to horizontal velocity is horizontal RPM (velocity). Results obtained for tests run at lower velocities is therefore more reliable results than tests run at higher velocities. The sampling rate may explain some of these variations. The computer is supposed to register average values once each cycle, but as seen in Figure 78 these recordings has not been made in the same horizontal position. In Figure 83 there can be seen that the actual velocity are varying with horizontal position. So if the distance between the measurements is not 400 mm, but can be both shorter and longer, this might influence the calculated average values. However, it is difficult to say for sure as Figure 82 seems to indicate that the average values are having the same variations independent of horizontal position.

Average contact pressure and load history is found to be consistent for the specimens tested under the same conditions. However, pressure is adjusted by registered loads in the vertical load cells. When ice is consumed, load decreases and the ice abrasion rig starts to add more load by pushing the piston downwards. There is a time delay and the load drops until the test rig is able to adjust the position of the piston. This effect is compensated, by adding higher load than what is set in the software, and as Figure 85 and Figure 86 shows, the average is kept around the set values but it is never kept at a constant value. All tested products show this type of development and the internal difference of the results due to this should therefore be minimal. Another fact to consider is that the ice abrasion rig uses some time and distance before the piston is able to restore the load on the concrete surface after ice specimens are replaced. By comparing the average ice consumption for Densit and B60 test for contact pressure of 1 MPa, it is found that ice has to be replaced almost three times as often for the B60. Total accumulated distance where load is too low is therefore larger for specimens where ice has to be replaced often. This effect is however small, and with 2,5 km of effective sliding it is most certainly negligible. Average load also seem to be even over the sliding distance. But as shown in Figure 88 and Figure 89 there seem to be higher registered loads on the edges of the y-axis compared to the center of the specimens. This could be an explanation for the difference in abrasion seen on these places, as the abrasion results clearly indicate a connection between load and abrasion. This should be investigated further to see if it is the case for the whole specimen, not only one half. If so, either calibration of abrasion rates for the actual average load on each position, or report rates as a function of the abrasion in the midsection of the specimens should be considered. There is found no good explanations to why the load is higher in the edges.

As illustrated with the ATOS optical image scans there is tendency of increased abrasion, in particular for the products with highest rate of abrasion, on the edges of the specimens where the ice specimen turns. This effect was also found by Egil Møen. The analysis of sliding velocity as a function of horizontal position shows that the internal variations over the surface position are larger than the relatively small variations in average velocity. As showed in Figure 81 and Figure 82 variations of average velocities are the same over both sliding distance and horizontal position. But when analyzing the horizontal velocity (Figure 83) as function of horizontal position there is a distinctive difference at the edge and center of the specimen. When the ice turns, it is accelerated by the rig and the edges is therefore experiencing “low” and “high” velocities depending on which direction the ice is moving. Velocity is lower in these outer areas in close to 50 % of the ice exposed time. This can be a possible explanation to the uneven abrasion. Whether the increased load described in the previous section is a consequence of sliding velocities or something else is difficult to say.

Even though average velocity is what it is supposed to, the variations of actual velocity over the cross section are high and the highest registered values are almost two times the average velocity. Results presented in Figure 84 also indicate that this effect is unrelated to sliding distance. Results for tests run with the same velocities in the NTNU rig are therefore comparable to each other, but has limited direct comparability to other test rigs.

Experiments are supposed to be performed at -10° C. As showed in Figure 91 temperature is varying regularly during the tests. Since these variations occur for all tested specimens it should influence all them almost equally. In addition, results presented by (Nawwar, et al., 1988) indicate that for temperatures higher than -10°C there is small variations of abrasion. Measured abrasion in this study should therefore be representative for temperatures >- 10°C. If the effect of different temperatures is to be tested in the NTNU laboratory, it should be considered to improve the temperature control. When comparing to other studies at same temperatures this variation should at least be taken into consideration and mentioned, even if there is little pointing towards any connection between changing temperatures and variations of abrasion rates for the tests in this study.

Density measurement shows that there are some variations in the ice density with a standard deviation of 13 kg/ m^3. However, since each ice abrasion test uses in the range of 6-20 ice specimens, it is unlikely that this should influence the abrasion results. The fact that the measured ice density is lower than the theoretical shouldn’t be a problem, as reported density of sea ice seems to have greater variations and tends to be lower than the ice used in this this study. Density of ice in this study might be classified as high and conservative when comparing to real life exposure. The difference between seawater and fresh water ice has not been tested. Results by (Hara, et al., 1995) and (Itoh, et al., 1994) suggest that the difference are small for temperatures < -10°C and therefore the choice of ice should be irrelevant.

Control measurements of surfaces gave an average deviation of 0,005 mm. This is larger than the margin of error on the digital indicator, which is 0,003 mm according to the manufacture. However, there might be many explanations for this. To measure the exact same point for two independent measurements would be next to impossible. Small deviations of < 1 mm could give different measured deviations.

None of the above mentioned effects is likely to cause differences between products tested under the same conditions in the NTNU rig. All variations seem to be the similar for the different products and therefore the results can be compared to each other. However, the differences in observed load and horizontal velocities at the edges would suggest that comparability to other test rigs and studies are limited.

Measuring on broken specimens is a possible source of error. There has been put a lot of effort to make the conditions for how the specimens are measured as equal as possible. When measuring on the broken specimens there is a possibility that different positioning on the measurement table and reduced number of points that can be measured could cause some variations.

5.2 Bond tests

Even if there are some variations in strength, all products have high bond strength compared to usual requirements for repair mortars. A target is to achieve a bond strength > 2 MPa (Kværner Engineering, 2012), and based on the results, all tested repair mortars has this potential, even if there are some lower registered values.

Bond tests were performed according to NS-EN 1542 and a minimum three tests were performed for all panels. The variations in the results from the Densit tests are high, and difficult to explain. Reforcetech also shows a similar tendency with a distinct difference of average values of nearly 1 MPa between the two test panels. Pretreatment has been performed equally after the same procedures, and results should in principal be similar. This indicates that execution is critical and can easily affect the bond strength.

For Densit and Reforcetech all failures occurred in the transition zone between substrate and repair mortar. For Rockbond which had more even results there was a combination of different failures, from failure in substrate to failure in adhesion between repair mortar and the glue. This indicates that the observed strength is in the range of what is possible to achieve. In total, Rockbond is better than Densit which again is slightly better than Reforcetech. Rockbond has both the highest individual and average strength. The difference in average values between Densit and Reforcetech are small, but a higher maximum value is obtained for Densit, and shows that Densit has a potential to obtain bond strength, similar to Rockbond.

Rockbond has considerably lower compressive strength compared to Densit (and Reforcetech). Therefore it may be reasonable to propose that reinforcement fibers have positive effect on the bond strength, as well as the abrasion resistance. This also indicates that, as for abrasion resistance, tensile strength/capacity may be a more relevant parameter to measure and use to predict both bond strength capacity and abrasion resistance.

5.3 Further work

Some suggestions for things to investigate in future studies:

- Full-scale tests of the repair mortars (at least one) should be performed to evaluate how good results from the ice abrasion rig represent real abrasion in the field.
- Full scale tests should also be performed on possible application methods for repair products. This to see what it take, and if it is possible to get good bond in large scale for the tested repair mortars. As they all have fairly good abrasion and bond properties, this might be an important parameter influencing the decision on which product to use.
- Sandblasted specimens should be tested for increased distances to see if and when the abrasion rate is stabilizing.
- Find a way to avoid cracking of test specimens, results from Rockbond with low compressive strength indicates that fiber reinforcement and high tensile strength is beneficial. It should also be considered making some adjustments on the rig. Stiffer steel plate and/or more load cells should decrease the chance of specimens cracking.
- Fiber reinforcement also seems to be beneficial for improving abrasion resistance, and ice abrasion experiments investigating this as a parameter should be performed.
- Perform a study to evaluate the effect of increased sliding velocity, to find if the spread of average values are continuing to increase at even higher velocities and investigate why increased sliding velocity are giving reduced abrasion.
- Find the reason why load is higher in the edges when using the NTNU ice abrasion rig.
- Longer sliding distance for MapeCoat and Polyurethane specimens so abrasion resistance can be measured. The coatings should be applied on a strong substrate concrete to avoid cracking. A suggestion would be to use some of the already tested repair mortars specimen to this.
- Investigate the relationship between density and abrasion resistance.
- Learn how to use ATOS image scans to measure abrasion and calculate roughness parameters. Together with the manual measurements, this should increase the validity of the measurements.
- Investigate the influence of tensile strength of concrete and find if tensile or flexural strength can give a better indication of the abrasion resistance than compressive strength.
- Test specimens should be casted as double size specimen, and the saw-cut surface should be tested. This to ensure a representative fraction of aggregate and paste on the test surface.

6 Conclusion

- Seven different materials are tested; Densit, Reforcetech, Rockbond, B60, B70, MapeCoat and Polyurethane.
- Ice abrasion is investigated in the ice abrasion rig at department of structural engineering at NTNU. Pull-out bond strength tests are performed according to NS-EN 1542.
- Variables of the test conditions were: Sliding velocity, contact pressure and initial surface roughness.
- Abrasion rates after 2,5 km sliding : - Densit: 0,009-0,026 [mm/km]
  - Reforcetech: 0,014-0,033 [mm/km]
  - Rockbond: 0,024-0,042 [mm/km]
  - B70: 0,024-0,052 [mm/km]
  - B60: 0,025-0,090 [mm/km]
- No measurable abrasion at MapeCoat and Polyurethane specimens.
- Measured bond strength: - 0,78 - 3,19 MPa with an average of 2,10 for Densit
  - 0,95 - 2,69 MPa with an average of 1,82 for Reforcetech
  - 2,20 - 3,80 MPa with an average of 2,90 for Rockbond
- All repair mortars have better abrasion resistance than the standard B60 offshore concrete, and are therefore suitable as repair products, with Densit as the best product when it comes to abrasion resistance.
- B70, which according to ISO19906 has acceptable abrasion properties, shows better abrasion resistance than B60, but not as good as the repair mortars.
- Acceptable bond strength ($>\approx 2$ MPa) is possible for all the repair mortars and they are therefore suitable as repair products. Rockbond has the best bond strength properties.
- Increased sliding velocity reduces abrasion.
- Indications towards reduced abrasion for increased tensile strength.
- Indications towards that higher compressive strength and density are increasing the abrasion resistance.
- Steel reinforcement fibers seem to improve abrasion resistance and bond strength. It also has a positive effect on avoiding cracking of ice abrasion specimens.
- Increasing coefficient of friction for loads $< \approx 2000$ N.
- Friction coefficient is found to be independent of sliding velocities.
- Sources of error and uncertainties of the test method and equipment are influencing the specimens similarly and results are therefore comparable to each other and other studies in the NTNU rig.
- Used sampling rate only gives recordings of data for one half of the specimen surface.

7 References

Amaral Ron and Chong Leonal Ho Surface Roughness [Report]. - 2002.
Anderson Don L and Weeks Wilford F A theoretical Analysis of Sea-Ice strength [Article] // Transaction, American Geophysical Union. - 1958. - 4 : Vol. 39. - pp. 632-640.
Barrett T S, Stachowiak G W and Batchelor A W Effect of roughness and sliding speed on the wear and friction of ultra-high molecular weight polyethylene [Article] // Wear. - 1991. - Vol. 153. - pp. 331-350.
Bloomfield Dr. Max Roughness Concepts [Online] // Dr. Max Bloomfield: Researcher in Modeling and Simulation, Computation Center for Nanotechnology Innovation. - Rensselaer Polytechnic Institute, 06 01, 2006. - 04 04, 2013. - http://homepages.rpi.edu/~bloomm2/roughness.pdf.
Byggeindustrien Concrete under The Northern Lights. - 2012.
Bøhn Olav Ice abrasion of concrete, background theory and testing at the NTNU laboratory [Report]. - Trondheim: [s.n.], 2012.
Chaplin Martin Cubic Ice [Online] // Water structure and science. - London South Bank University, 04 10, 2012. - 05 11, 2013. - http://www.lsbu.ac.uk/water/ice1c.html.
Cox Gilbert ROCKBOND STAINLESS STEEL FIBRE. - Newton's Farm Estate, Wissington, Nayland, Suffolk: ROCKBONDSCP SPC LTD, 2012.
Dhir R K, Hewlett P C and Chan Y N Near-surface characteristics of concrete: abrasion resistance [Journal]. - [s.l.]: Materials and structures, 1991. - Vol. 24. - pp. 122-128.
Fiorio Bruno Wear characterization and degradation mechanisms of a concrete surface under ice friction [Journal] // Construction and building Materials. - [s.l.]: Construction and building Materials, 2004. - 19. - pp. 366-375.
Fosså Kjell Tore Improvement of the ice zone on structures for sub artic areas [Conference] // Proceedings of WORKSHOP "Ice Abrasion on Concrete Structures". - Helsingfors: The Nordic concrete Federation, 2007. - pp. 1-4.
Furukawa Yosinori Ice [Book Section] // Encyclopedia of Snow, Ice and Glaciers. - [s.l.]: Springer Netherlands, 2011. - pp- 557-560.
Garbacz Andrzej, Courard Luc and Kostana Katarzyna Characterization of concrete surface roughness and its relation to adhesion in repair systems [Article] // Materials Characterization. - 2006. - 4-5 : Vol. 56. - pp. 281-289.
Gorlenko O A Assessment of surface roughness parameters and their independence [Article] // Precision engineering. - 1981. - 3. - Vol. 2. - pp. 105-108.
Hanada M. [et al.] Abrasion rate of various materials due to movement of ice sheets [Conference] // Proceedings of the sixth International Offshore and polar Engineering conference. - Los Angeles: [s.n.], 1996. - Vol. 2. - pp. 433-437.
Hara F. [et al.] Evaluation of the test methods of abrasion by ice movements on the surface of reinforced concrete structures [Conference] // Proceedings of CONSEC'95: Concrete under Severe Conditions- Environment and loading. - Sapporo: [s.n.], 1995.
Hara F. [et al.] Prediction of the degree of abrasion of bridge piers by fresh water ice and the protective measures [Conference] // Proceedings of CONSEC'95: Concrete under Severe Conditions- Environment and loading. - Sapporo: [s.n.], 1995. - pp. 484-494.
Huovinen Seppo Abrasion of concrete by ice in artic sea structures [Report] / Laboratory of structural Engineering; Helsinki University of Technology. - Espoo: Technical research Centre of Finland, 1990. - 951-38-3572-3.
Huovinen Seppo Abrasion of concrete structures by ice [Journal] // Cement and Concrete Research. - 1993. - 1: Vol. 3. - pp. 69-82.

Ice [Online] // Wikipedia. - Wikimedia Foundation, 01 28, 2013. - 01 28, 2013. - http://en.wikipedia.org/wiki/Ice.
Itoh Y. [et al.] The mechanism of the abrasion of concrete structures due to the movement of ice sheets [Conference] // Proceedings of CONSEC'95: Concrete under Severe Conditions-Environment and loading. - Sapporo: [s.n.], 1995. - Volume one. - pp. 465-475.
Itoh Y., Tanak Y. and Saeki H. Estimation method for abrasion of concrete structures due to sea ice movement [Conference] // Proceedings of the fourth International Offshore and polar engineering conference. - Osaka: [s.n.], 1994. - Vol. 2. - pp. 545-552.
Jacobsen S. [et al.] Concrete Ice abrasion: Deteriation Mechanisms, testing and Modeling [Report]. - Trondheim: International Congress on Durability of Concrete, 2012.
Janson J. E. Results from the winter season 1988-1989, conclusion after three winters 1986-1989 [Report]. - [s.l.]: VBB, 1989.
Janson J.E Long term resistance of concrete offshore structures in ice environment [Conference] // International conference on offshore mechanics and artic engineering. - 1988.
Júlio Eduardo N.B.S, Branco Fernando A.B and Silva Victor D Concrete-to-concrete bond strength. Influence of the roughness of the substrate surface [Article] // Construction and Building Materials. - 2004. - 9: Vol. 18.
Kepconic Surface Roughness Measurements [Online] // kepconic.com. - Kalamazoo Electropolishing company, 04 04, 2013. - 04 04, 2013. - http://www.kepcoinc.com/downloads/Electro_Polishing/LC_surface-roughness-measurements.pdf.
Kim L. V [et al.] Ice-concrete abrasion study [Report]. - Trondheim: ICDC 2012, 2012.
Kirkhaug Joakim Rydningen Isabrasjon: Abrasjon- og heftprøving av reparasjonsmørtler [Report] : Project thesis. - Trondheim : [s.n.], 2012.
Kobrick Ryan, Klaus David and Street Jr. Kenneth W Validation of proposed metrics for two-body abrasion scratch test analysis standards [Journal]. - [s.l.]: Wear, 2011. - Vol. 270. - pp. 815-822.
Kværner Engineering Results from ice-abrasion and bond testing [Report]: Research report. - [s.l.]: Kværner Engineering, 2012.
Meddah Mohammed Seddik, Zitouni Salim and Belaabes Said Effect of content and particle size distribution of coarse and aggregate on the compressive strength of concrete [Journal]. - [s.l.] : Construction and building materials, 2010. - 4 : Vol. 24. - pp. 505-512.
Mitjan Kalin, Said Jahanmir and Lewis K Ives Effect of counterface roughness on abrasive wear of hydroxyapatite [Article] // Wear. - 2002. - 9-10: Vol. 252. - pp. 679-685.
Mitutoyo Corp. 1824 Digmatic Indicators.pdf [Online]. - 2013. - 11 12, 2012. - http://www.mitutoyo.com/wp-content/uploads/2012/11/1824_DigimaticIndicators.pdf.
Momayez A. [et al.] Comparison of methods for evaluating bond strength between concrete substrate and repair materials [Article] // Cement and concrete research 35. - [s.l.] : C, 2005. - pp. 748-757.
Morgan D. R. Compatibility of concrete repair materials and systems [Journal] // Construction and building materials. - February 1996. - 1: Vol. 10. - pp. 57-67.
Møen Egil Average abrasion depths for w/c = 0,60 concretes after 500 m accumulated (effective) sliding distance ice-concrete.pdf.
Møen Egil, Jacobsen Stefan and Myhra Håvard A Ice Abrasion Data On Concrete Structures- Overview [Conference] // Proceedings of WORKSHOP "Ice Abrasion on Concrete Structures". - Helsingfors: [s.n.], 2007.
Møen Egil, Jacobsen Stefan and Myhra Håvard Ice abrasion data on concrete structures- an overview state of the art [Report]. - Trondheim : SINTEF-COIN, 2007.

Nawwar A. M. and Malhotra V. M. Development of test method to determine the resistance of concrete to ice abrasion and/or impact [Report]. - [s.l.] : American Concrete Institute (ACI), 1988.
NIST Measures of Skewness and Kurtosis [Online] // Engineering statistics handbook. - National Institute of Standards and Technology, 04 04, 2013. - 04 04, 2013. - http://www.itl.nist.gov/div898/handbook/eda/section3/eda35b.htm.
NS-EN 1542 "Produkter og systemer for beskyttelse og reparasjon av betongkonstruksjoner. Prøvingsmetoder, Måling av heftfasthet ved uttrekksprøving". - [s.l.] : Standard Norge, 1999.
Ophardt Charles E Which is more dense - Ice or Liquid Water? [Online] // elmhurst.edu. - Elmhurst College, 01 01, 2003. - 04 12, 2013. - http://www.elmhurst.edu/~chm/vchembook/122Adensityice.html.
Petrovic J. J: Review: Mechanical properties of ice and snow [Article] // Journal of Material Science. - 2003. - 38. - 6 : Vol. 1.
Samen Ezeldin A. and Balaguru P. N. Bond behavior of Normal and High-strength Fiber Reinforced Concrete [Journal] // ACI Materials Journal. - [s.l.]: ACI, 1989. - 5: Vol. 86. - pp. 515-524.
Schulson Erland M. The structural and Mechanical Behavior of Ice [Article] // JOM. - 1999. - 51. - Vol. 2. - pp. 21-27.
Sedlacek Marko, Podgornik Bojan and Vizintin Joze Correlation between standard roughness parameters skewness and kurtosis and tribological behavior of contact surfaces [Article] // Tribology International. - 2012. - Vol. 48. - pp. 102-112.
Sedlacek M, Podgornik B and Vizintin J Influence of surface preparation on roughness parameters, friction and wear [Article] // Wear. - 2006. - 266. - pp. 482-287.
Sonebi M' and Khayat K H Testing Abrasion Resistance of High-Strength Concrete [Journal]. - [s.l.]: Cement, concrete and aggregates, 2001. - 1: Vol. 23. - pp. 34-43.
Sørensen Svein Ivar Betongkonstruksjoner. Beregning og dimensjonering etter Eurocode 2 [Book]. - Trondheim : Tapir Akademisk Forlag, 2009. - Vol. 1.
Talati Jigar Surface Roughness – Significance and symbol interpretation in drawing [Online] // hexagondesign.net. - Hexagon Product Development, 04 04, 2013. - 04 04, 2013. - http://www.hexagondesign.net/images/pdf/surface_roughness_jigar_talati.pdf.
Tatone Bryan Quantitative Characterization of Natural Rock Discontinuity [Report]. - 2009.
Technology overview [Online] // Schmitt industries INC. - Schmitt industries INC. - 04 03, 2013. - http://www.schmitt-ind.com/support-technical-papers-scatter.shtml.
Thomas T R Characterization of surface roughness [Article] // Precision Engineering. - 1981. - 2: Vol. 3. - pp. 97-104.
Timco G W and Weeks W F A review of the engineering properties of sea ice [Journal]. - [s.l.]: Cold Regions and Science Technology, 2009. - 60. - pp. 107-129.
Vorburger T V 8: Methods for Characterizing Surface Topography [Book Section] // Tutorials in Optics / ed. Moore Duncan T. - Massachusetts: Optical society of America, 2010.
Zeccihino Mike Characterizing Surface Quality: Why Average Roughness is Not Enough [Internet] // veeco.com. - Veeco, 04 04 2013. - 04 04 2013. - http://www.veeco.com/pdfs/appnotes/an511_roughness_64.pdf.
Zheng Jian Jun and Chun Qing Li Three-Dimensional Aggregate Density in Concrete with Wall Effect [Journal]. - [s.l.] : Material Journals, 2002. - 6: Vol. 99. - pp. 568-575.

List of figures

List of tables

List of formulas

Appendix 1: Abrasion rates. Summary along y-axis

Product:	Reforcetech					
Abrasion rate [mm/km] summary y-axis						
Specimen nr:	1	2	3	4	5	6
Contact pressure[MPa]:	1	1	1	1	0,5	0,5
Sliding velocity[cm/s]	16	25	16	25	16	16
x = 20	0,026	0,02	0,038	0,034	0,011	0,017
x = 30	0,029	0,024	0,025	0,021	0,017	0,014
x = 40	0,036	0,032	0,044	0,025	0,013	0,022
x = 50	0,031	0,027	0,026	0,026	0,02	0,019
x = 60	0,039	0,036	0,031	0,03	0,015	0,018
x = 70	0,038	0,033	0,019	0,025	0,013	0,018
x = 80	0,024	0,041	0,039	0,036	0,014	0,022
Average:	0,032	0,030	0,033	0,028	0,015	0,019

Product:	Densit									
Abrasion rate [mm/km] summary y-axis										
Specimen nr:	9	10	13	13(7,5 km)	14	14(7,5 km)	11	12	8 SB	39 SB
Contact pressure[MPa]:	1	1	1	1	1	1	0,5	0,5	1	1
Sliding velocity[cm/s]	16	16	25	25	25	25	16	16	16	16
x = 20	0,021	0,025	0,016	0,017	0,016	0,015	0,013	0,012	0,024	0,025
x = 30	0,023	0,025	0,013	0.012	0,019	0,021	0,009	0,015	0,027	0,022
x = 40	0,025	0,025	0,015	0.016	0,013	0,011	0,011	0,013	0,016	0,026
x = 50	0,030	0,027	0,015	0,013	0,012	0,017	0,011	0,010	0,021	0,022
x = 60	0,032	0,026	0,013	0,015	0,011	0,019	0,012	0,011	0,012	0,021
x = 70	0,030	0,028	0,015	0,017	0,015	0,017	0,013	0,007	0,021	0,026
x = 80	0,025	0,026	0,018	0,016	0,012	0,016	0,011	0,013	0,024	0,023
Average:	0,026	0,026	0,015	0,016	0,014	0,017	0,011	0,011	0,021	0,024

Product:	Rockbond					
Abrasion rate [mm/km] summary y-axis						
Specimen nr:	50	51	53	55	52	54
Contact pressure[MPa]:	1	1	1	1	0,5	0,5
Sliding velocity[cm/s]	16	16	25	25	16	16
x = 20	0,048	0,034	0,036	0,041	0,027	0,028
x = 30	0,037	0,041	0,037	0,033	0,014	0,017
x = 40	0,038	0,044	0,036	0,037	0,027	0,027
x = 50	0,039	0,038	0,028	0,038	0,024	0,028
x = 60	0,042	0,037	0,029	0,035	0,023	0,028
x = 70	0,036	0,038	0,037	0,038	0,024	0,021
x = 80	0,045	0,041	0,034	0,033	0,024	0,022
Average:	0,041	0,039	0,034	0,036	0,024	0,024

Product:	B70							
Abrasion rate [mm/km] summary y-axis								
Specimen nr:	15	17	19	19(7,5km)	20	20(7,5km)	16	18
Contact pressure[MPa]:	1	1	1	1	1	1	0,5	0,5
Sliding velocity[cm/s]	16	16	25	25	25	25	16	16
20	0,051	0,056	0,031	0,029	0,048	0,053	0,028	0,03
30	0,056	0,048	0,034	0,037	0,048	0,047	0,029	0,027
40	0,054	0,042	0,035	0,035	0,043	0,044	0,024	0,022
50	0,048	0,044	0,031	0,040	0,044	0,046	0,024	0,025
60	0,049	0,048	0,031	0,034	0,046	0,047	0,021	0,025
70	0,052	0,052	0,032	0,033	0,043	0,045	0,024	0,026
80	0,055	0,053	0,031	0,030	0,047	0,052	0,021	0,022
Average:	0,052	0,050	0,032	0,034	0,047	0,048	0,024	0,024

Product:	B60							
Abrasion rate [mm/km] summary y-axis								
Specimen nr:	33	36	34	35	31	32	37 SB	38 SB
Contact pressure[MPa]:	1	1	1	1	0,5	0,5	1	1
Sliding velocity[cm/s]	16	16	25	25	16	16	16	16
20	0,094	0,078	0,071	0,093	0,023	0,037	0,072306	0,069
30	0,099	0,093	0,073	0,087	0,030	0,035	0,073265	0,075
40	0,086	0,087	0,068	0,081	0,027	0,032	0,058007	0,071
50	0,087	0,086	0,065	0,077	0,022	0,028	0,069847	0,072
60	0,088	0,089	0,071	0,085	0,025	0,032	0,074889	0,07
70	0,089	0,092	0,073	0,089	0,030	0,033	0,07428	0,073
80	0,089457	0,09	0,073	0,087	0,024	0,031	0,076866	0,083
Average:	0,090	0,088	0,071	0,085	0,025	0,03200	0,072	0,073

Product:	Epoxies: MapeCoat and Polyuretahne					
Abrasion rate [mm/km] summary y-axis						
Specimen nr:	21(M)	22(M)	24(P)	26(P)		
Contact pressure[MPa]:	1	1	1	1		
Sliding velocity[cm/s]	16	16	16	16		
X = 20	0,000	-0,002	0,001	0,002		
X = 30	0,000	-0,001	-0,002	-0,003		
X = 40	0,001	0,002	0,001	-0,002		
X = 50	0,004	0,003	0,004	-0,002		
X = 60	0,001	-0,002	-0,003	0,004		
X = 70	-0,002	-0,002	0,000	0,003		
X = 80	-0,003	0,003	-0,002	0,000		
Average:	0,000	0,000	0,000	0,000	#DIV/0!	#DIV/0!

Appendix 2: Abrasion rates. Summary along x-axis:

Abrasion rate [mm/km]summary x-axis						
Product:	Reforcetech					
Specimen nr:	1	2	3	4	5	6
Contact pressure[MPa]:	1	1	1	1	0,5	0,5
Sliding velocity[cm/s]	16	25	16	25	16	16
y= -100	0,032	0,024	0,030	0,038	0,018	0,022
y= -80	0,030	0,026	0,034	0,037	0,020	0,026
y= -60	0,033	0,034	0,031	0,022	0,015	0,027
y= -40	0,039	0,033	0,034	0,024	0,014	0,016
y= -20	0,026	0,040	0,027	0,024	0,015	0,022
y= 0	0,022	0,027	0,026	0,023	0,011	0,014
y= 20	0,030	0,032	0,026	0,024	0,014	0,018
y= 40	0,057	0,032	0,036	0,026	0,016	0,022
y= 60	0,024	0,033	0,030	0,027	0,010	0,012
y= 80	0,031	0,025	0,034	0,033	0,017	0,021
y= 100	0,024	0,025	0,038	0,031	0,016	0,005
Average	0,032	0,030	0,033	0,028	0,015	0,019

Abrasion rate [mm/km]summary x-axis										
Product:	Densit									
Specimen nr:	9	10	13	13(7,5 km)	14	14(7,5 km)	11	12	8 SB	39 SB
Contact pressure[MPa]:	1	1	1	1	1	1	0,5	0,5	1	1
Sliding velocity[cm/s]	16	16	25	25	25	25	16	16	16	16
y= -100	0,029	0,030	0,015	0,015	0,014	0,017	0,027	0,004	0,013	0,017
y= -80	0,024	0,026	0,021	0,020	0,011	0,015	0,028	0,011	0,015	0,025
y= -60	0,021	0,031	0,018	0,019	0,010	0,015	0,020	0,013	0,024	0,024
y= -40	0,023	0,030	0,015	0,014	0,014	0,020	0,016	0,017	0,017	0,017
y= -20	0,021	0,021	0,016	0,017	0,010	0,012	0,008	0,006	0,024	0,024
y= 0	0,027	0,021	0,010	0,016	0,017	0,016	0,006	0,012	0,030	0,030
y= 20	0,030	0,023	0,012	0,014	0,022	0,018	0,005	0,005	0,021	0,021
y= 40	0,034	0,024	0,013	0,013	0,017	0,014	0,008	0,020	0,016	0,018
y= 60	0,029	0,028	0,016	0,018	0,012	0,019	0,004	0,011	0,024	0,024
y= 80	0,028	0,026	0,018	0,018	0,014	0,021	0,000	0,015	0,028	0,028
y= 100	0,024	0,025	0,012	0,017	0,014	0,017	0,004	0,013	0,020	0,020
Average	0,027	0,026	0,015	0,016	0,014	0,017	0,011	0,011	0,021	0,024

Abrasion rate [mm/km]summary x-axis						
Specimen nr:	Rockbond					
Contact pressure[MPa]:	50	51	53	55	52	54
Sliding velocity[cm/s]	1	1	1	1	0,5	0,5
Sliding velocity	16	16	25	25	16	16
y= -100	0,038	0,035	0,023	0,027	0,022	0,023
y= -80	0,044	0,039	0,039	0,036	0,030	0,029
y= -60	0,042	0,046	0,031	0,042	0,029	0,026
y= -40	0,038	0,036	0,028	0,032	0,026	0,025
y= -20	0,037	0,039	0,026	0,033	0,024	0,024
y= 0	0,038	0,038	0,038	0,034	0,019	0,021
y= 20	0,041	0,034	0,027	0,037	0,024	0,025
y= 40	0,036	0,037	0,039	0,032	0,028	0,024
y= 60	0,047	0,036	0,041	0,042	0,027	0,028
y= 80	0,045	0,042	0,036	0,039	0,031	0,030
y= 100	0,041	0,034	0,035	0,037	0,022	0,022
Average	0,041	0,039	0,034	0,036	0,024	0,024

Abrasion rate [mm/km]summary x-axis								
Product:	B70							
Specimen nr:	15	17	19	19(7,5km)	20	20(7,5km)	16	18
Contact pressure[MPa]:	1	1	1	1	1	1	0,5	0,5
Sliding velocity[cm/s]	16	16	25	25	25	25	16	16
y= -100	0,047	0,048	0,026	0,028	0,050	0,047	0,020	0,025
y= -80	0,071	0,052	0,025	0,029	0,050	0,053	0,029	0,025
y= -60	0,051	0,063	0,036	0,036	0,043	0,052	0,025	0,027
y= -40	0,044	0,052	0,035	0,035	0,043	0,048	0,024	0,023
y= -20	0,049	0,048	0,031	0,032	0,045	0,048	0,024	0,023
y= 0	0,051	0,049	0,034	0,033	0,047	0,046	0,021	0,023
y= 20	0,050	0,047	0,029	0,031	0,046	0,047	0,022	0,021
y= 40	0,049	0,046	0,029	0,036	0,043	0,049	0,026	0,026
y= 60	0,053	0,050	0,037	0,042	0,051	0,047	0,025	0,026
y= 80	0,054	0,051	0,035	0,036	0,048	0,051	0,021	0,027
y= 100	0,051	0,047	0,032	0,033	0,048	0,044	0,025	0,022
Average	0,052	0,050	0,032	0,034	0,047	0,048	0,024	0,024

Abrasion rate [mm/km]summary x-axis								
Product:	B60							
Specimen nr:	33	36	34	35	31	32	37 SB	38 SB
Contact pressure[MPa]:	1	1	1	1	0,5	0,5	1	1
Sliding velocity[cm/s]	16	16	25	25	16	16	16	16
y= -100	0,088	0,083	0,069	0,080	0,026	0,020	0,065	0,065
y= -80	0,093	0,100	0,068	0,096	0,024	0,036	0,072	0,087
y= -60	0,095	0,099	0,074	0,098	0,024	0,043	0,078	0,076
y= -40	0,097	0,087	0,071	0,077	0,021	0,029	0,082	0,083
y= -20	0,086	0,087	0,070	0,082	0,023	0,031	0,066	0,067
y= 0	0,087	0,078	0,071	0,081	0,024	0,028	0,080	0,073
y= 20	0,083	0,082	0,071	0,079	0,028	0,030	0,068	0,069
y= 40	0,086	0,081	0,073	0,094	0,019	0,029	0,078	0,072
y= 60	0,099	0,095	0,075	0,086	0,032	0,031	0,073	0,074
y= 80	0,097	0,097	0,076	0,086	0,031	0,037	0,072	0,075
y= 100	0,085	0,080	0,067	0,082	0,025	0,032	0,064	0,071
Average	0,090	0,088	0,071	0,085	0,025	0,031	0,072	0,073

Abrasion rate [mm/km]summary x-axis						
Specimen nr:	Epoxies: MapeCoat and Polyuretahne					
Contact pressure[MPa]:	21(M)	22(M)	24(P)	26(P)		
Sliding velocity[cm/s]	1	1	1	1		
Sliding velocity	16	16	16	16		
y= -100	0,000	0,001	0,000	-0,002		
y= -80	0,000	-0,002	0,000	0,001		
y= -60	-0,002	-0,002	-0,002	0,002		
y= -40	-0,003	0,003	0,004	0,001		
y= -20	-0,002	-0,003	-0,003	0,003		
y= 0	0,001	0,004	0,001	0,000		
y= 20	0,001	0,001	-0,002	-0,003		
y= 40	-0,002	-0,002	0,002	-0,002		
y= 60	0,001	-0,002	0,001	-0,002		
y= 80	0,004	0,001	0,004	0,001		
y= 100	0,001	-0,002	0,000	-0,001		
Average	0,000	0,000	0,000	0,000		

Appendix 3: Roughness parameters and standard deviations

Densit Distance [km]		Specimen:	9	10	11	12	13	14	SBB1	SBB2
Ra	0,00	Ra	0,058	0,019	0,103	0,153	0,023	0,017	0,438	0,324
		Std.dev	0,023	0,008	0,049	0,073	0,008	0,007	0,016	0,014
		%	40 %	41 %	47 %	48 %	35 %	43 %	4 %	4 %
	1,25	Ra	0,071	0,021	0,121	0,176	0,056	0,056	0,427	0,557
		Std.dev	0,035	0,004	0,063	0,132	0,039	0,039	0,021	0,034
		%	50 %	21 %	52 %	75 %	69 %	69 %	5 %	6 %
	2,50	Ra	0,042	0,021	0,025	0,023	0,039	0,021	0,425	0,371
		Std.dev	0,005	0,004	0,008	0,007	0,005	0,005	0,011	0,013
		%	12 %	21 %	31 %	28 %	12 %	24 %	3 %	4 %
	5,00	Ra		0,023			0,023			
		Std.dev		0,006			0,008			
		%		26 %			35 %			
	7,50	Ra		0,061			0,021			
		Std.dev		0,023			0,002			
		%		38 %			10 %			
Rq	0,00	Rq	0,097	0,023	0,180	0,208	0,026	0,020	0,432	0,432
		Std.dev	0,051	0,010	0,097	0,105	0,008	0,006	0,029	0,025
		%	52 %	45 %	54 %	51 %	31 %	31 %	7 %	6 %
	1,25	Rq	0,072	0,026	0,201	0,266	0,087	0,087	0,524	0,124
		Std.dev	0,026	0,006	0,103	0,103	0,055	0,055	0,031	0,061
		%	36 %	23 %	51 %	39 %	63 %	63 %	6 %	49 %
	2,50	Rq	0,068	0,026	0,029	0,029	0,055	0,025	0,591	0,500
		Std.dev	0,011	0,006	0,007	0,008	0,008	0,006	0,019	0,026
		%	16 %	23 %	25 %	27 %	15 %	23 %	3 %	5 %
	5,00	Rq		0,028			0,027			
		Std.dev		0,007			0,008			
		%		25 %			30 %			
	7,50	Rq		0,061			0,042			
		Std.dev		0,044			0,005			
		%		72 %			11 %			
Rk	0,00	Rk	6,736	-0,286	7,786	2,340	-0,742	-0,475	1,995	1,623
		Std.dev	4,059	0,151	3,878	1,325	0,439	0,353	1,482	1,021
		%	60 %	53 %	50 %	57 %	59 %	74 %	74 %	63 %
	1,25	Rk	6,856	0,037	6,102	2,795	6,861	6,961	2,750	6,479
		Std.dev	4,337	0,024	3,733	3,733	4,742	4,432	0,156	0,272
		%	63 %	65 %	61 %	134 %	69 %	64 %	6 %	4 %
	2,50	Rk	1,307	0,037	0,385	0,926	0,576	0,915	2,645	2,155
		Std.dev	1,037	0,024	0,263	0,757	0,372	0,649	0,361	0,398
		%	79 %	65 %	68 %	82 %	65 %	71 %	14 %	18 %
	5,00	Rk		-0,051			5,668			
		Std.dev		0,014			1,524			
		%		27 %			27 %			
	7,50	Rk		0,966			0,383			
		Std.dev		0,302			0,144			
		%		31 %			38 %			
Rsk	0,00	Rsk	-2,148	0,283	-2,377	-1,414	0,113	-0,016	0,155	-0,222
		Std.dev	1,096	0,075	0,944	0,631	0,097	0,008	0,014	1,300
		%	51 %	27 %	40 %	45 %	86 %	50 %	9 %	585 %
	1,25	Rsk	6,102	0,128	-1,808	-0,440	-1,935	-1,935	0,013	-2,015
		Std.dev	3,950	0,089	1,226	1,809	1,665	1,665	0,498	1,074
		%	65 %	69 %	68 %	411 %	86 %	86 %	3967 %	53 %
	2,50	Rsk	-0,491	0,128	0,321	-0,683	0,089	-0,115	-0,387	-1,221
		Std.dev	1,256	0,043	1,081	1,016	0,144	1,034	1,359	1,122
		%	256 %	34 %	337 %	149 %	161 %	895 %	351 %	92 %
	5,00	Rsk		0,213			0,148			
		Std.dev		0,162			0,099			
		%		76 %			67 %			
	7,50	Rsk		-0,742			-0,816			
		Std.dev		0,861			1,050			
		%		116 %			129 %			

	Reforcetech	Specimen	1	2	3	4	5	6
Parameter	Distance [km]							
Ra [mm]	0,00	Ra	0,050	0,050	0,048	0,045	0,056	0,039
		Std.dev	0,029	0,027	0,028	0,013	0,033	0,018
		%	58 %	54 %	58 %	29 %	59 %	46 %
	1,25	Ra	0,070	0,333	0,030	0,032	0,058	0,038
		Std.dev	0,055	0,052	0,019	0,007	0,011	0,047
		%	77 %	16 %	63 %	23 %	20 %	123 %
	2,50	Ra	0,136	0,140	0,084	0,075	0,082	0,046
		Std.dev	0,051	0,074	0,069	0,050	0,059	0,050
		%	38 %	53 %	83 %	67 %	71 %	109 %
Rq [mm]	0,00	Rq	0,199	0,105	0,076	0,068	0,087	0,055
		Std.dev	0,060	0,082	0,044	0,030	0,063	0,083
		%	30 %	79 %	57 %	44 %	73 %	150 %
	1,25	Rq	0,189	0,532	0,037	0,050	0,120	0,057
		Std.dev	0,115	0,097	0,041	0,053	0,039	0,085
		%	61 %	18 %	111 %	105 %	33 %	149 %
	2,50	Rq	0,218	0,191	0,119	0,129	0,135	0,073
		Std.dev	0,078	0,107	0,090	0,088	0,102	0,091
		%	36 %	56 %	76 %	69 %	76 %	124 %
Rk	0,00	Rk	5,632	0,642	5,985	4,951	4,853	0,038
		Std.dev	3,142	3,874	4,456	4,273	3,500	0,385
		%	56 %	603 %	74 %	86 %	72 %	1003 %
	1,25	Rk	6,031	3,549	3,140	3,684	6,256	2,112
		Std.dev	2,811	2,462	3,624	3,601	4,180	4,686
		%	47 %	69 %	115 %	98 %	67 %	222 %
	2,50	Rk	5,221	2,684	6,041	8,515	6,742	3,110
		Std.dev	3,028	3,609	2,994	2,378	3,722	4,559
		%	58 %	134 %	50 %	28 %	55 %	147 %
Rsk	0,00	Rsk	-0,018	-0,438	1,902	-1,774	-0,594	-0,379
		Std.dev	0,877	1,313	1,545	1,053	1,982	1,253
		%	4912 %	300 %	81 %	59 %	334 %	331 %
	1,25	Rsk	1,332	-0,216	0,485	-0,418	1,572	0,641
		Std.dev	0,166	0,630	1,306	1,366	1,705	1,529
		%	12 %	291 %	269 %	327 %	108 %	239 %
	2,50	Rsk	-0,018	1,386	2,364	-1,174	1,910	0,447
		Std.dev	0,002	0,978	0,545	1,212	1,467	0,916
		%	10 %	71 %	23 %	103 %	77 %	205 %

Rockbond Parameter	Distance [km]	Specimen	50	51	52	53	54	55
Ra [mm]	0,00	Ra	0,046	0,044	0,050	0,071	0,038	0,075
		Std.dev	0,018	0,021	0,020	0,015	0,008	0,048
		%	39 %	49 %	40 %	21 %	20 %	64 %
	1,25	Ra	0,070	0,066	0,055	0,106	0,043	0,113
		Std.dev	0,030	0,024	0,037	0,063	0,034	0,050
		%	43 %	37 %	68 %	59 %	80 %	44 %
	2,50	Ra	0,093	0,102	0,066	0,105	0,052	0,130
		Std.dev	0,043	0,063	0,033	0,074	0,037	0,092
		%	46 %	62 %	51 %	71 %	72 %	71 %
Rq [mm]	0,00	Rq	0,066	0,060	0,072	0,104	0,055	0,105
		Std.dev	0,029	0,038	0,036	0,049	0,015	0,071
		%	45 %	63 %	50 %	47 %	27 %	68 %
	1,25	Rq	0,088	0,099	0,044	0,045	0,065	0,085
		Std.dev	0,037	0,042	0,019	0,026	0,023	0,020
		%	42 %	42 %	43 %	58 %	35 %	23 %
	2,50	Rq	0,128	0,154	0,090	0,172	0,071	0,176
		Std.dev	0,058	0,109	0,052	0,133	0,045	0,140
		%	45 %	70 %	57 %	77 %	64 %	79 %
Rk	0,00	Rk	2,332	1,627	2,522	2,297	3,460	3,651
		Std.dev	1,408	1,144	1,616	1,652	1,459	1,585
		%	60 %	70 %	64 %	72 %	42 %	43 %
	1,25	Rk	2,124	1,125	3,257	2,759	3,646	2,525
		Std.dev	0,803	0,597	1,975	0,918	1,302	1,371
		%	38 %	53 %	61 %	33 %	36 %	54 %
	2,50	Rk	3,285	3,647	3,123	6,203	2,420	2,712
		Std.dev	1,385	2,033	1,670	2,070	1,342	1,562
		%	42 %	56 %	53 %	33 %	55 %	58 %
Rsk	0,00	Rsk	-0,772	-0,750	-0,176	-0,989	0,696	-1,101
		Std.dev	1,185	1,064	1,504	0,248	1,556	1,496
		%	153 %	142 %	854 %	25 %	224 %	136 %
	1,25	Rsk	-0,503	-0,633	-0,907	-1,250	-0,724	-0,397
		Std.dev	0,347	1,033	1,440	0,313	1,256	0,936
		%	69 %	163 %	159 %	25 %	174 %	236 %
	2,50	Rsk	-0,973	-0,906	-1,493	-2,206	-0,679	-0,601
		Std.dev	0,839	1,336	0,970	0,653	1,274	1,382
		%	86 %	147 %	65 %	30 %	188 %	230 %

B70		Specimen	15	16	17	18	19	20
	Distance [km]							
Ra	0,000	Ra	0,039	0,029	0,022	0,031	0,041	0,016
		Std.dev	0,019	0,008	0,009	0,008	0,048	0,005
		%	48 %	28 %	42 %	27 %	118 %	28 %
	1,250	Ra	0,103	0,100	0,041	0,100	0,100	0,048
		Std.dev	0,014	0,024	0,024	0,020	0,033	0,010
		%	14 %	24 %	58 %	20 %	33 %	21 %
	2,500	Ra	0,139	0,143	0,060	0,169	0,170	0,097
		Std.dev	0,018	0,071	0,034	0,035	0,045	0,055
		%	13 %	49 %	56 %	21 %	27 %	56 %
	5,000	Ra	0,142					0,139
		Std.dev						
		%	106 %					0 %
	7,500	Ra	0,150					0,157
		Std.dev						
		%	0 %					0 %
Rq	0,000	Rq	0,058	0,038	0,024	0,038	0,061	0,020
		Std.dev	0,036	0,010	0,009	0,010	0,022	0,005
		%	61 %	26 %	39 %	27 %	36 %	23 %
	1,250	Rq	0,168	0,075	0,060	0,002	0,080	0,066
		Std.dev	0,025	0,024	0,018	0,033	0,023	0,015
		%	15 %	31 %	30 %	1809 %	29 %	22 %
	2,500	Rq	0,204	0,190	0,087	0,281	0,120	0,159
		Std.dev	0,259	0,097	0,055	0,610	0,077	0,084
		%	127 %	51 %	63 %	217 %	65 %	53 %
	5,000	Rq	0,237					0,263
		Std.dev	0,070					0,175
		%	30 %					67 %
	7,500	Rq	0,266					0,247
		Std.dev	0,124					0,099
		%	47 %					40 %
Rk	0,000	Rk	3,696	1,096	1,203	0,480	1,253	0,186
		Std.dev	1,330	2,509	0,529	1,516	1,793	0,820
		%	36 %	229 %	44 %	316 %	143 %	441 %
	1,250	Rk	3,850	2,259	2,524	3,200	5,700	2,247
		Std.dev	4,938	1,418	1,127	1,024	1,715	2,575
		%	128 %	63 %	45 %	32 %	30 %	115 %
	2,500	Rk	3,456	2,095	2,453	2,106	5,160	2,119
		Std.dev	1,690	1,231	2,546	2,461	1,388	2,568
		%	49 %	59 %	104 %	117 %	27 %	121 %
	5,000	Rk	3,257					2,246
		Std.dev						
		%	0 %					0 %
	7,500	Rk	3,009					3,102
		Std.dev						
		%	0 %					0 %
Rsk	0,000	Rsk	-0,238	-0,475	-0,123	0,403	0,013	0,140
		Std.dev	1,699	0,973	0,287	0,797	0,014	0,639
		%	714 %	205 %	233 %	198 %	107 %	457 %
	1,250	Rsk	-0,907	0,002	-0,300	0,300	0,300	0,257
		Std.dev	1,440	1,025	0,070	1,059	1,369	1,298
		%	159 %	65705 %	23 %	353 %	456 %	505 %
	2,500	Rsk	-0,885	-1,415	0,398	-0,405	1,236	0,326
		Std.dev	1,596	0,895	0,933	1,532	1,827	1,849
		%	180 %	63 %	234 %	378 %	148 %	568 %
	5,000	Rsk	-0,926					-0,483
		Std.dev	0,569					1,237
		%	61 %					256 %
	7,500	Rsk	-0,886					-1,529
		Std.dev	0,658					1,225
		%	74 %					80 %

B60 Parameter	Distance [km]	Specimen	31*	32*	33*	34,000	35*	36,000	32sb	33sb
Ra [mm]	0,000	Ra	0,088	0,047	0,100	0,028	0,074	0,063	0,284	0,186
		Std.dev	0,035	0,038	0,080	0,013	0,034	0,097	0,040	0,038
		%	40 %	82 %	80 %	45 %	46 %	155 %	14 %	20 %
	1 (1,25)	Ra	0,064	0,067	0,120	0,131	0,124	0,240	0,315	0,186
		Std.dev	0,022	0,025	0,049	0,084	0,033	0,102	0,064	0,032
		%	35 %	37 %	41 %	64 %	26 %	43 %	20 %	17 %
	1,25 (2,5)	Ra	0,396	0,230	0,141	0,096		0,194		
		Std.dev	0,012	0,402	0,153	0,092		0,160		
		%	3 %	175 %	109 %	96 %		82 %		
Rq [mm]	0,000	Rq	0,135	0,071	0,139	0,040	0,106	0,096	0,193	0,186
		Std.dev	0,060	0,072	0,052	0,022	0,059	0,087	0,043	0,184
		%	45 %	102 %	37 %	55 %	56 %	90 %	22 %	99 %
	1 (1,25)	Rq	0,106	0,112	0,195	0,198	0,286	0,321	0,213	0,312
		Std.dev	0,050	0,052	0,065	0,119	0,062	0,073	0,028	0,045
		%	47 %	46 %	33 %	60 %	22 %	23 %	13 %	14 %
	1,25 (2,5)	Rq	0,444	0,388	0,208	0,129		0,260		
		Std.dev	0,020	0,070	0,023	0,027		0,046		
		%	5 %	18 %	11 %	21 %		18 %		
Rk	0,000	Rk	4,542	3,781	3,603	2,752	2,530	1,600	2,513	5,208
		Std.dev	2,358	3,098	4,359	2,382	3,146	3,662	0,817	1,553
		%	52 %	82 %	121 %	87 %	124 %	229 %	33 %	30 %
	1 (1,25)	Rk	6,557	5,790	3,855	3,595	3,458	1,257	4,876	5,208
		Std.dev	4,050	3,626	2,986	1,716	2,237	2,080	1,306	1,664
		%	62 %	63 %	77 %	48 %	65 %	166 %	27 %	32 %
	1,25 (2,5)	Rk	2,661	5,251	3,768	1,346		3,048		
		Std.dev	2,489	4,238	4,504	3,556		4,055		
		%	94 %	81 %	120 %	264 %		133 %		
Rsk	0,000	Rsk	0,679	-1,694	-1,066	-0,824	-0,119	-0,903	-0,903	-0,374
		Std.dev	1,524	0,760	1,451	1,044	1,134	1,017	1,339	1,055
		%	225 %	45 %	136 %	127 %	956 %	113 %	148 %	282 %
	1 (1,25)	Rsk	1,855	1,700	-0,547	-1,349	0,254	-0,840	-1,845	-0,374
		Std.dev	1,418	1,168	1,024	0,715	0,857	0,568	1,239	0,956
		%	76 %	69 %	187 %	53 %	337 %	68 %	67 %	255 %
	1,25 (2,5)	Rsk	-0,636	-0,278	-1,484	-0,576		-1,719		
		Std.dev	1,251	1,033	1,319	1,291		1,025		
		%	197 %	372 %	89 %	224 %		60 %		

MapeCoat and Polyuretahne		Specimen	m1	m2	P1	p2
Parameter	Distance [km]					
Ra [mm]	0,000	Ra	0,020	0,019	0,031	0,025
		Std.dev	0,010	0,014	0,024	0,022
		%	47 %	71 %	77 %	89 %
	1,250	Ra	0,022	0,016	0,032	0,024
		Std.dev	0,012	0,008	0,011	0,006
		%	56 %	51 %	35 %	25 %
	2,500	Ra		0,018		
		Std.dev		0,012		
		%		70 %		
Rq [mm]	0,000	Rq	0,024	0,018	0,039	0,034
		Std.dev	0,011	0,005	0,005	0,004
		%	46 %	29 %	14 %	12 %
	1,250	Rq	0,026	0,022	0,040	0,033
		Std.dev	0,016	0,011	0,014	0,018
		%	61 %	50 %	34 %	56 %
	2,500	Rq		0,029		
		Std.dev		0,006		
		%		21 %		
Rk	0,000	Rk	4,520	4,502	3,437	7,280
		Std.dev	0,787	1,255	1,091	3,377
		%	17 %	28 %	32 %	46 %
	1,250	Rk	4,767	4,757	3,773	10,136
		Std.dev	1,236	1,022	1,362	1,097
		%	26 %	21 %	36 %	11 %
	2,500	Rk		5,558		
		Std.dev		1,367		
		%		25 %		
Rsk	0,000	Rsk	0,064	0,064	0,041	0,181
		Std.dev	0,029	0,508	0,209	0,192
		%	44 %	797 %	514 %	106 %
	1,250	Rsk	0,087	0,085	0,001	-0,186
		Std.dev	0,090	0,104	0,136	0,269
		%	103 %	122 %	11057 %	-145 %
	2,500	Rsk		0,029		
		Std.dev		0,036		
		%		126 %		

Appendix 4 Ice abrasion rig quick guide and test procedures

This appendix is a quick guide on how to use and operate the NTNU ice abrasion rig. The rig is built at NTNU and the performed tests of this study have given a great insight on how the rig is working. This includes everyday operating procedures and on how to avoid problems and thus be able to run tests more efficient. Problems and unforeseen events that occurred using the ice abrasion rig is described so that they can be avoided in the future.

The following equipment and tools should be available when using the ice abrasion rig: Silicone based lubricant, Oil, Wrench, mallet, flat head screwdriver, Gaffer tape, anti-freeze liquid (on spray bottle), extra rubber rings.

Ice: One of the first things that should be done is to make ice. This could be done either by drilling out cores from ice sheets or by filling plastic cylinders with water and freeze them in a freezer. If the latter method is chosen there are a couple of things to be aware of:
First and foremost, there should be made enough ice before testing is started, so that unwanted stop caused by a higher consumption than the capacity of production is avoided.
The volume expansion when water freezes to ice generates huge forces on the plastic cylinder used to make ice specimens. An unwanted consequence of this is that the plastic cylinders seem to have limited capacity to withstand the forces from this expansion, and is therefore cracking easily. A large number of the plastic cylinders made for this study cracked in the freezer causing a problem to produce enough ice. Having too few cylinders made it necessary to postpone some tests, so that enough ice could be made available. Even small cracks make the cylinders unable to keep water from leaking out, and are therefore making them useless. However, instead of throwing them away gaffer tape has been found to be a useful product. Small cracks can be taped and cracked cylinders can be used at least a couple of extra times. The used plastic material is obviously too weak and it should be considered to make cylinders from a stronger material like for instance PVC-plastic.

Already produced ice can be stored in the ice abrasion laboratory. However, ice that has been stored over longer time periods was found to melt slowly, even if the laboratory temperature is -10^{0}C. Another challenge is that the fuse, for the circuit where the temperature regulator is connected, blows for none apparent reason. The ice abrasion laboratory is good insulated and a blown fuse during the night is not too critical. However, if the fuse is not turned back on within a day or so, all the stored ice will melt completely. It is therefore recommended to store ice in the freezer for periods where the laboratory is not kept under regular observation.

A last tip is not to fill the cylinders completely with water, as the height of the specimens is going to be too high for the ice container in the ice abrasion rig,

Testing: After completing initial surface treatment and measurement, the specimen is ready to be mounted in the ice abrasion rig. If the specimen is taken straight from room temperature the concrete surface are going to be warm. Placing it in the freezer for half an hour before testing is found to reduce the surface temperature to approximately 0^{0}C.

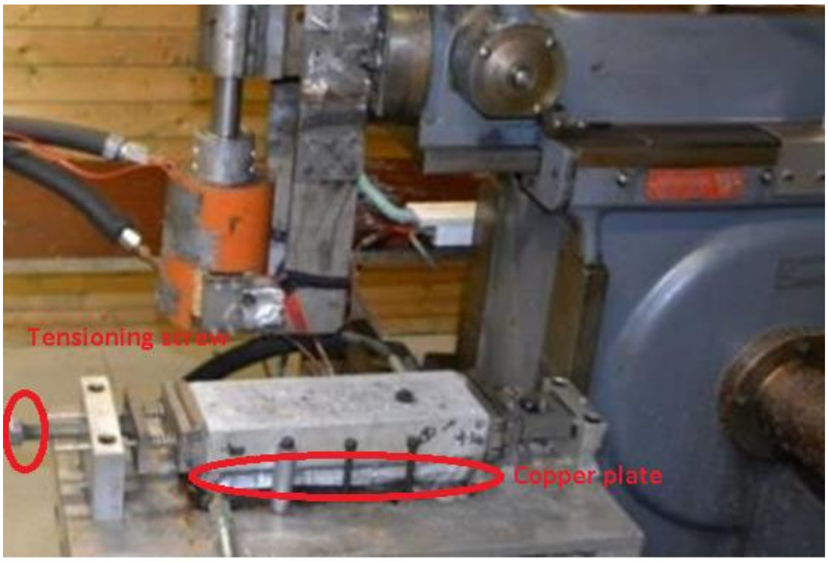

Picture 1Concrete specimen placed in the test rig

Test specimens should be placed on the copper bedding and before tightening the tensioning screw (showed in Picture 1) the vertical load cells should be calibrated. This is done so that the load cells can register applied ice load. Calibration is done by entering the calibration tab in “Isabrasiv” program in Labview. In the calibration tab, click on the “zero” buttons for both vertical load cells, as showed in Picture 2.

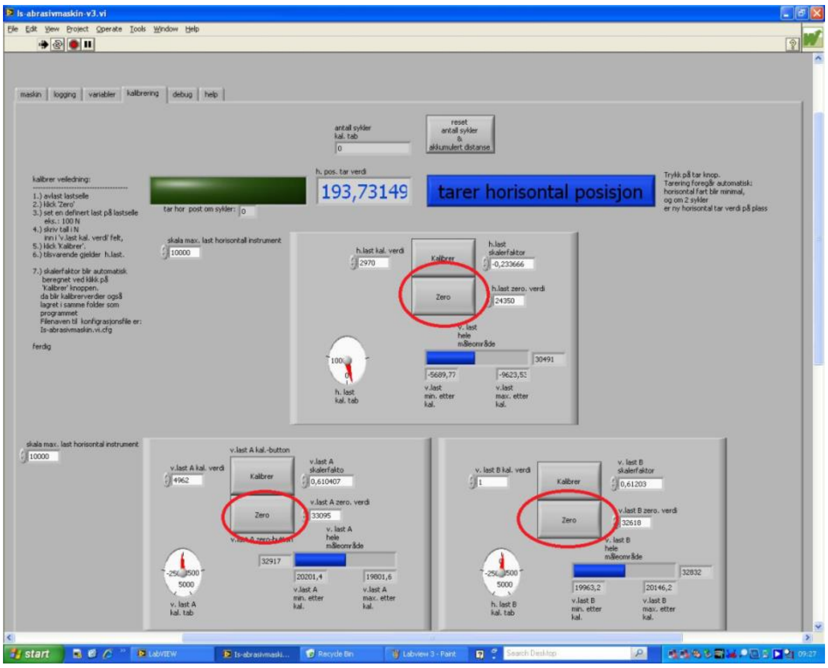

Picture 2 Calibration of load cells. Calibration buttons inside the red rings.

After this is done the tensioning screw should be tightened so that the specimen is kept in place during testing. In order to get meaningful values of horizontal load and thus also friction the next thing to do is to calibrate the horizontal load cell. This is done the same way as the vertical cells are calibrated. After calibration is performed ice can be placed in the ice container and the bedding could be swung back under the ice. It is important that the concrete specimen is placed with its center under the center of the ice specimen container, as showed in Picture 3.

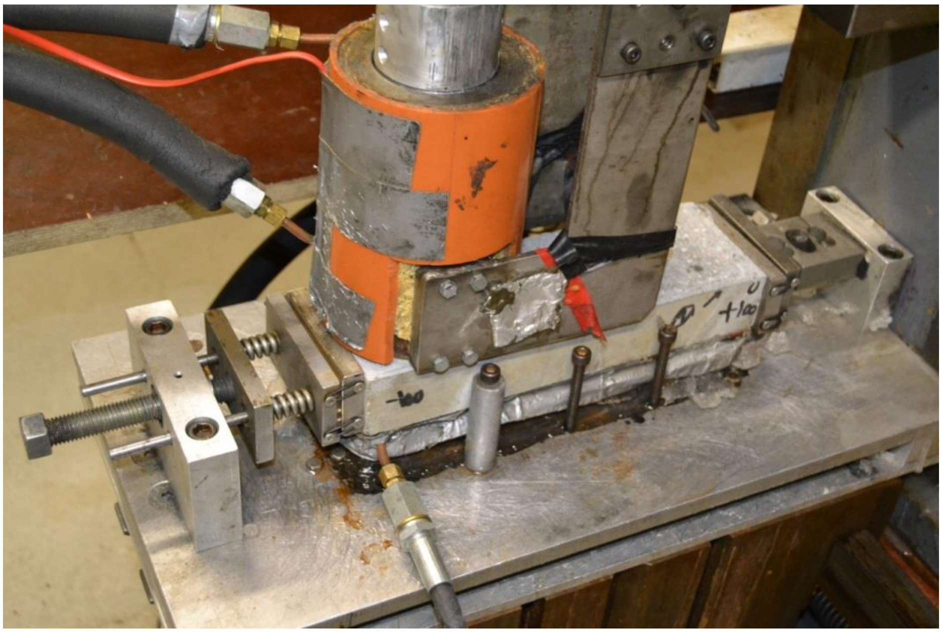
Picture 3 Concrete specimen is placed in correct position for testing.

If the specimen is casted with temperature sensors these should now be connected.
To get meaningful results test parameters and test settings have to be decided and entered into the Labview software. Sampling rate can be chosen in the “logging” tab of the Labview program. Available options are frequency or cycle controlled logging.

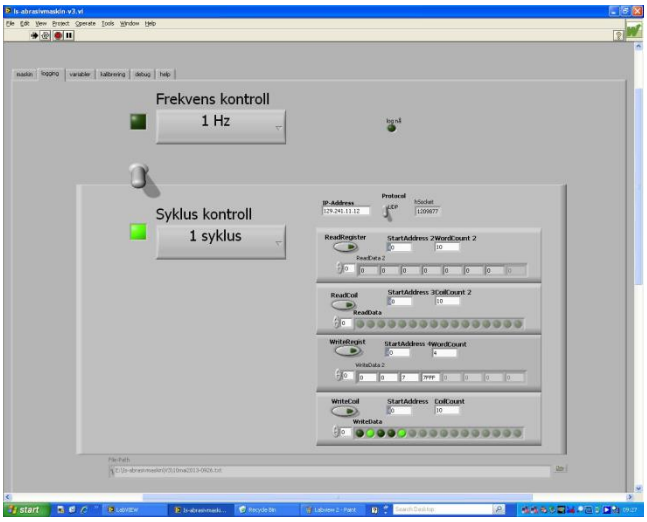

Picture 4 “Logging” tab in Labview. Either frequency or cycle controlled logging can be used

Contact pressure is entered as a load [N] and can be found by multiplying desired contact pressure with the surface area of the ice specimen, which is 43000 mm^2.

Vertical gain [mm] and vertical speed [RPM] has to be set for making the ice abrasion rig able to apply load. Low gain and a high vertical speed would be preferable to get as stable load as possible. Then the rig is adjusting the piston fast and often. In (Bøhn, 2012) it is suggested to use a vertical speed of 1350 RPM. My experience is that this is too high and causes some sort of overload on the horizontal engine which starts to get overheated. A vertical speed in the range of 500-800 RPM combined with a gain on 0,02 mm is found to give reasonable stable loading and avoiding engine problems

.

The next parameter to be set in Labview is horizontal sliding velocity. This entered as RPM in the “Horisontal turtall” box. A spare test specimen should be used to find which RPM is giving the desired velocity. 850 RPM is found to give a velocity of approximately 16 cm/sec.

The last thing to do before testing, sliding distance for when the rig is going to stop automatically should be entered. Then it stops automatically after a given accumulated distance. Unless this parameter is set, the rig runs until ice is consumed or to it is stopped manually. Picture 5 shows the main operating window in labview and where to make inputs of test settings parameters.

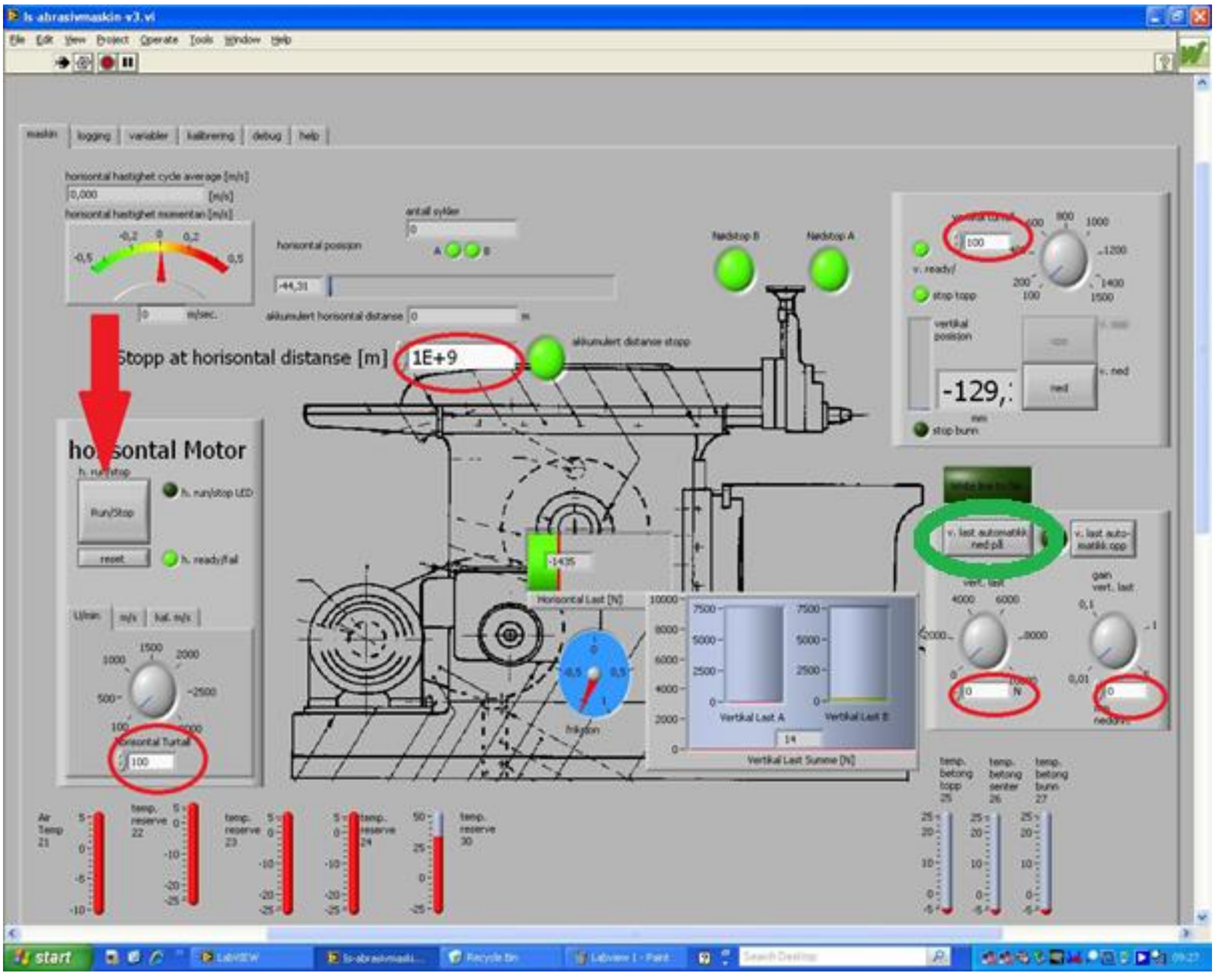

Picture 5 Red rings around parameters which have to be set before testing. Green ring around the vertical load automatic down on button and the red arrow is placed over the start/stop button.

To avoid water freezing on the test specimen surface, the heating circulator should be switched on. Temperature should be adjusted so that the copper plate transfers enough energy to keep the concrete surface at a temperature ≈ 0^0C. Different concretes will have different heat transfer properties. Specimen with temperature sensors should be used to find the correct temperature of the heating circulator. The products tested in this study are found to need a temperature in the range of 12-13 ^{0}C to avoid ad-freeze. It is important to check that the gauges for the copper bedding circuit are open. Picture 6 is showing the heating circulator and gauges.

Picture 6 Heating circulator. Copper bedding circuit is marked with a green circle and the ice specimen circuit is marked with a red circle

Before starting the test it is important to remember to push the “Vert.last automatisk ned på” button, marked with a green circle at Picture 5. If this is not done no load will be applied and the ice is going to move back and forth without performing any testing (load).

To start testing, push the “Run/stop” button in Labview, marked with red arrow in Picture 5. The rig runs by itself to accumulated distance is reached or the ice is consumed and a new ice specimen has to be inserted.

When ice is consumed the rig is supposed to automatically set horizontal sliding speed to 400 RPM and vertical speed to 1350 RPM so that the piston can be reversed to its top position. However, there should be kept an eye on the rig when the position of the vertical piston is getting close to zero. For some reason the reversing seem to hang up from time to time. If the vertical engine is not stopped when this happens it could cause the engine to overheat and “burn up”. This is found to be avoided by stopping the engine and reducing the vertical speed before restarting the engine again.

To get the old ice out of the ice container the gauge on the heating circulator, on the circuit connected to the ice specimen container, should be opened for half a minute or so. Then the ice melts enough to be removed and replaced. A mallet can be used on the ice to help speed things along. Remember to close the gauge to avoid the new ice to melt.

Things to remember/ precautionary measures: Murphy's Law definitely seems to apply for the ice abrasion rig and laboratory equipment. Experiments have been delayed due to many different unforeseen events and problems.

The first breakdown happened as a consequence of what is believed to be water freezing on one of the vertical load cells. This made the load cell unable to register loads. Then the rig tried to adjust the load by pushing down the piston even more. But as long as this load was only registered by one of the cells, the load never became high enough. In the end this caused the vertical engine to overload, it overheated and had to be replaced. Originally the ice abrasion rig is designed to keep water away from the load cells, but it seems as if a leakage in the sealing allows water to get in contact with one of the load cells. To prevent this from happening again, an anti-freeze liquid has been sprayed over the sealing and on the load cell. This should be done regularly when performing tests In addition to prevent the water from freezing, it is also easier to remove slush instead of ice from the area around the load cells.

The sealing should be repaired, and it should also be considered to install some sort of heating on the plates under the concrete specimen bedding to make the removal of ice easier.

When an ice specimen is consumed the rig is supposed to set horizontal velocity to 400 RPM and reverse the piston to its top position. After some while of testing it was unable to reverse the piston automatically. A temporally solution that seemed to work was to stop the rig manually and use a lower vertical speed (800-1000 RPM) when reversing the piston. However, after doing this for a while it became impossible to adjust the piston at all.

One likely cause of this problem is that the repeated movement up and down lead to large friction on some of the components, as they were practically welded together. In addition one component needed for adjusting vertical position of the piston had fallen out. Because of this the rig had to be dismantled and rebuilt. The rig has been working fine after this, but no components have been replaced, and the problem could therefore reoccur. Using silicon based lubricant on the vertical moving parts once a day or so is used as a solution to prevent this problem. If it should reoccur, there is little that can be done and there should be kept an eye on it when ice level is getting close to zero and the rig is entering "maintenance" modus. If the piston is not reversed automatically, the laboratory staff (Steinar or Gøran) should be contacted to assess the situation.

In the last part of the tests of this study, the ice abrasion rig shut down completely, blowing the main fuse every time it was tried to be restarted. After troubleshooting this problem from many angels the solution was found to be quite simple. As the vertical piston is moving up and down the insulation of a cable to the sensor indicating vertical position of the piston, had been "chewed" up causing a short circuit of the electrical system. The problem was fixed by applying some electrical tape on the damaged cable, and it should be easy to prevent this from happing again if there is kept an eye on the cable. This problem also affected some of the computer chips in the control unit, which had to be replaced.

The sensor registering the vertical position of the piston is fastened relatively loosely loose to the rig. It happened more than once that the vibration from the rig made it change its position. It is therefore important to be in the proximity of the test rig when ice level is closing into zero, to make sure that the piston is not pushed too far down.

The bedding where the test specimens are mounted can be swung back and forth to be able to mount new concrete specimens or changing ice. The track it slides on should be lubricated with oil in the following situations:

- After temperature in the ice abrasion laboratory has been higher than 0°C
- When it starts to get difficult to swing the wheel
- Once a week in periods of testing, or before testing if it has been a while since the rig has been used.

The ice abrasion rig contains of many individual components, carefully put together. Vibrations and other stresses have been found to loosen screws. Therefore, all visible screws should be checked and tightened regularly to avoid any unnecessary damage to the rig. Also the rubber stretches used on the plate in front of the horizontal load cell should be kept an eye on. These seem to get “crunchy” due to the low temperatures and have to be replaced regularly. Make sure to always have some extra on hand.

A very time efficient tip is to connect the laboratory computer to internet and create a Teamviewer account. The computer is easily connected to internet by a wireless LAN usb-stick. By installing Teamviewer and connecting the computer to your account, tests can be monitored also outside the laboratory, on a Teamviewer supported device connected to internet. This makes it possible to do some other work in the laboratory and still be able to respond quickly the ice abrasion tests.

A new log file is created for each time the “Automatisk last ned” button is being hit. Values like distance and number of cycles are continued to be counted in the next log file. However, if the labview software is restarted values are being counted from zero again. This should be done if new specimens are to be tested. It is also important to have an organized system of sorting log files for different specimens, as the number of files can get high and difficult to get a good overview of.

Ice abrasion test rig test procedure quick guide, step by step (Modified and updated version of the guide found at page 35 in (Bøhn, 2012)**):**

Preparations:

1 Start making ice, at least a couple of day before the experiments are going to take place
2 Perform preabrasion surface measurement
3 Decide test settings; ice contact pressure, sliding velocity, sliding distance, temperature of ice, laboratory and copper bedding, to prevent surface freezing.

Testing:

4 Mount test specimen on the copper bedding and pretension.
5 Calibrate vertical and horizontal load cells
6 Insert ice in the ice specimen container
7 Make sure concrete specimen is located directly under the ice specimen.
8 Make sure there is a gap between ice specimen container and concrete specimen
If not: Loosen the screws holding the ice container and level it so that there is a gap
9 Hit Run/stop button in Labview
10 Hit the apply vertical load button in Labview
11 The rig will now run automatically to wanted sliding distance is reached or ice has to be replaced
12 The ice abrasion rig is entering maintenance-mode, adjusting horizontal speed to 400 RPM and the piston is reset to its top vertical position
13 Stop horizontal movement by hitting the run/stop button
14 Before removing ice, open the gauge to the ice container circuit on the heating circulator for approximately 30 seconds, before closing them again
15 Use the mallet to give the ice a kick. This will make the removal of ice faster.
16 Remove old ice
17 Insert new ice
18 Reset vertical and horizontal velocity
19 Hit run/stop button and continue testing by performing step 5-17 until wanted distance is reached
20 Remove concrete specimen from the bedding.
21 Measure abrasion
22 Obtain log file. Log files should be obtained immediately and archived in a well-organized system for each specimen.
23 Remember to lubricate the described moving parts on the rig
24 Keep an eye on ice growth on vertical load cells

Appendix 5: How to use the ATOS surface scanner (quick guide)

The ATOS 3D scanner was found to be a very demanding equipment to learn how to use and operate. A complete user manual is available in the laboratory. This is a short, simplified version that can be used as a quick start.

1) Turn on the computer
2) Open the ATOS software
3) Remove camera lens protection and turn on the cameras. First push the main power button and wait a while before hitting the green button.
4) The cameras takes some time to start and warm up, and by waiting a few minutes the rest of the scanning will run more smoothly
5) The equipment has to be calibrated. However, this is only necessary if the equipment has been moved or in some way has been decalibrated, and is normally unnecessary.
6) Attach contrast marks on the surface which is to be measured. It is important to attach them in an irregular pattern so that the software can recognize them when stitching together individual photos to a final digitalized version of the surface.
7) Place the specimen on the table under the cameras
8) Create a new file in the ATOS software and follow the instructions on the screen
9) Enter Measuring mode
10) When cameras and lasers are turned on, set camera in wanted angle and adjust the height so that the two laser beams are crossing each other on the specimen surface.
11) Start measuring by hitting the measurement button.
12) Move specimen or camera to a new position to include a larger part of the surface. A certain number of contrast marks from one of the previous scans have to be visible.
13) After the whole surface is photographed, the images are ready to be polygonized
14) Enter evaluation mode and select the parts of the surface to be polygonized.
15) Click Polygonize project and follow the instructions on the screen
16) Polygonizing takes a while, depending on the number of pictures to be digitalized!
17) Set a coordinate system. The easiest way is to use the 3-2-1 transformation function. You will be asked to set out 5 points to create a reference coordinate system. This is the tricky part. In order to get good results the chosen points should be on unabraded places on the surface and preferably not in pores.
18) Use the surface deviation function. Remember to select the parts of the surface the function should be applied for. A color map of the surface shall then occur.
19) Create snapshots and/or export the digitalized version to an wanted file format
20) When done. Click the close senor button in labview.
21) Turn off the cameras and wait until the light on the red button is getting brighter
22) Turn off the red button.
23) Reattach the camera lens protectors